Geomagnetically induced currents by solar storms: how we model and measure them

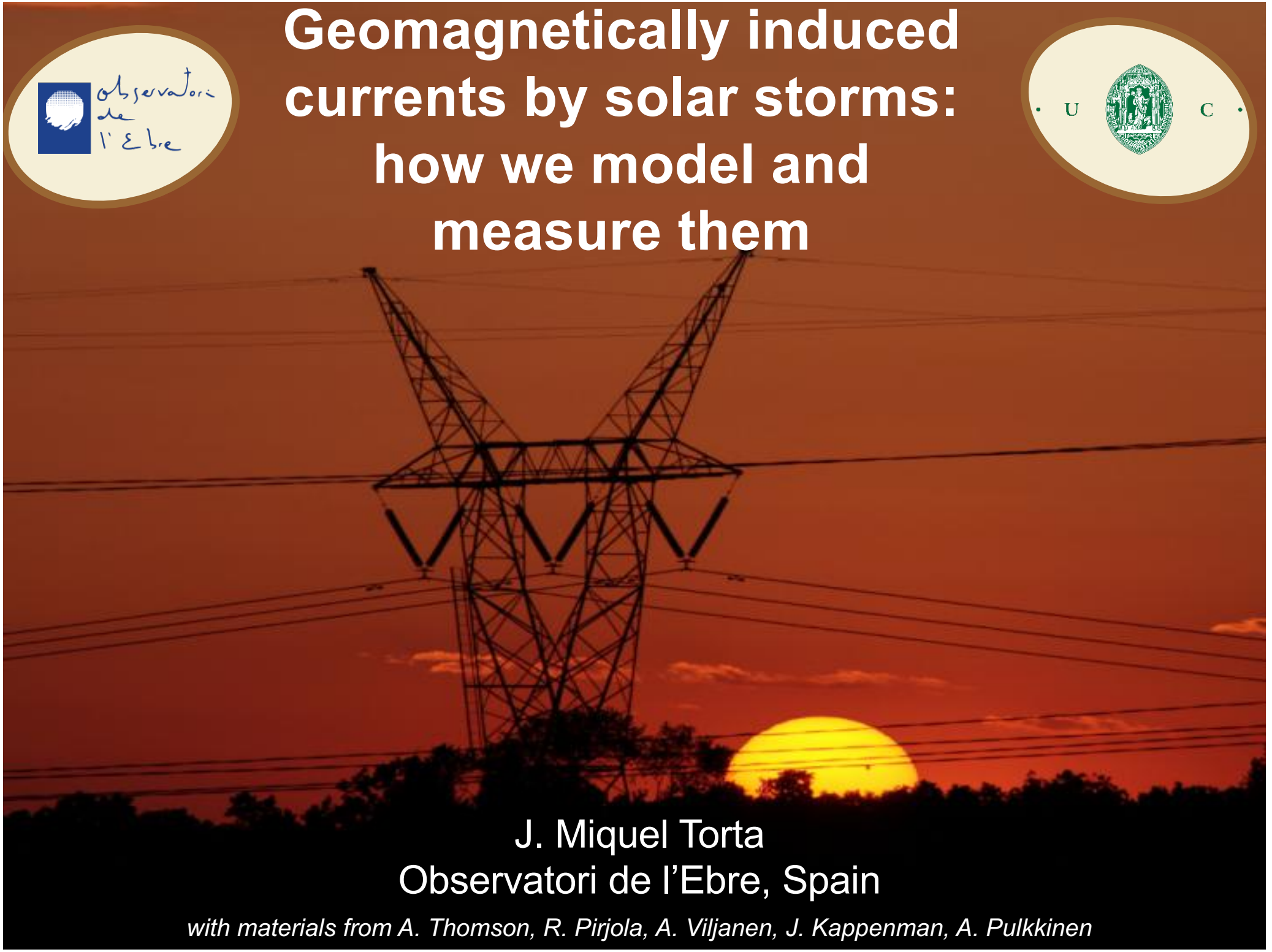

J. Miquel Torta
Observatori de l'Ebre, Spain

with materials from A. Thomson, R. Pirjola, A. Viljanen, J. Kappenman, A. Pulkkinen

SPACE WEATHER

It refers to conditions on the sun, in the solar wind, and within Earth's magnetosphere, ionosphere and thermosphere that can influence the performance and reliability of space-borne and ground-based technological systems and can endanger human life or health.

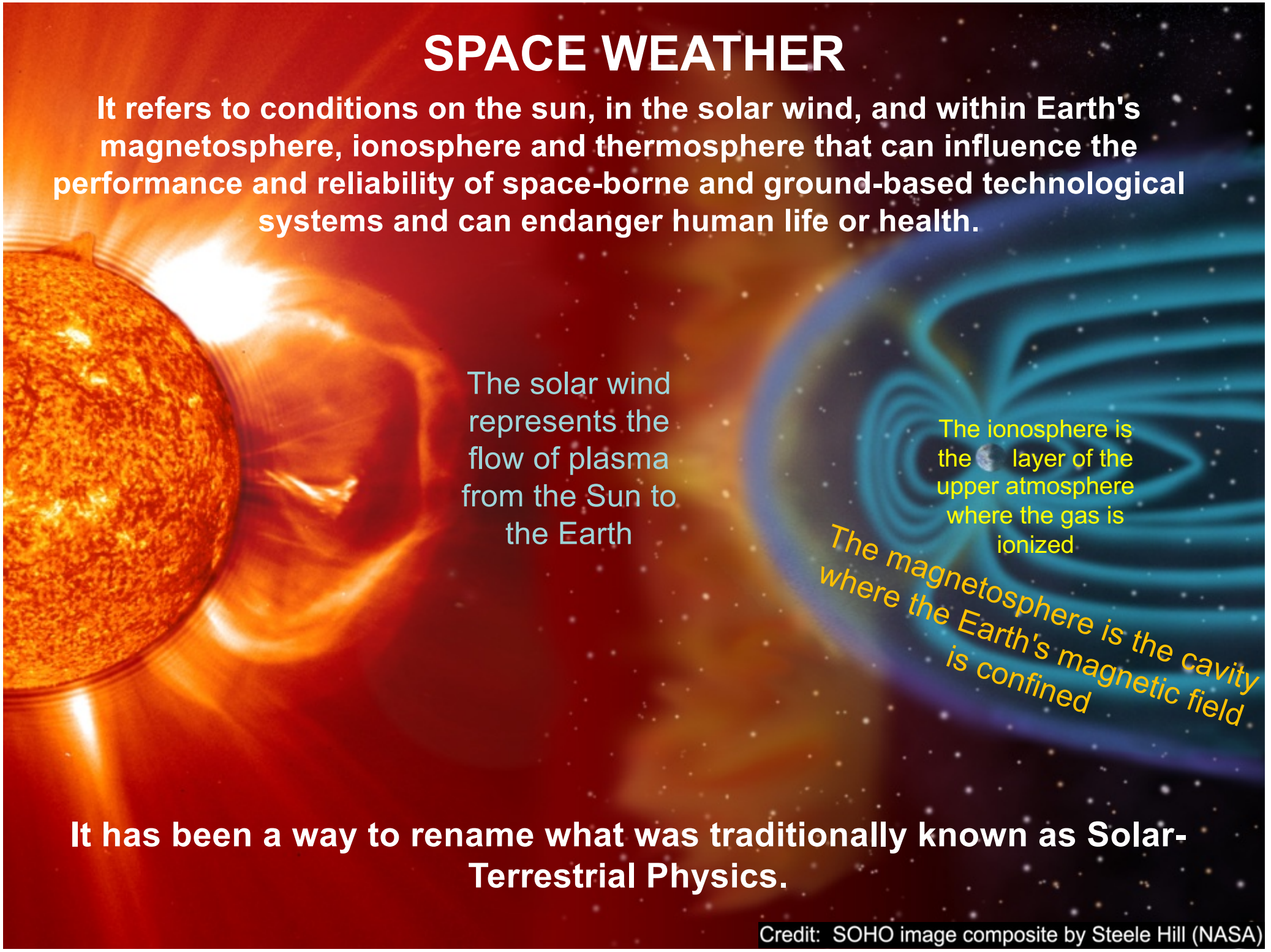

It has been a way to rename what was traditionally known as Solar-Terrestrial Physics.

Credit: SOHO image composite by Steele Hill (NASA)

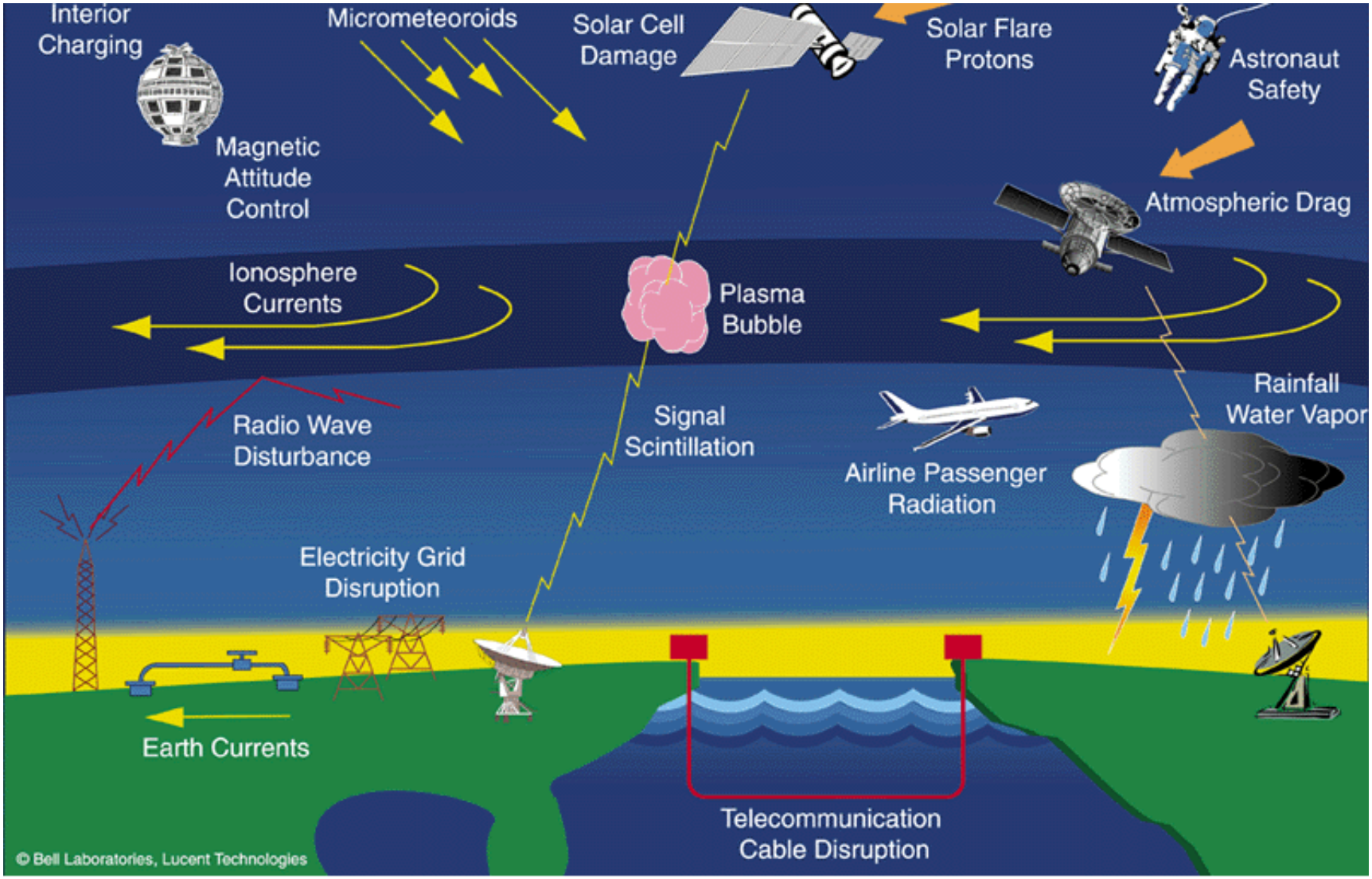

The effects of magnetic storms - what scientists call space weather - extend from the ground to geostationary orbit and beyond.

Geomagnetically induced currents (GICs) at the surface of the Earth in:

- **Power transmission grids**
- **Oil and gas pipelines**
- **Telecommunication cables**
- **Railway equipment**

Outline of the talk

- **Description of the phenomenon. Latitudinal extent**
- **Determination of the electric field occurring in connection with a magnetic storm at the Earth's surface**
- **Calculation of the resulting GIC**
- **Case Study: Modelling and measuring GIC in the Spanish power transmission network**

Under disturbed conditions of the Sun, the degree of ionization in the magnetosphere and the ionosphere increases and there is a significant increase in their electrical current systems, which are the source of the magnetic fields at the Earth's surface (superposed on the main geomagnetic field, whose origin is in the Earth's liquid core).

The auroral electrojects can reach values of MA.

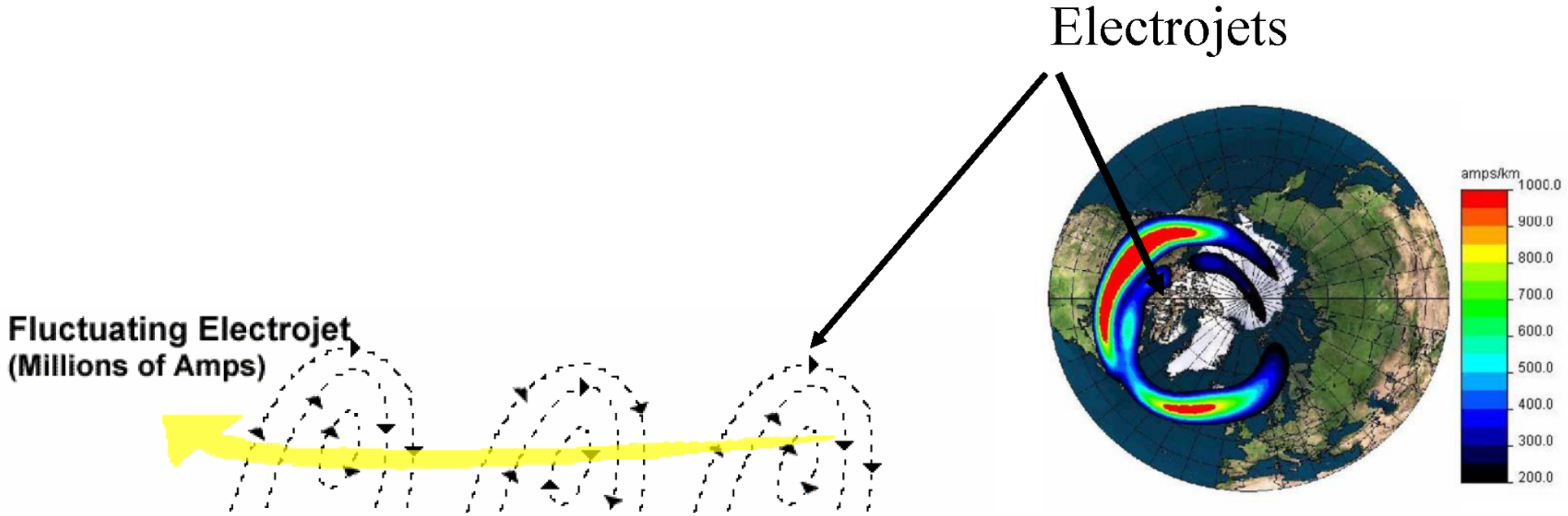

As a consequence of Faraday's law, associated with the variations in time of the geomagnetic field, an electric field is induced on the Earth's surface. This electric field acts as a voltage source through the networks.

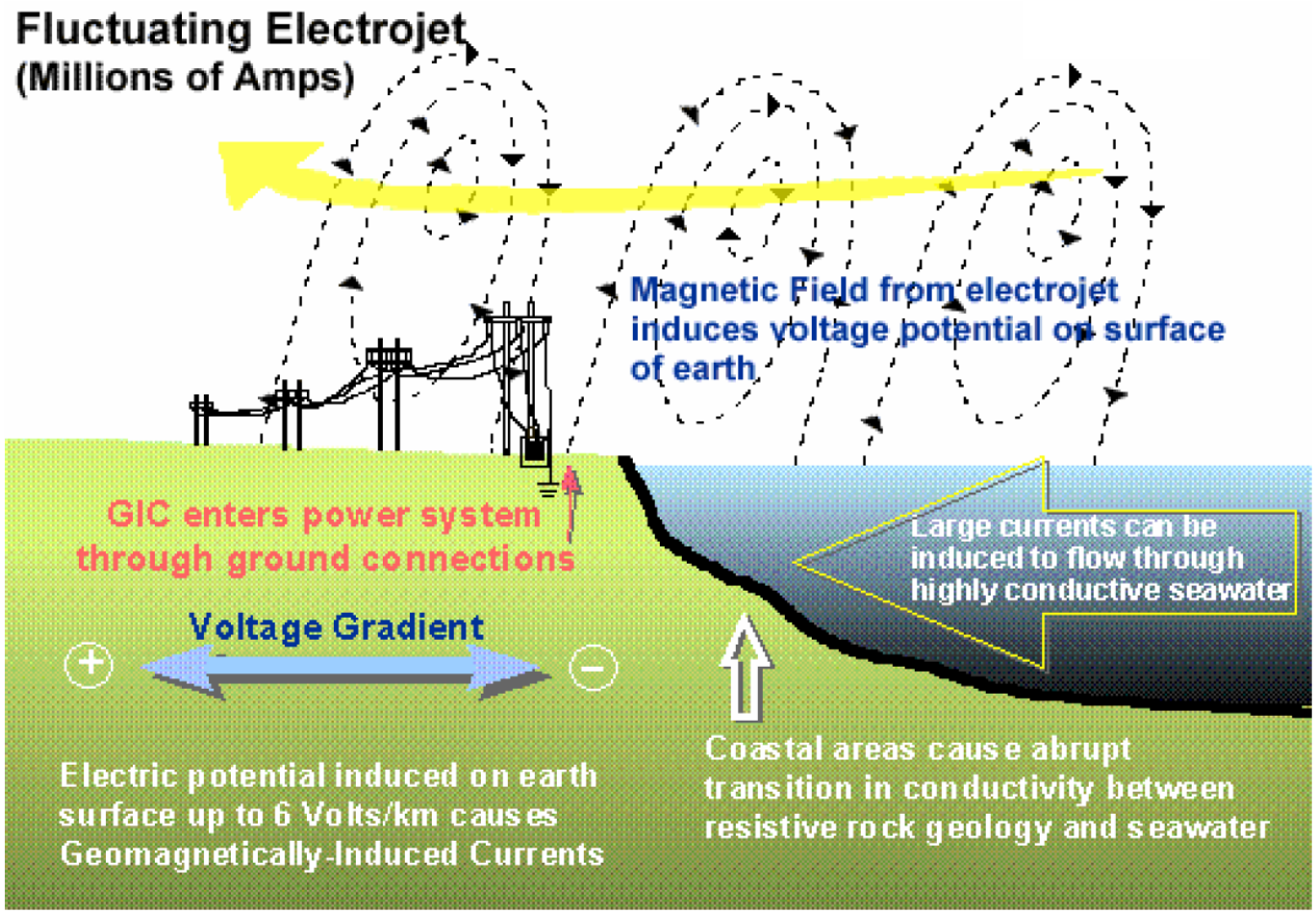

Figure: John Kappenman (Metatech)

Transformer failures in regions incorrectly considered to have low GIC-risk

Failure in a 700 MVA generator transformer in South Africa after the Halloween storms of 2003.
[Thomson et al., Adv. Space Res., 2010]

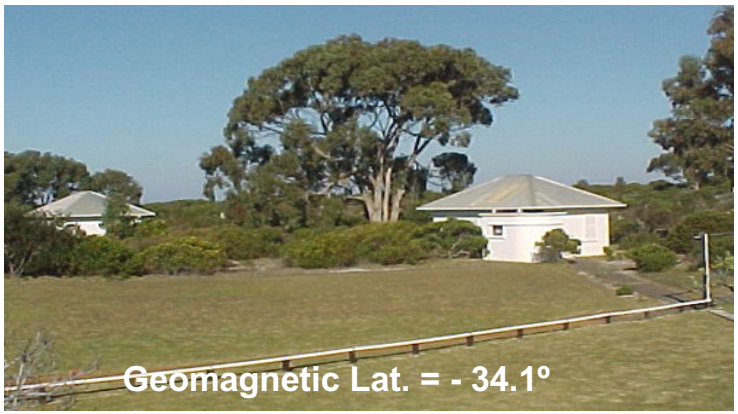

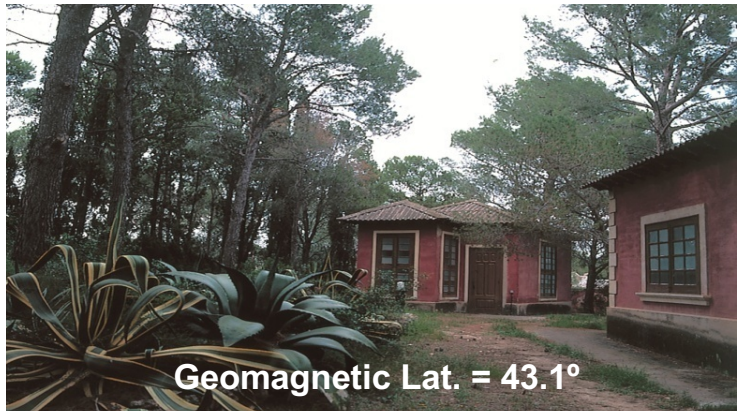

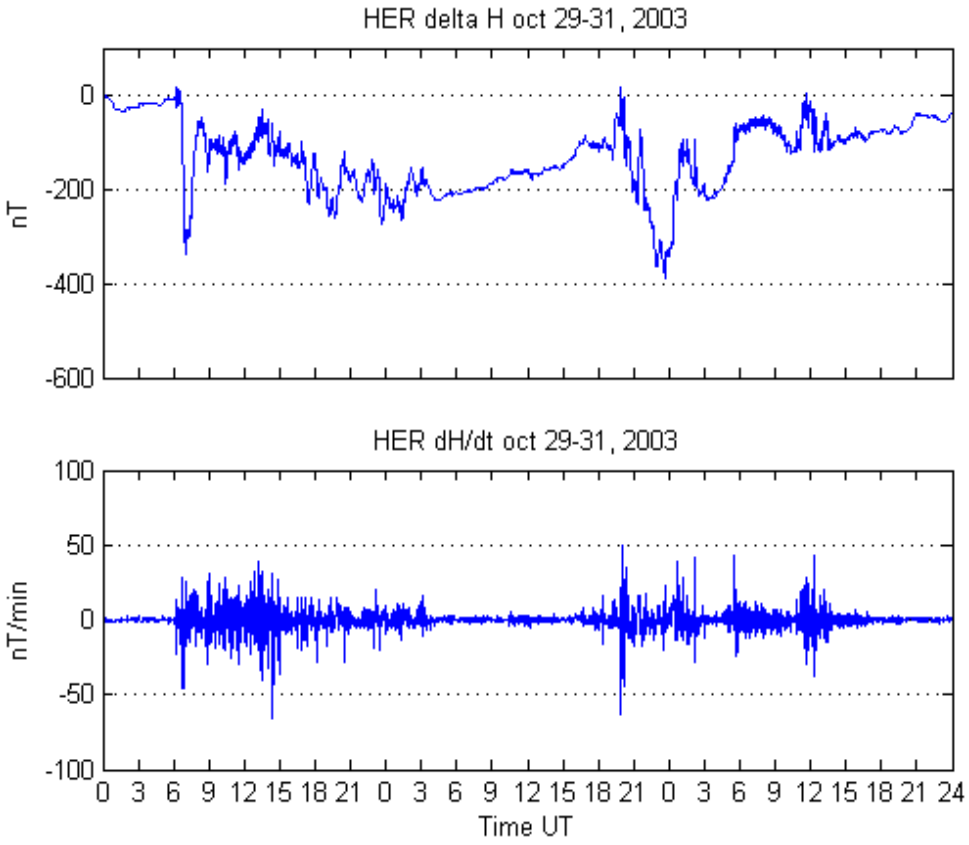

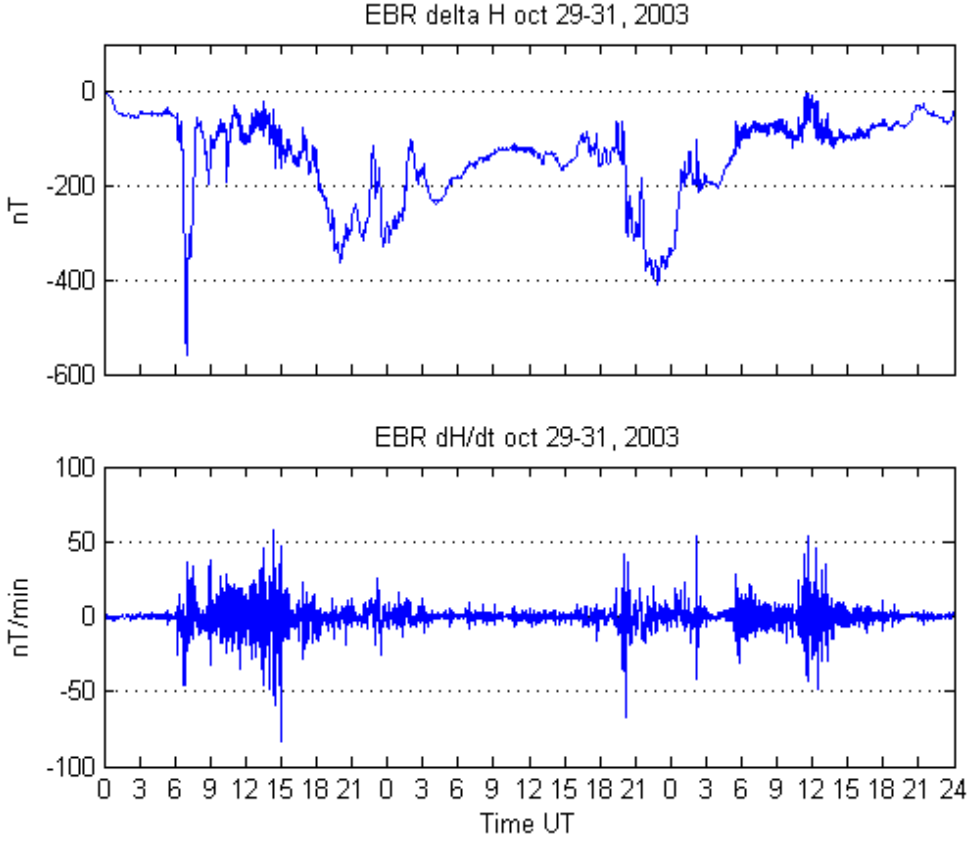

Left: H component of the HER (South Africa) magnetic field (top) and time derivative (bottom) during the Halloween storm. Right: the same event as recorded at EBR (Spain)

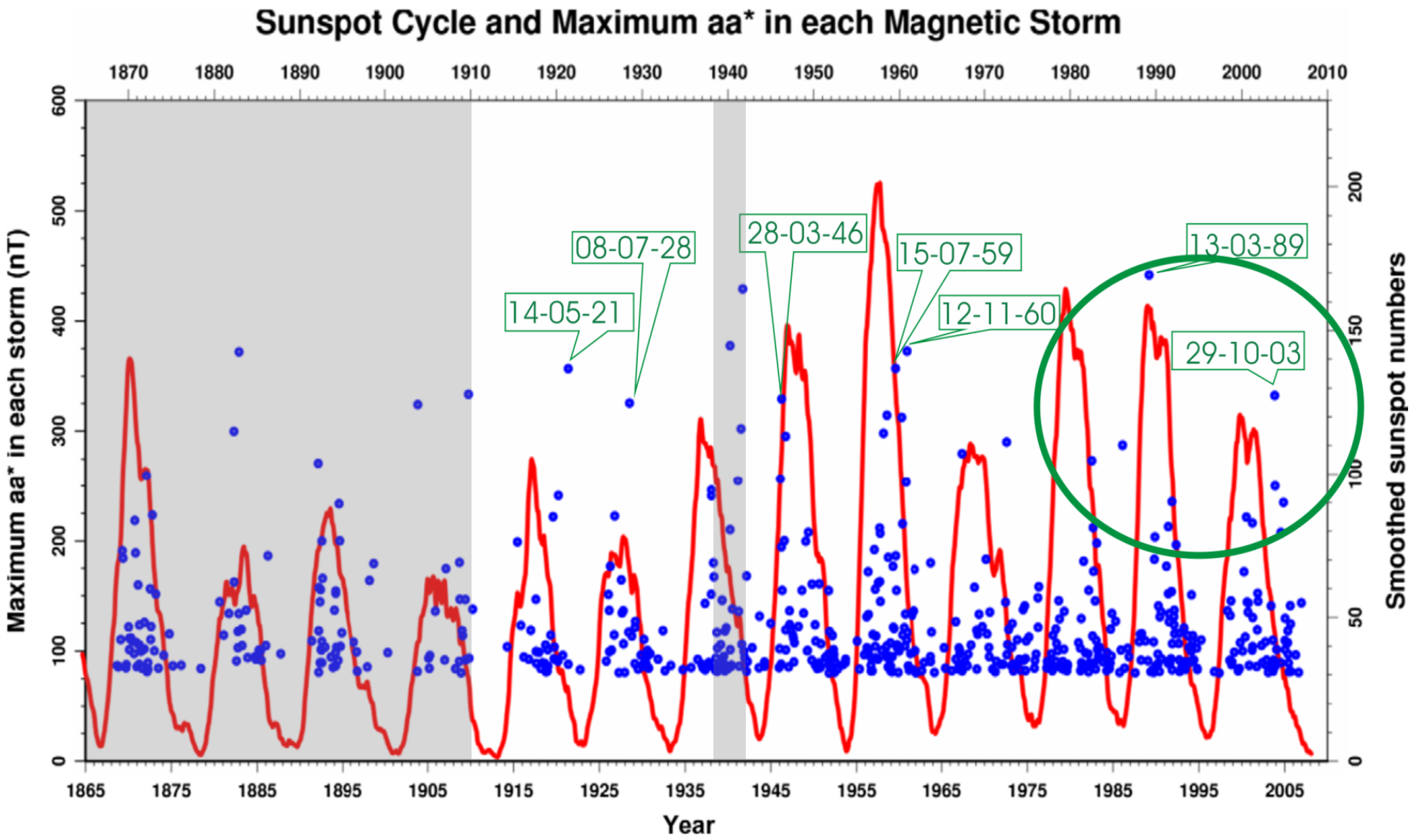

Large storms identified by the peak in the 24-h running average of the aa index, overlain with monthly smoothed SSN. The largest storms recorded at EBR and those during the last three solar cycles that provide large rates of change are indicated. [Adapted from Thomson et al., Adv. Space Res., 2010].

Rank	Date	Peak aa (nT)	Peak dB_H/dt (nT/min)
1	24 Mar 1991	363	**177**
2	14 May 1921	680	**135**
3	15 Jul 2000	440	**112**
4	13 Jul 1982	497	**110**
5	13 Mar 1989	715	**92**
6	29 Oct 2003	715	**83**
7	26 Jul 2004	228	**82**
8	31 Mar 2001	284	**72**
9	28 Mar 1946	656	**70**
10	24 Nov 2001	445	**69**
11	06 Nov 2001	306	**64**
12	05 Jun 1991	363	**64**
13	13 Nov 1960	568	**55**
14	09 Nov 2004	363	**55**
15	08 Nov 1991	578	**50**
16	08 Jul 1928	656	**50**

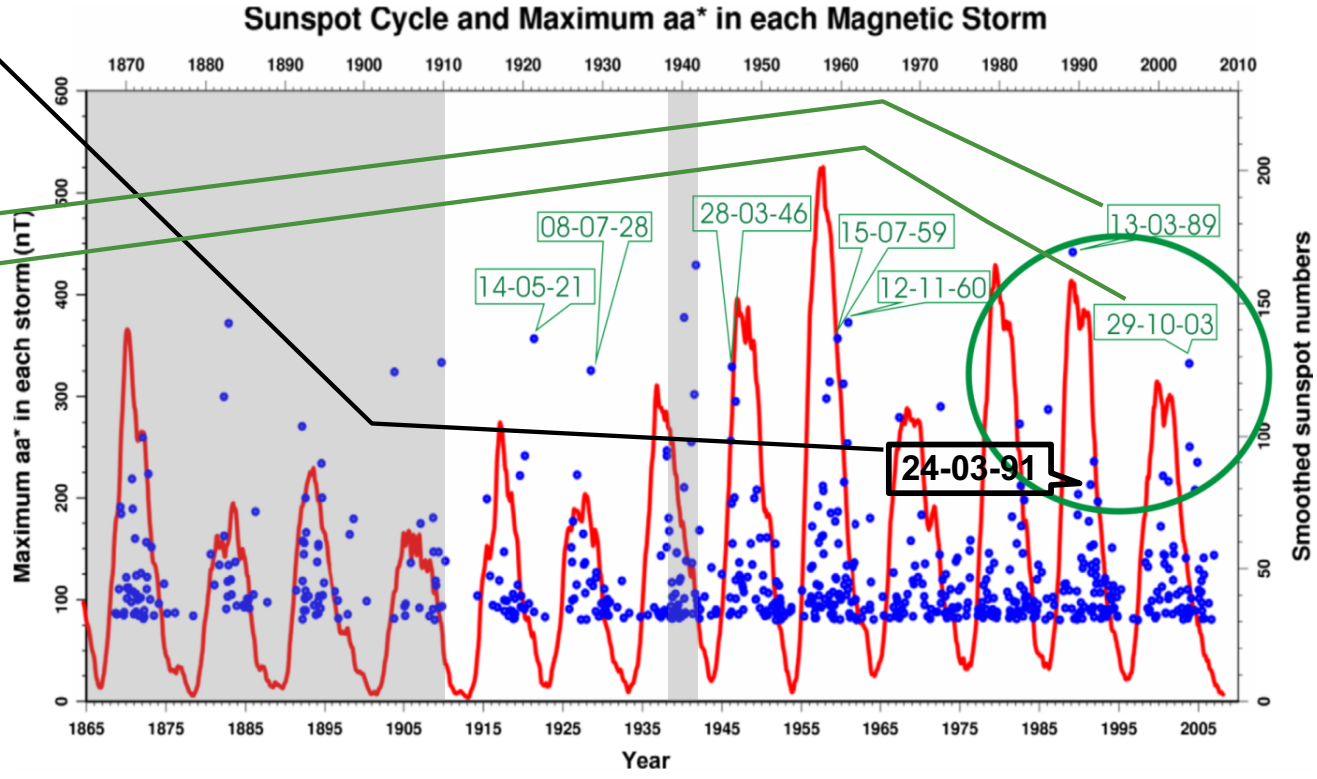

Rank	Date	Peak aa (nT)	Peak dB_H/dt (nT/min)
1	24 Mar 1991	363	**177**
2	14 May 1921	680	**135**
3	15 Jul 2000	440	**112**
4	13 Jul 1982	497	**110**
5	13 Mar 1989	715	**92**
6	29 Oct 2003	715	**83**
7	26 Jul 2004	228	**82**
8	31 Mar 2001	284	**72**
9	28 Mar 1946	656	**70**
10	24 Nov 2001	445	**69**
11	06 Nov 2001	306	**64**
12	05 Jun 1991	363	**64**
13	13 Nov 1960	568	**55**
14	09 Nov 2004	363	**55**
15	08 Nov 1991	578	**50**
16	08 Jul 1928	656	**50**

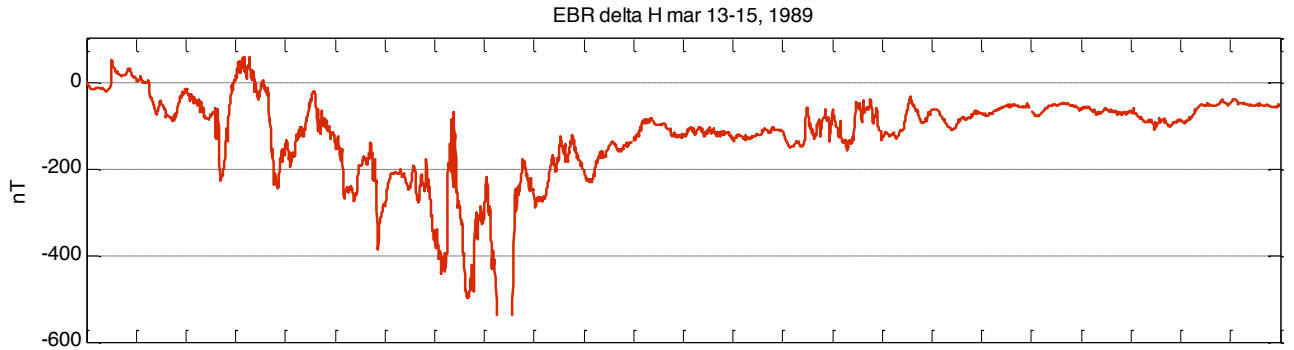

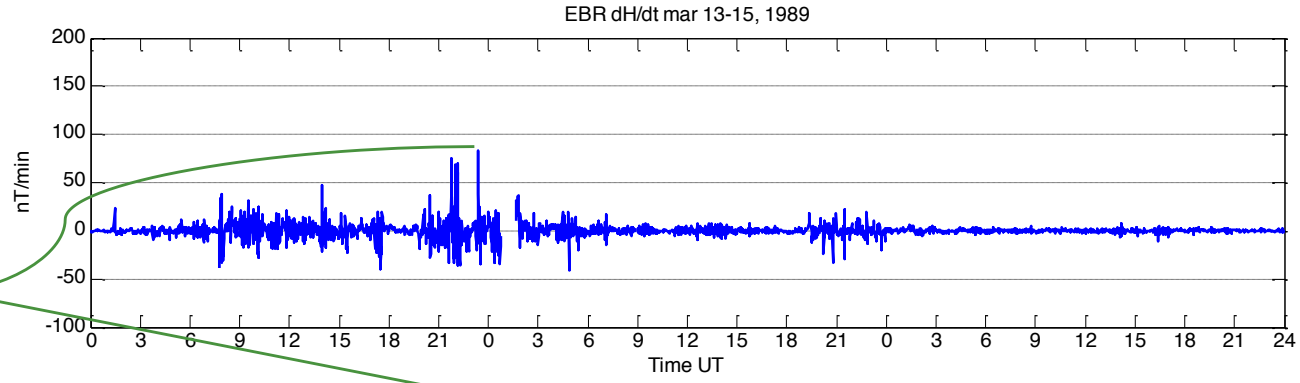

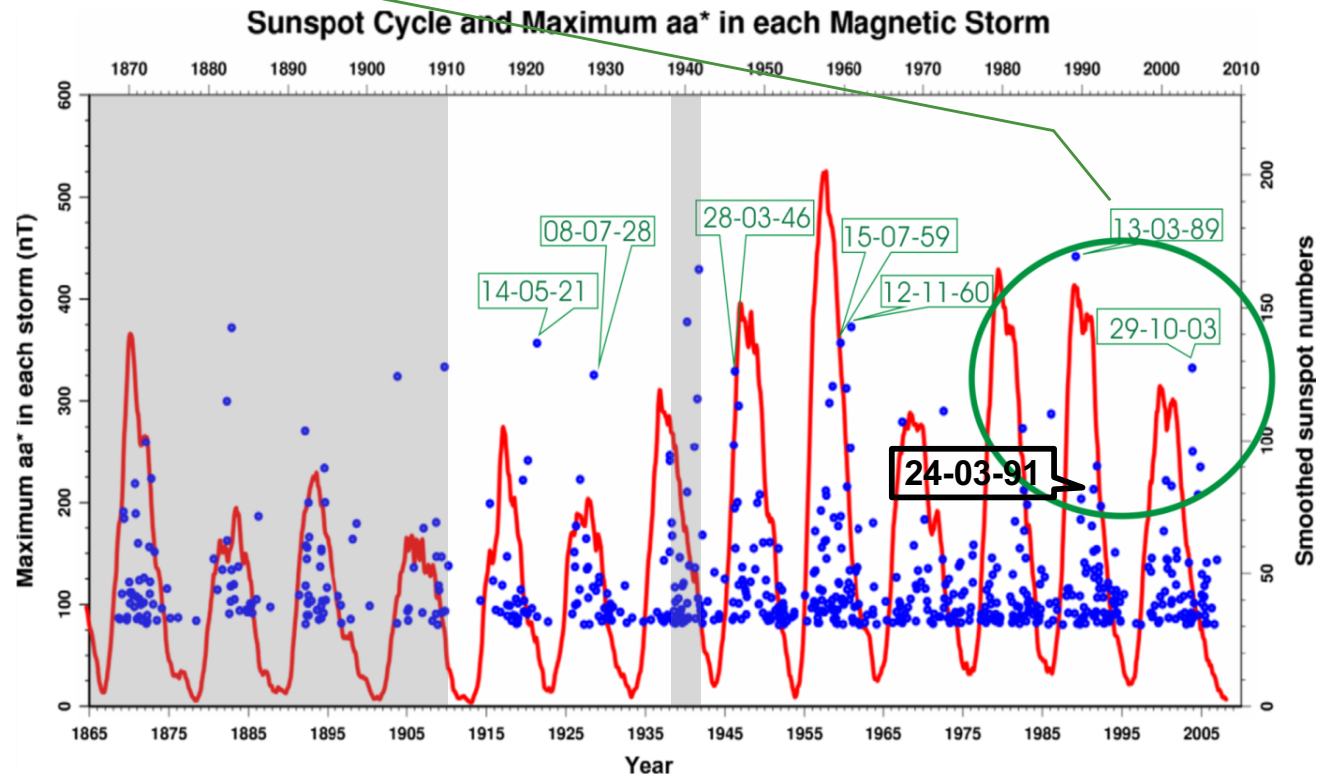

Rank	Date	Peak aa (nT)	Peak dB_H/dt (nT/min)
1	24 Mar 1991	363	**177**
2	14 May 1921	680	**135**
3	15 Jul 2000	440	**112**
4	13 Jul 1982	497	**110**
5	13 Mar 1989	715	**92**
6	29 Oct 2003	715	**83**
7	26 Jul 2004	228	**82**
8	31 Mar 2001	284	**72**
9	28 Mar 1946	656	**70**

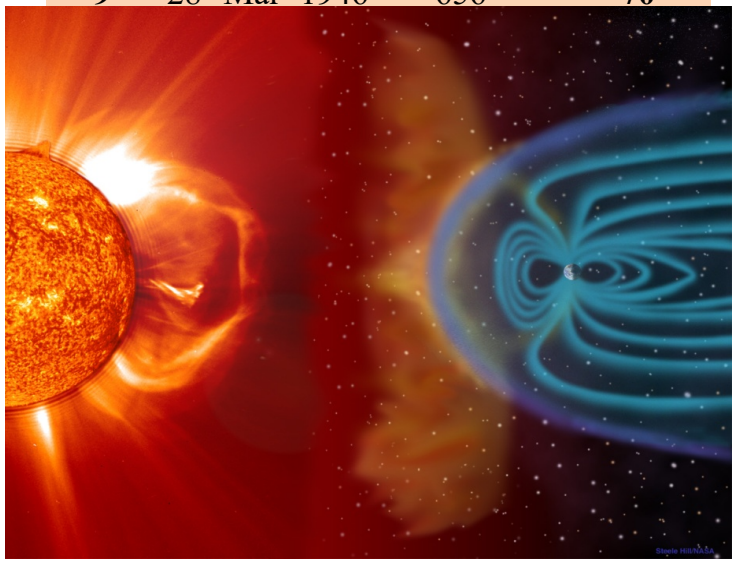

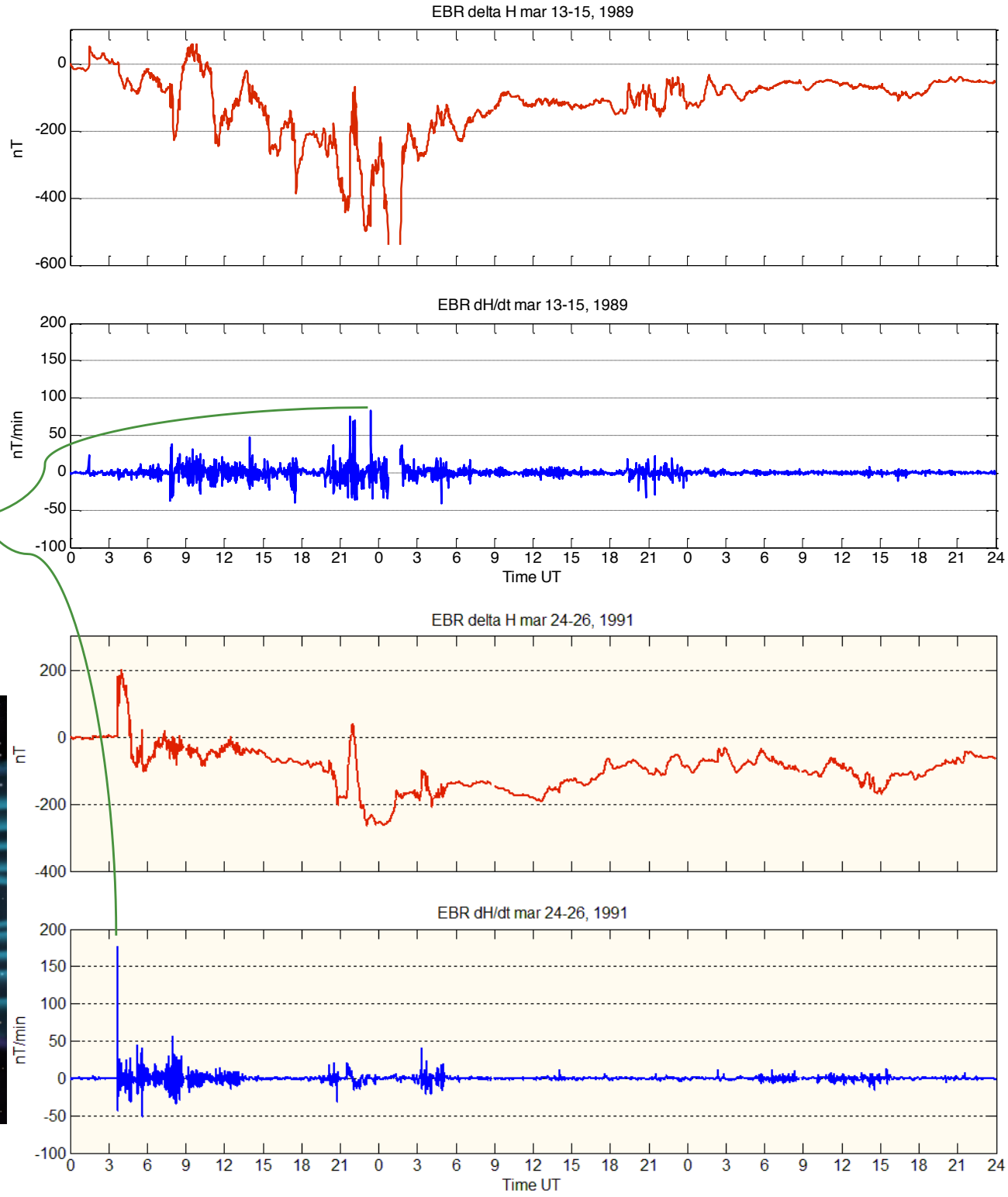

E fields associated with the auroral electrojet are complicated by the effect of currents induced in the Earth. In turn, induced currents in the transformer neutrals depend on the network topology and characteristics.

Electrojets

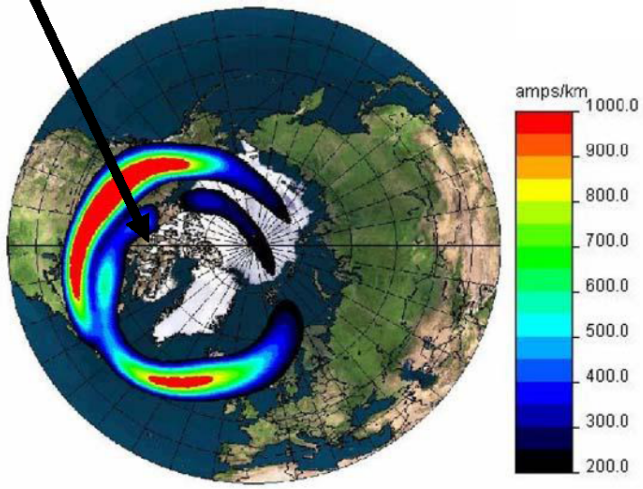

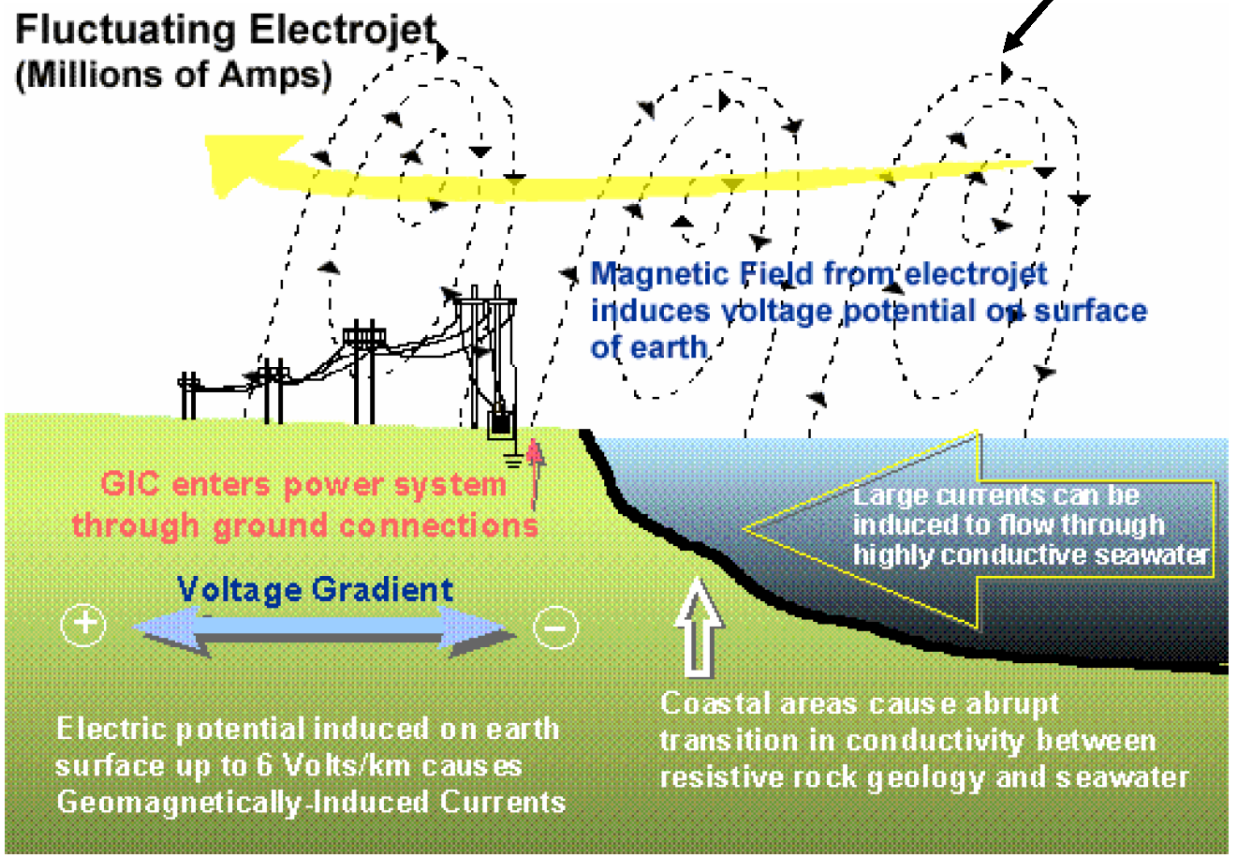

Figure: Alan Thomson (BGS)

3D Conducting Earth

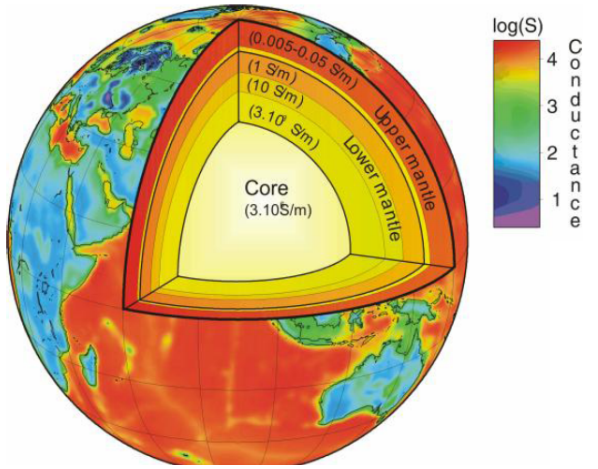

A problem to be solved in two steps:

1) Determination of the geoelectric field from the rate of change of the magnetic field (Faraday's Law):

$$\oint \boldsymbol{E} \cdot d\boldsymbol{l} = -\int \frac{\partial \boldsymbol{B}}{\partial t} \cdot d\boldsymbol{A}$$

$$\left(\nabla \times \boldsymbol{E} = -\frac{d\boldsymbol{B}}{dt} \right)$$

This a purely geophysical problem, which is independent of the technological system

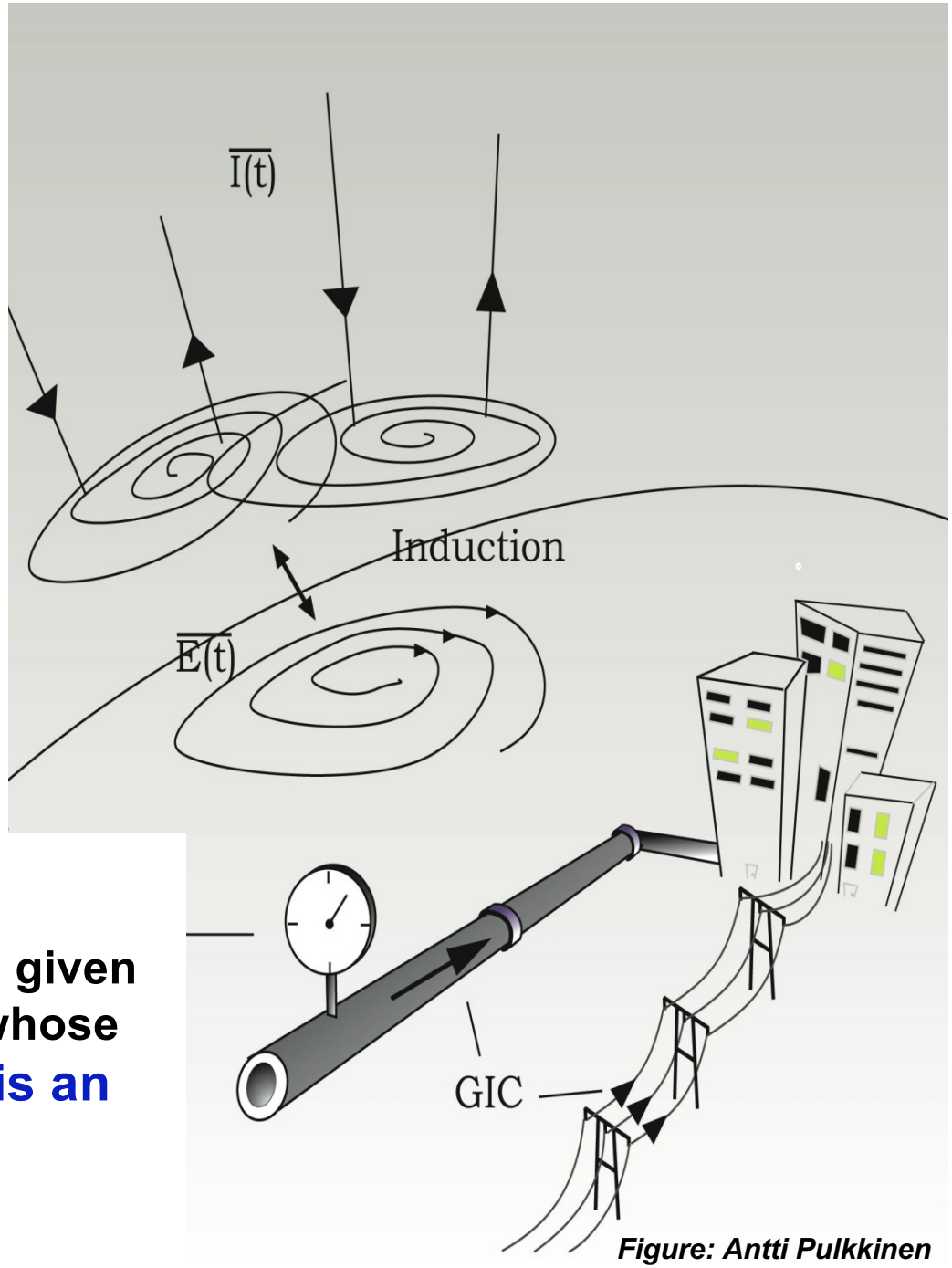

Figure: Antti Pulkkinen

2) Determination of the GICs due to the given geoelectric field in a conductor system whose topology and resistances are known. This an engineering problem

A problem to be solved in two steps:

1) Geophysical step

- **Assuming a plane wave**

- The electric and magnetic fields are horizontal and spatially constant at the Earth's surface.

- If the Earth is uniform:

$$E_{x,y}(t) = \pm \frac{1}{\sqrt{\pi \mu_0 \sigma}} \int_{-\infty}^{t} \frac{1}{\sqrt{t - t'}} \frac{dB_{y,x}(t')}{dt'} dt'$$

-The electric field is affected by past values of the magnetic field variation

-The integral can be obtained numerically:

$$E(t_n) = \frac{2}{\sqrt{\pi \mu_0 \sigma \Delta}} \left(R_{n-1} - R_n - \sqrt{m} b_{n-m} \right)$$

where: $b_n = B_n - B_{n-1}$ $\qquad R_n = \sum_{i=n-m+1}^{n} b_i \sqrt{n - i + 1}$

Δ = sampling interval $\qquad m$ = integration time

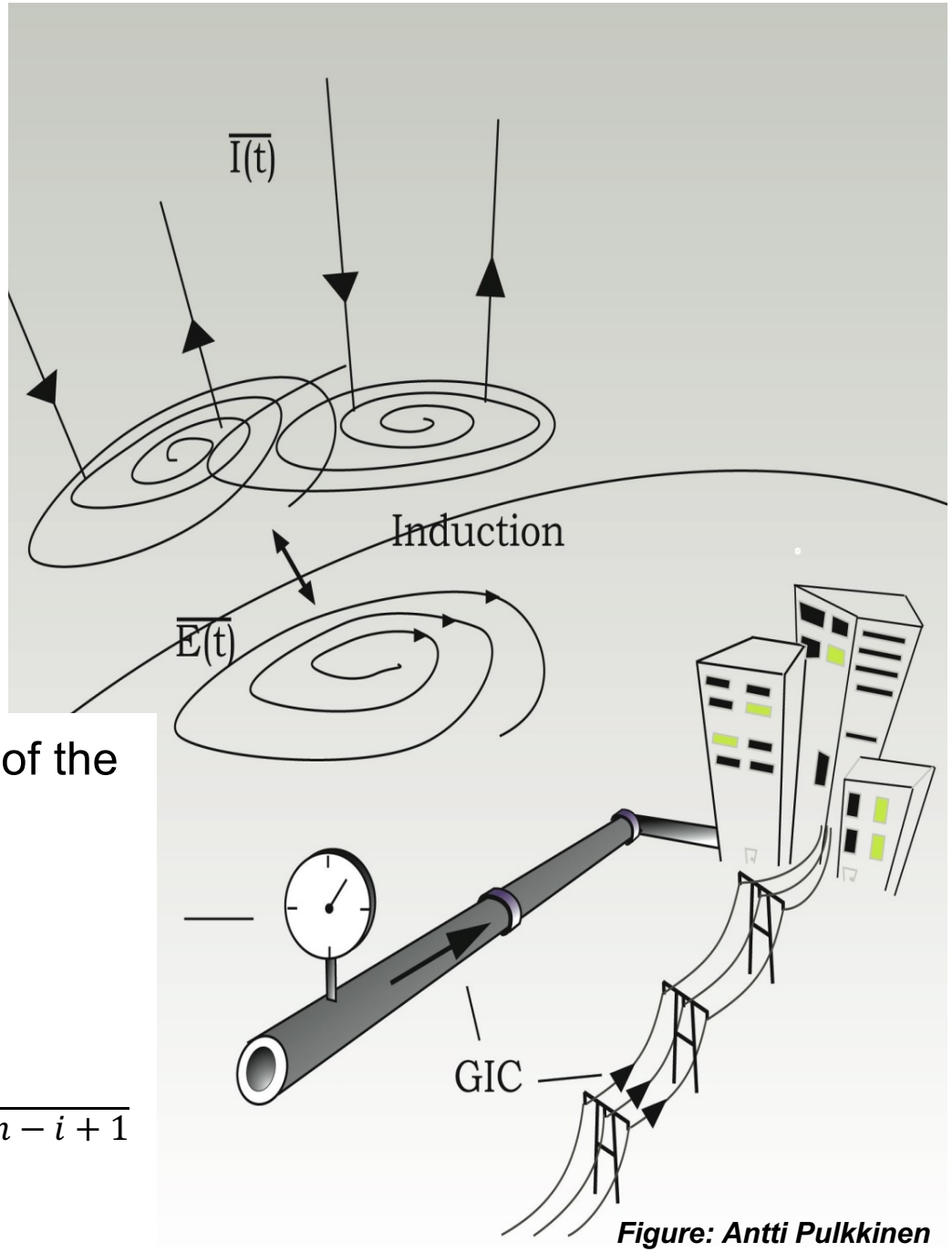

Figure: Antti Pulkkinen

East (E_y) and North (E_x) components of the geoelectric field ($\sigma = 10^{-3}$ S/m)

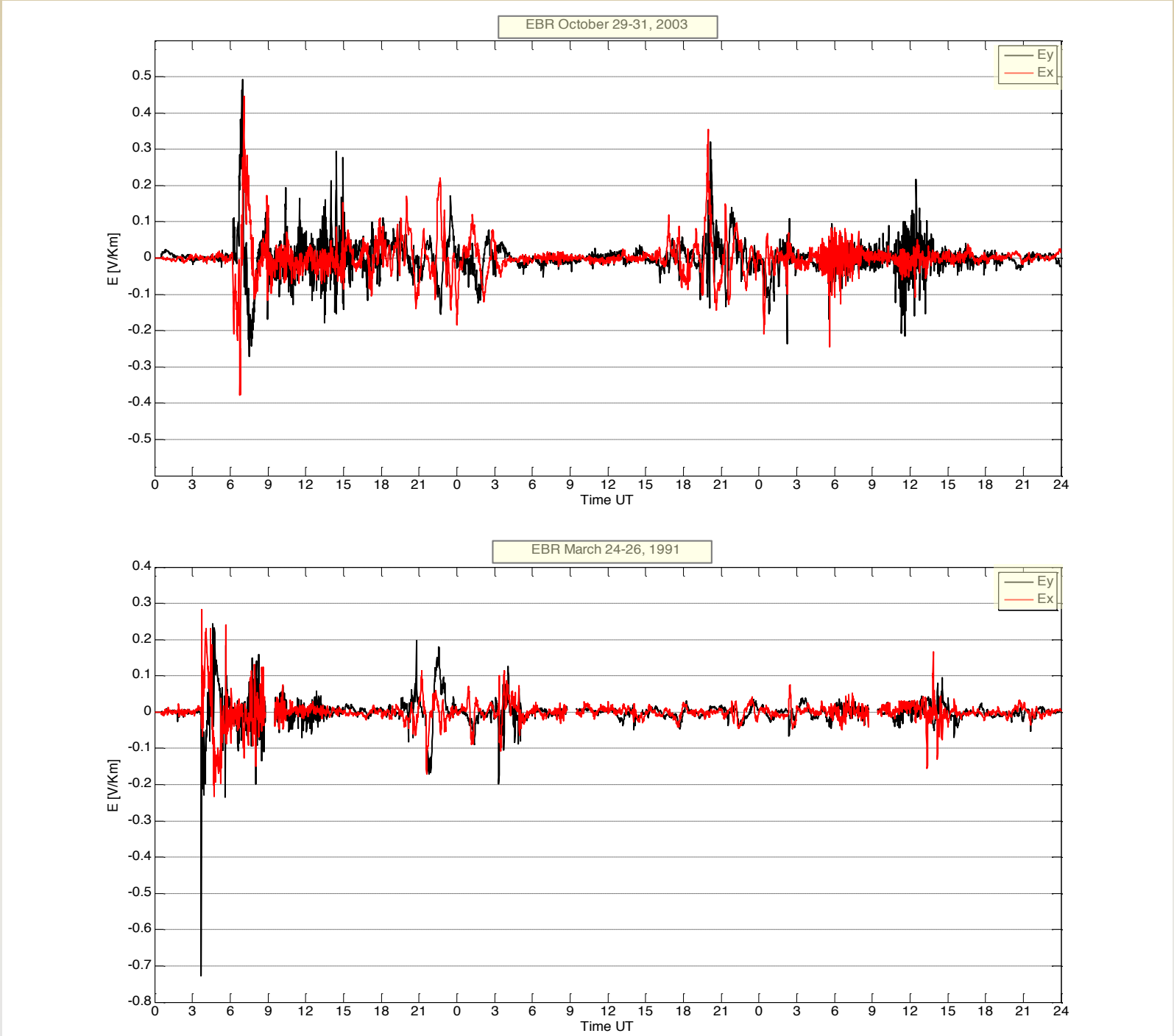

A problem to be solved in two steps:

2) Engineering step

Determine GIC due to the given geoelectric field in a conductor system whose topology and resistances are known.

Basic configurations of conductor networks:

- **Continuous contact with the ground (buried pipeline): Distributed source transmission line theory.**

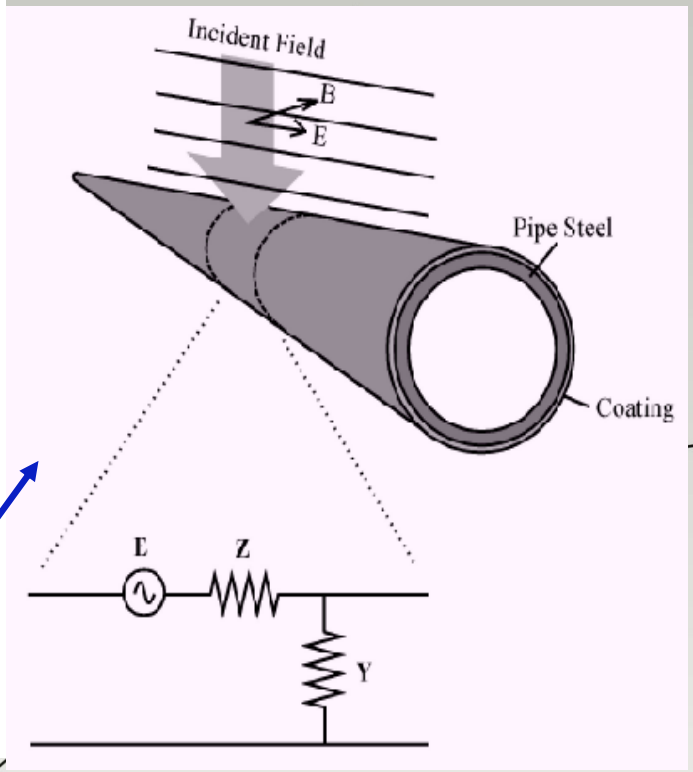

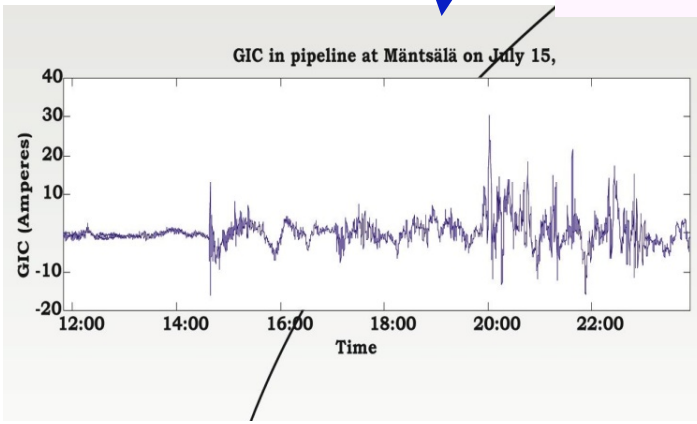

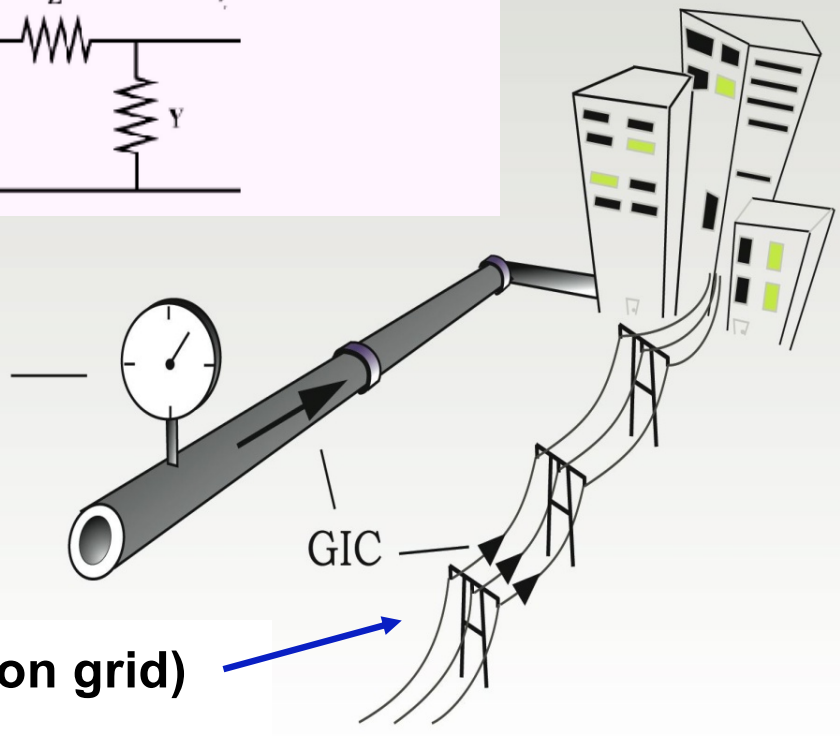

- **Discretely grounded system (power transmission grid)**

Power grid modelling:

- Circuit in DC-current by applying Ohm's and Kirchhoff's laws

- Grid divided in a series of grounded nodes → **Matrix formulation**

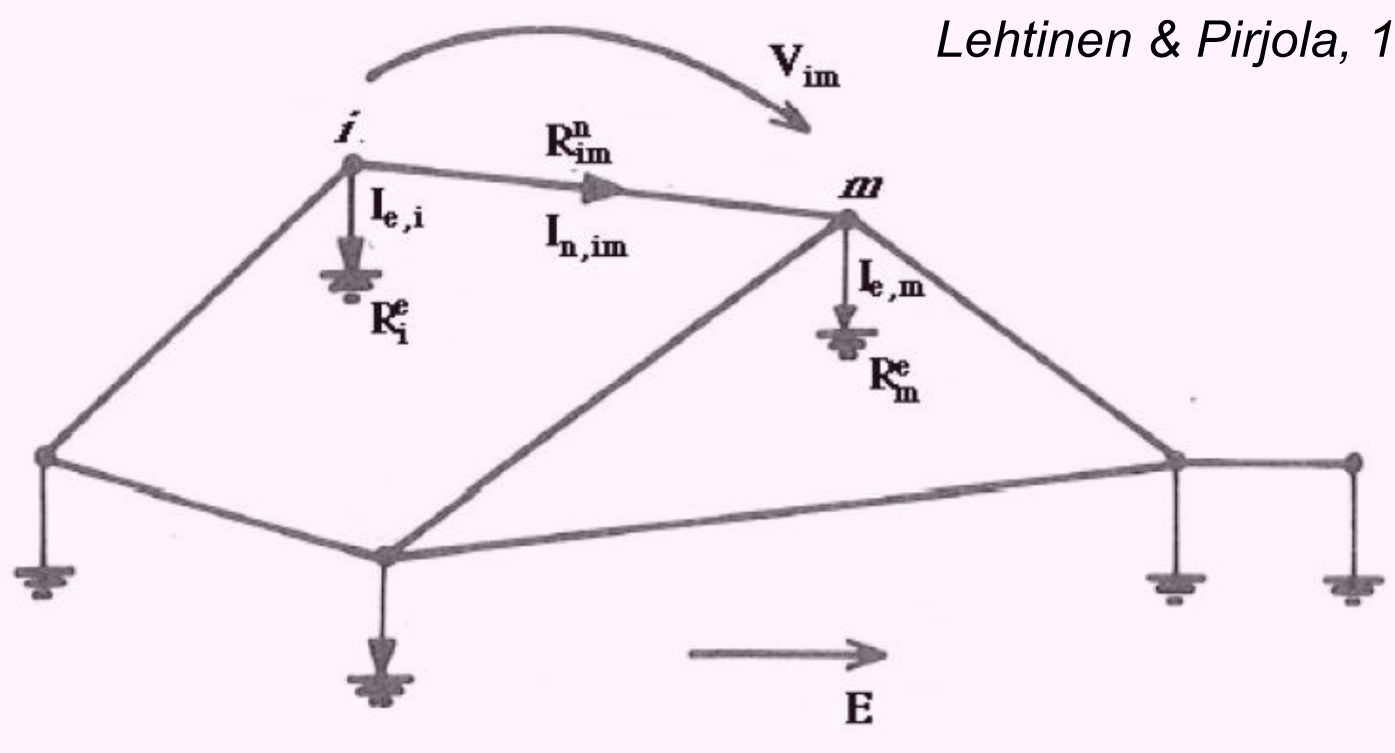

Lehtinen & Pirjola, 1985

GIC flowing into the Earth at each node

$$I_i = -\sum_{j \neq i} \frac{V_{ij}^o}{R_{ij}} - \sum_j Y_{ij}\, U_j^{cor} \quad \Longrightarrow \quad \mathbf{I = (1 + YZ)^{-1}\, J}$$

where: $V_{ij}^o = \int_{L_{ij}} \boldsymbol{E}^o \cdot d\boldsymbol{l}$, $U_j^{cor} = \sum_{i=1}^{m} Z_{ji}\, I_i$

$$Y_{ij} = \begin{Bmatrix} \frac{-1}{R_{ij}}, & i \neq j \\ \sum_{k \neq i} \frac{1}{R_{ik}}, & i = j \end{Bmatrix}, \quad Z_{ij} = \begin{Bmatrix} 0, & i \neq j \\ R_i^e, & i = j \end{Bmatrix}, \quad J_i = \sum_{j \neq i} \frac{V_{ij}^o}{R_{ij}}$$

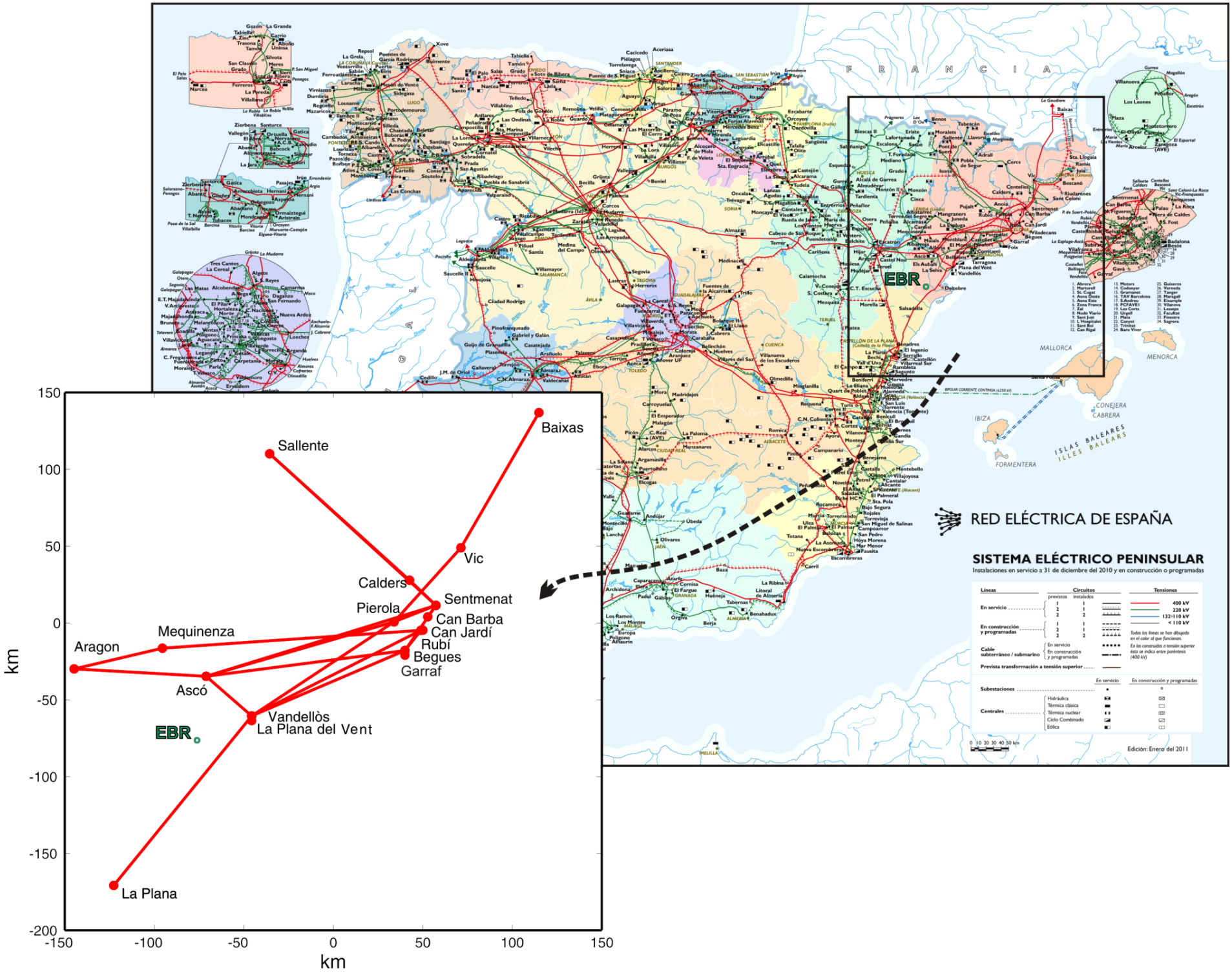
Baixas
Sallente
Vic
Calders
Sentmenat
Pierola
Can Barba
Can Jardí
Rubí
Begues
Garraf
Mequinenza
Aragon
Ascó
Vandellòs
La Plana del Vent
EBR
La Plana
km
km
150
100
50
0
-50
-100
-150
-200
-150
-100
-50
0
50
100
150
EBR
MALLORCA
MENORCA
IBIZA
FORMENTERA
CONEJERA
CABRERA
ISLAS BALEARES
ILLES BALEARS
FRANCIA
RED ELÉCTRICA DE ESPAÑA
SISTEMA ELÉCTRICO PENINSULAR
Instalaciones en servicio a 31 de diciembre del 2010 y en construcción o programadas
Líneas
Circuitos
previstos
instalados
Tensiones
En servicio
En construcción y programadas
Cable subterráneo / submarino
Prevista transformación a tensión superior
400 kV
220 kV
132÷110 kV
< 110 kV
Todos los líneas se han dibujado en el color al que funcionan.
En las construidas a tensión superior ésta se indica entre paréntesis (400 kV)
Subestaciones
Centrales
Hidráulica
Térmica clásica
Térmica nuclear
Ciclo Combinado
Eólica
0 10 20 30 40 50 km
Edición: Enero del 2011

Data used to compute the admittance (Y) and the earthing impedance (Z) matrices for GIC calculation:

· **Geographical positions of each substation and links**

· **Line resistances**

Resistance per unit length, length, no. of conductors/phase and no. of lines

· **Resistances of each substation**

Sum of the transformer resistances with all phases in parallel and any reactor resistance.

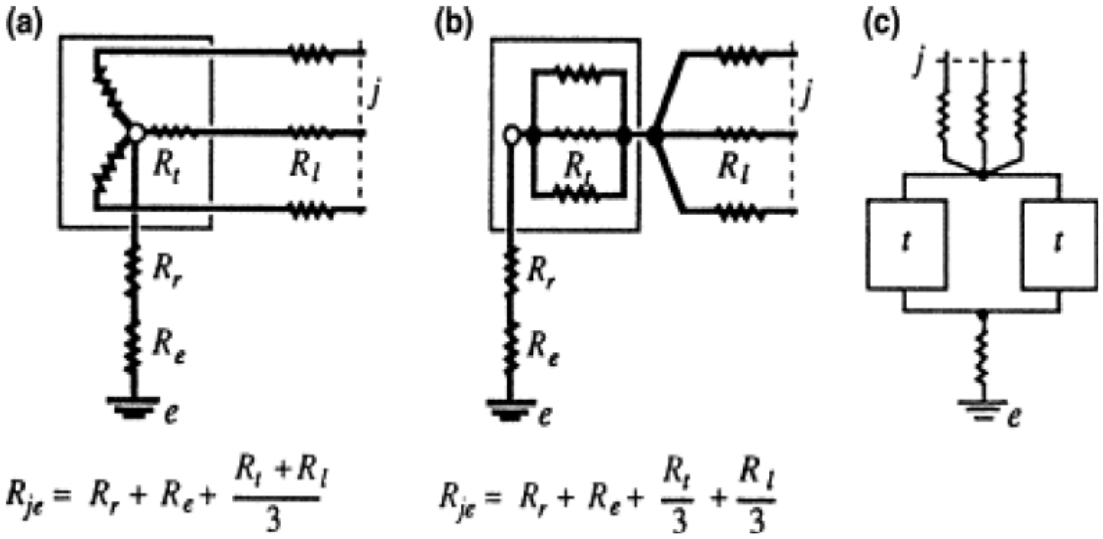

Possible transformer configurations

Transformer at Vandellòs subestation

GIC Modelling

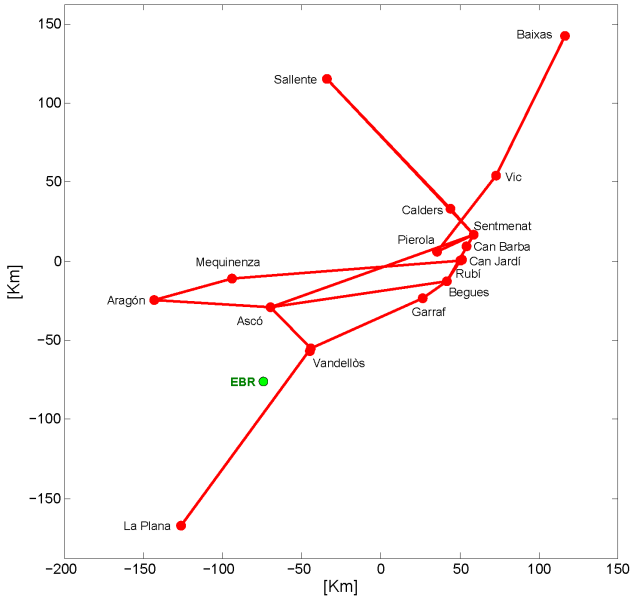

Electric grid model

Grid admittance matrix

Earthing impedance matrix

GIC → $\mathbf{I} = (1 + \mathbf{YZ})^{-1}\,\mathbf{J}$

Contains information of the source:

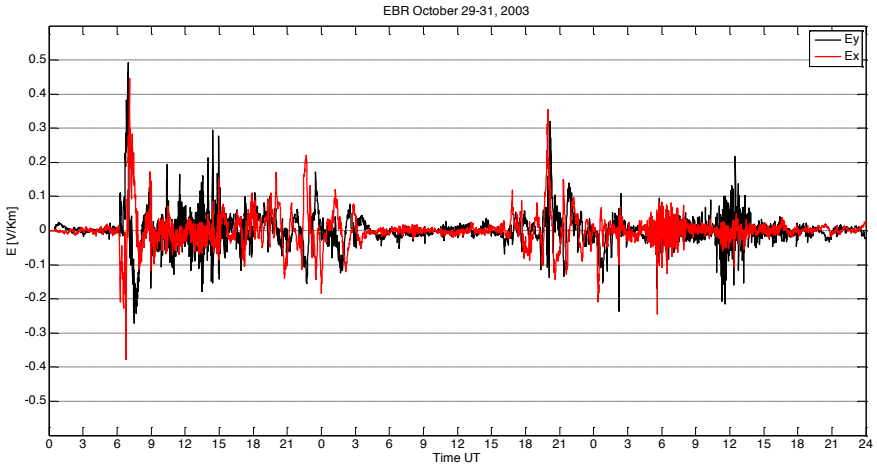

Electric field from Ebro Observatory magnetograms

Combining the Geophysical and Engineering Steps:

1) CALCULATION OF GIC's IN EACH NODE

When the electric field associated with the geomagnetic variations is considered spatially constant in the region of analysis, once it is known and the matrix elements of network impedances resolved, the calculation of GIC's is straightforward:

$$I_{GIC}(t) = aE_x(t) + bE_y(t)$$

where a and b are constant parameters [A km / V] for each node, which depend on the geometry and the resistances of the network. They are obtained by applying fields of 1 V / km in the N and E directions, respectively.

Station	*a*	*b*
ASCÓ	2.87	-81.14
BEGUES	-9.07	59.57
CALDERS	12.46	26.22
CAN BARBA	-16.62	51.81
CAN JARDÍ	12.80	44.85
GARRAF	-11.29	26.02
MEQUINENZA	6.86	-26.76
PIEROLA	-45.60	-22.79
PLANA DEL VENT	-31.78	4.54
RUBÍ	19.33	64.96
SALLENTE	83.90	-63.63
SENTMENAT	9.52	102.88
VANDELLÒS	-25.57	7.14
VIC	-8.45	2.22

Constants for end of October, 2011

2) CALCULATION OF GIC's IN EACH TRANSFORMER

The total GIC flowing in the node is shared among their neutrals. The constants a_T and b_T are derived from the constants a and b using the corresponding current divider:

$$I_{GIC}(t) = a_T E_x(t) + b_T E_y(t)$$

GICs depend on the length and geometry of the lines that converge at that node with respect to the direction of the incident field and, in turn, on the number and resistance of transformers.

Results published at:

Torta et al. (2012): Geomagnetically induced currents in a power grid of northeastern Spain, ***Space Weather***, **10**, S06002, doi:10.1029/2012SW000793

Station	Number of trafos	Transformer	a	b	a_T	b_T
ASCÓ	3	TG1	2.87	-81.14	1.22	-34.51
		TG2			1.22	-34.51
		TR3			0.43	-12.12
BEGUES	2	ATR3	-9.07	59.57	-4.53	29.78
		ATR4			-4.53	29.78
CALDERS	1	TR1	12.46	26.22	12.46	26.22
CAN BARBA	2	TR6	-16.62	51.81	-8.31	25.91
		TR7			-8.31	25.91
CAN JARDÍ	1	ATR4	12.80	44.85	12.80	44.85
GARRAF	1	TR1	-11.29	26.02	-11.29	26.02
MEQUINENZA	1	ATR2	6.86	-26.76	6.86	-26.76
PIEROLA	2	TR1	-45.60	-22.79	-22.61	-11.30
		ATR4			-22.99	-11.49
PLANA DEL VENT	2	TG1	-31.78	4.54	-15.89	2.27
		TG2			-15.89	2.27
RUBÍ	2	ATR7	19.33	64.96	10.20	34.29
		ATR8			9.13	30.67
SALLENTE	4	TG1	83.90	-63.63	21.54	-16.34
		TG2			21.20	-16.08
		TG3			20.63	-15.65
		TG4			20.52	-15.57
SENTMENAT	3	ATR2	9.52	102.88	3.12	33.72
		ATR3			3.34	36.07
		ATR4			3.06	33.09
VANDELLÒS	3	TR1	-25.57	7.14	-5.76	1.61
		TR2			-6.92	1.93
		TG1			-12.89	3.60
VIC	4	ATR1	-8.45	2.22	-1.01	0.27
		ATR2			-1.25	0.33
		ATR3			-1.25	0.33
		ATR4			-4.95	1.30

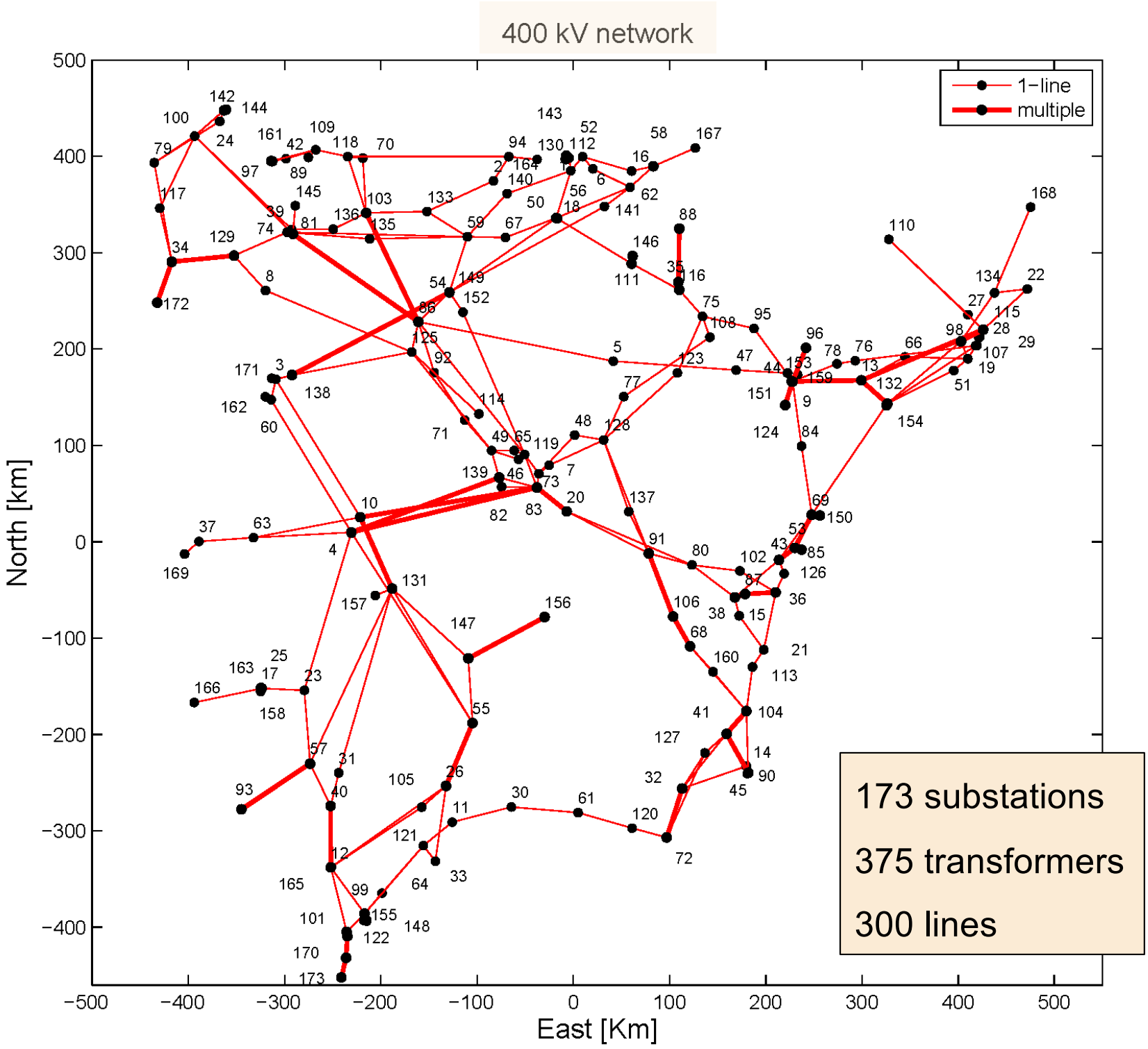
400 kV network
1−line
multiple
North [km]
East [Km]
500
400
300
200
100
0
−100
−200
−300
−400
−500
173 substations
375 transformers
300 lines

PREDICTION OF GIC'S IN THE NETWORK NODES/ TRANSFORMERS

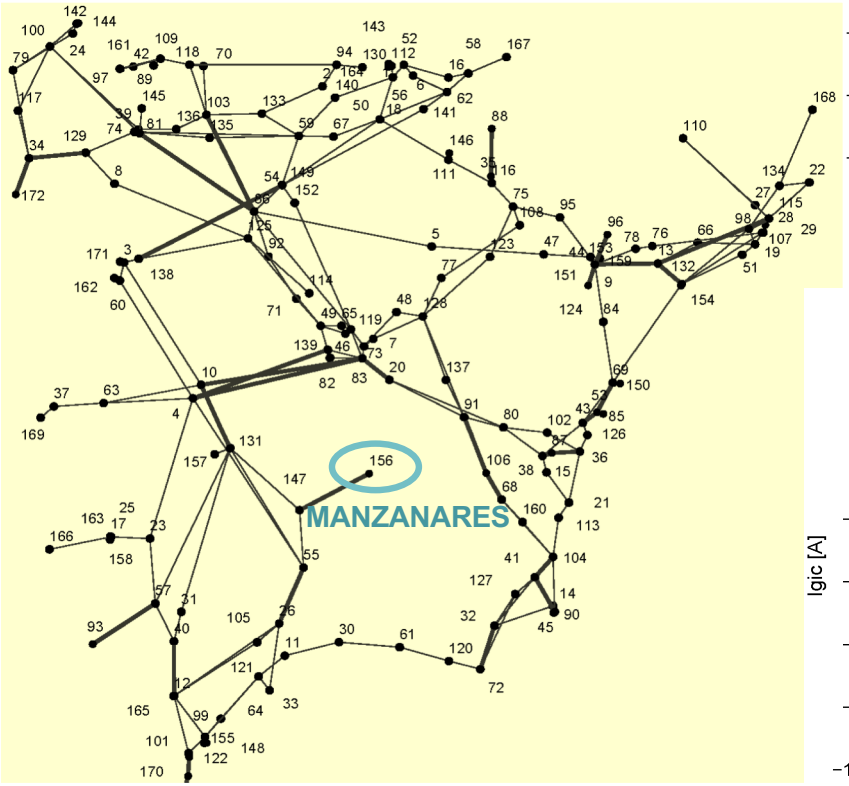

29-31 October 2003 (Halloween storm)

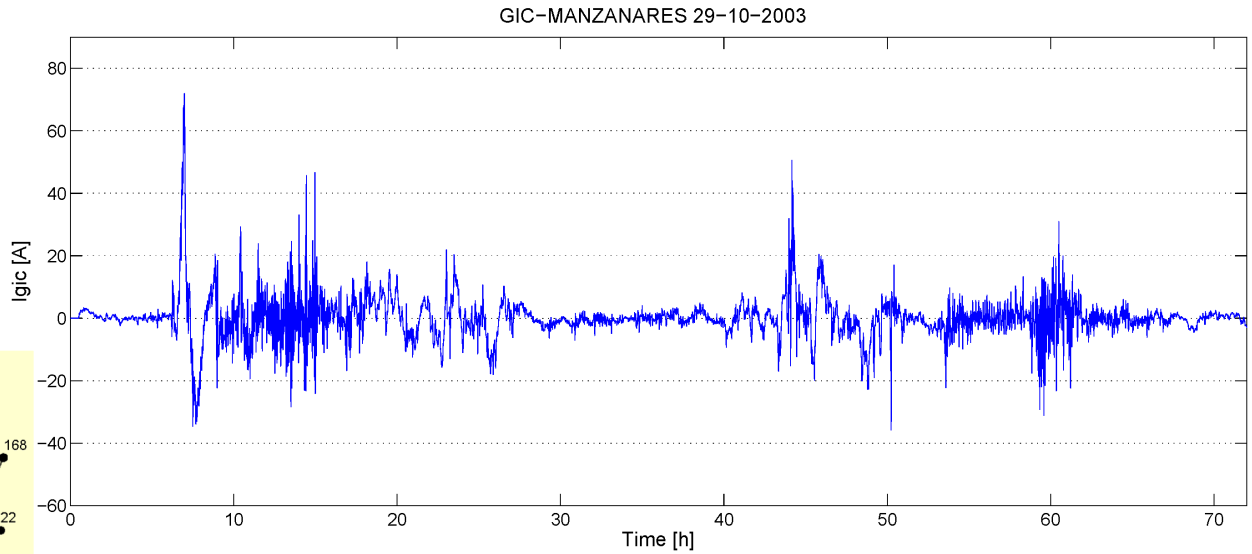

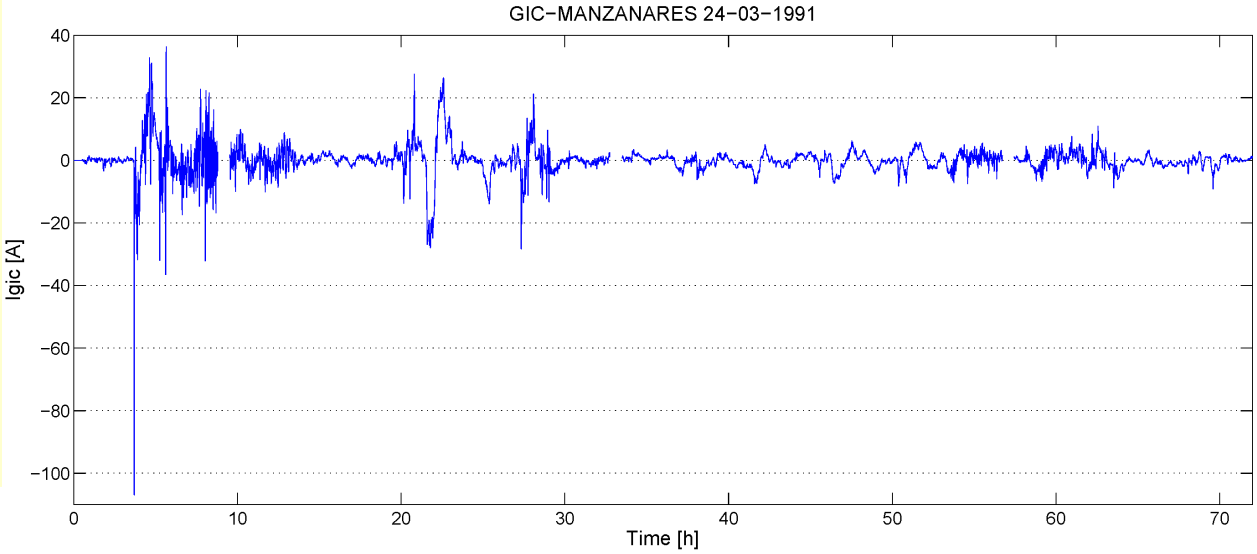

24-26 March 1991 (the most abrut SSC)

According to the current network configuration and all elements in operation

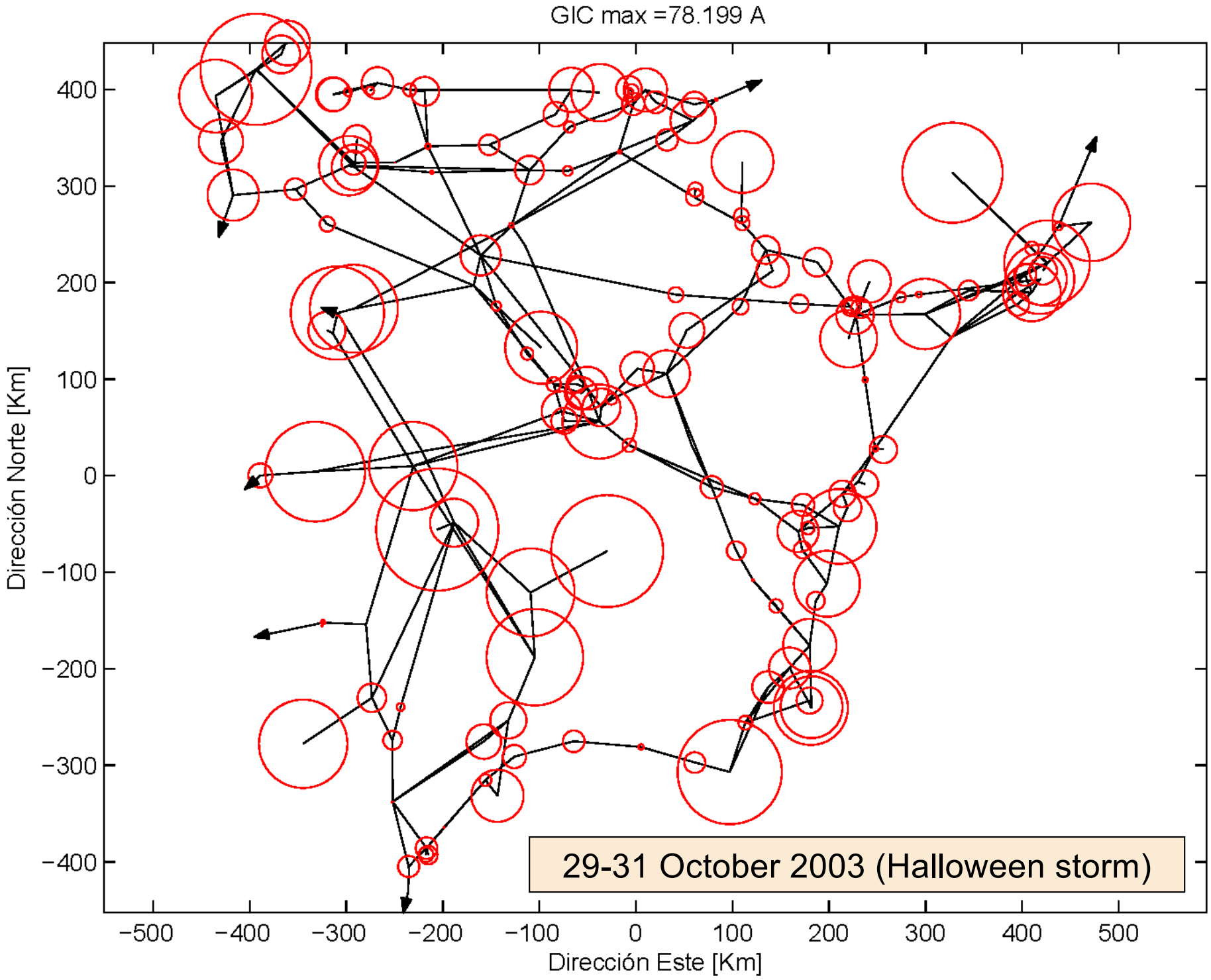
GIC max =78.199 A
Dirección Norte [Km]
Dirección Este [Km]
400
300
200
100
0
−100
−200
−300
−400
−500
−400
−300
−200
−100
0
100
200
300
400
500
29-31 October 2003 (Halloween storm)

Next step: extreme value statistics

SPACE WEATHER, VOL. 9, S10001, doi:10.1029/2011SW000696, 2011

Quantifying extreme behavior in geomagnetic activity

Alan W. P. Thomson,[1] Ewan B. Dawson,[1] and Sarah J. Reay[1]

SPACE WEATHER, VOL. 10, S02012, doi:10.1029/2011SW000734, 2012

On the probability of occurrence of extreme space weather events

Pete Riley[1]

Received 16 September 2011; revised 18 November 2011; accepted 22 December 2011; published 23 February 2012.

[1] By virtue of their rarity, extreme space weather events, such as the Carrington event of 1859, are difficult to study, their rates of occurrence are difficult to estimate, and prediction of a specific future event is virtually impossible. Additionally, events may be extreme relative to one parameter but normal relative to others. In this study, we analyze several measures of the severity of space weather events

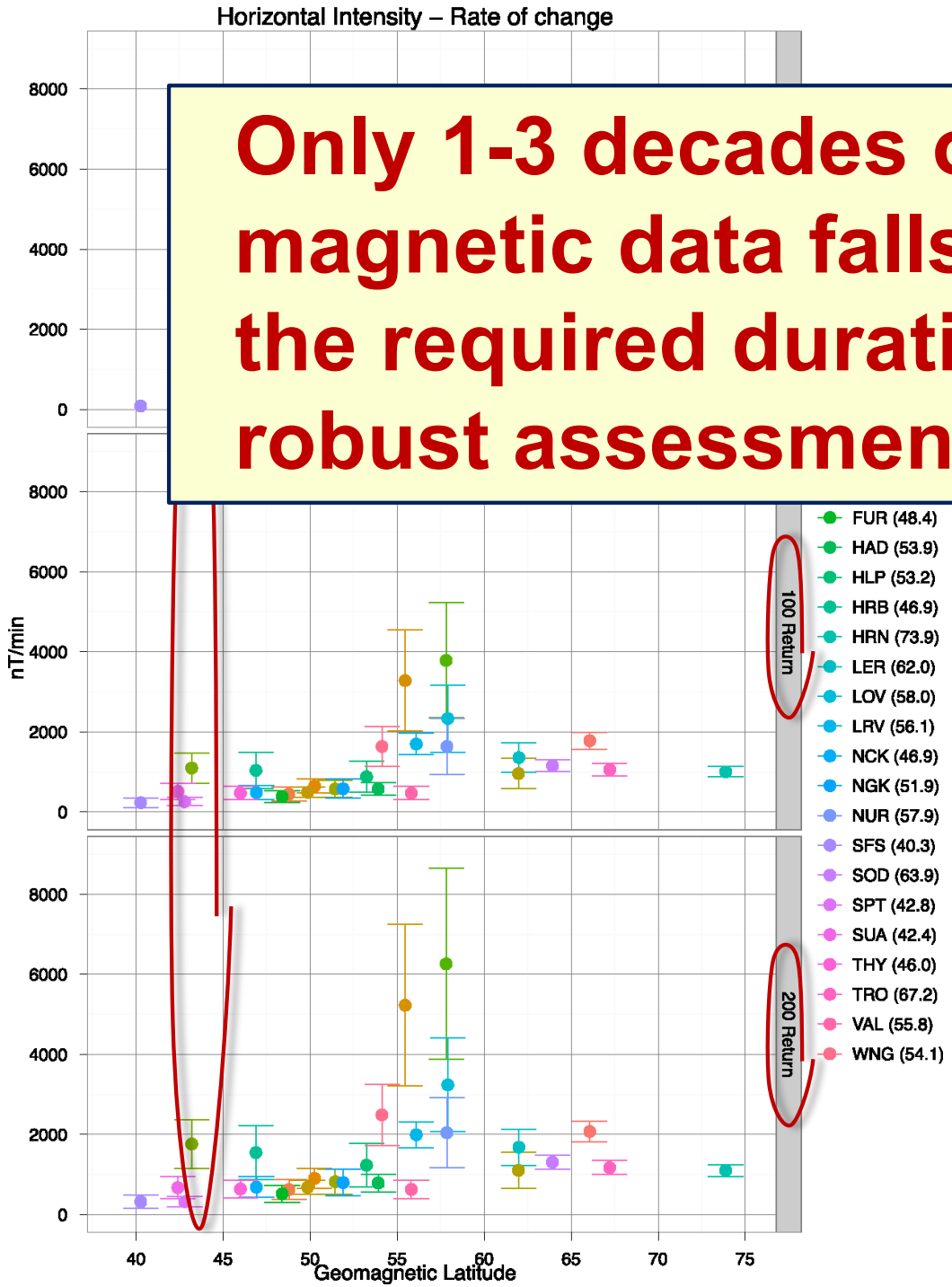

Only 1-3 decades of digital magnetic data falls far short of the required duration to provide robust assessments!!

The measured maximum and estimated 100-year and 200-year return levels, for the residual horizontal intensity, with respect to the observatory geomagnetic latitude, with their 95% confidence limits. From *Thomson et al. (2011).*

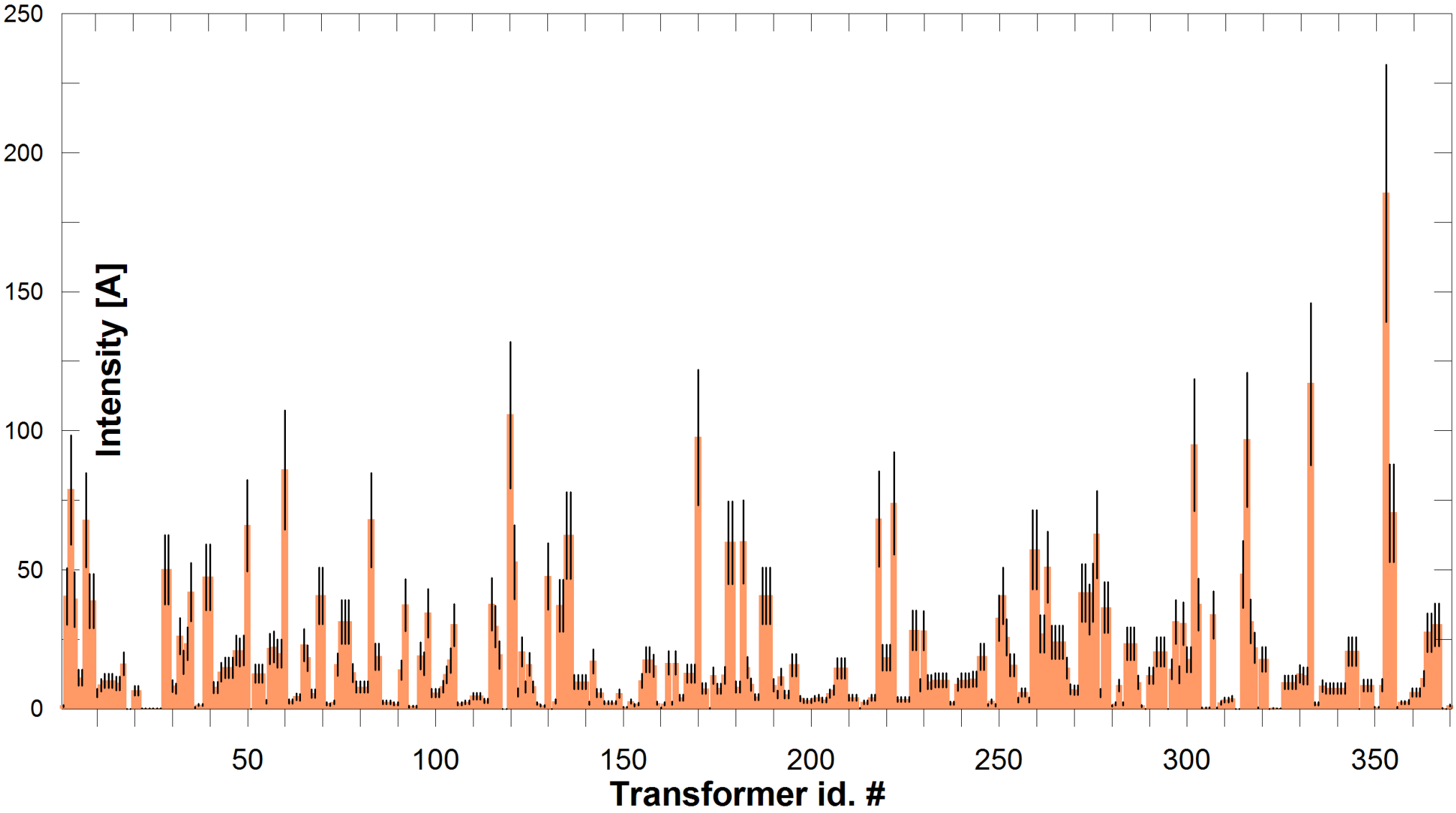

The maximum GICs in each transformer as a consequence of an extreme geomagnetic storm scenario for a return period of 100 years, from our network model and the results of Thomson et al. (2012) for EBR and assuming an impulsive event along the geomagnetic North. Vertical black lines indicate the 95% confidence levels.

Torta et al. Earth, Planets and Space 2014, 66:87
http://www.earth-planets-space.com/content/66/1/87

Earth, Planets and Space
a SpringerOpen Journal

FULL PAPER Open Access

Assessing the hazard from geomagnetically induced currents to the entire high-voltage power network in Spain

Joan Miquel Torta[1*], Santiago Marsal[1] and Marta Quintana[2]

Abstract

After the good results obtained from an assessment of geomagnetically induced currents (GICs) in a relatively small subset of the Spanish power transmission network, we now present the first attempt to assess vulnerability across the entire Spanish system. At this stage, we have only included the power grid at the voltage level of 400 kV, which contains 173 substations along with their corresponding single or multiple transformers and almost 300 transmission lines; this type of analysis could be extended to include the 220-kV grid, and even the 110-kV lines, if more detailed information becomes available. The geoelectric field that drives the GICs can be derived with the assumption of plane wave geomagnetic variations and a homogeneous or layered conductivity structure. To assess the maximum expected GICs in each transformer as a consequence of extreme geomagnetic storms, a post-event analysis of data from the Ebre Geomagnetic Observatory (EBR) during the 2003 Halloween storm was performed, although other episodes coincident with very abrupt storm onsets, which have proven to be more hazardous at these mid-latitudes, were analyzed as well. Preferred geomagnetic/geoelectric field directions in which the maximum GICs occur are automatically given from the grid model. In addition, EBR digital geomagnetic data were used to infer statistical occurrence probability values and derive the GIC risk at 100-year or 200-year return period

GIC Monitoring

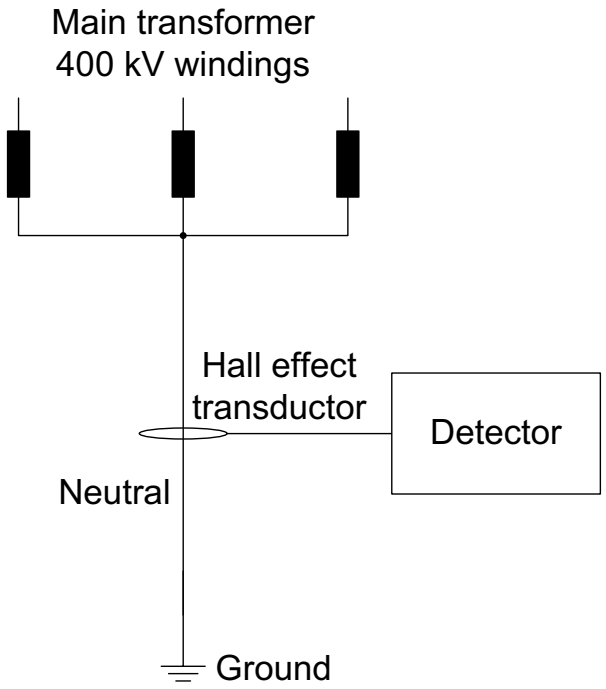

- System based in a Hall effect transducer.

- The 50-Hz signal and its harmonics are also monitored to evaluate the degree of saturation of the 400 kV transformers.

- Current and temperature data are digitized and saved by means of a real-time acquisition system. The data is transferred using an UMTS connection or a satellite modem.

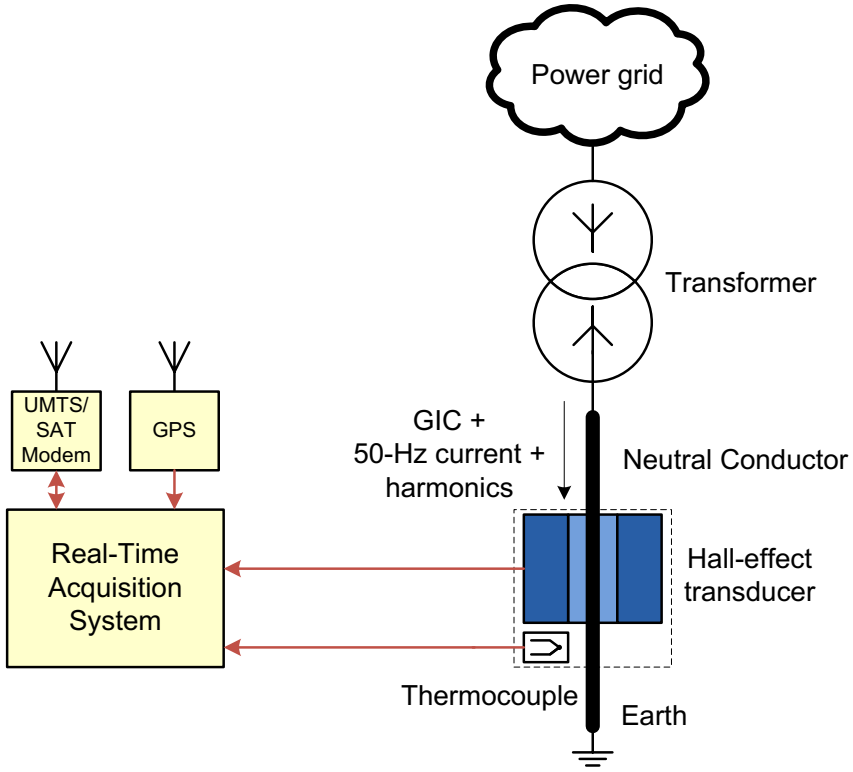

GIC Monitoring

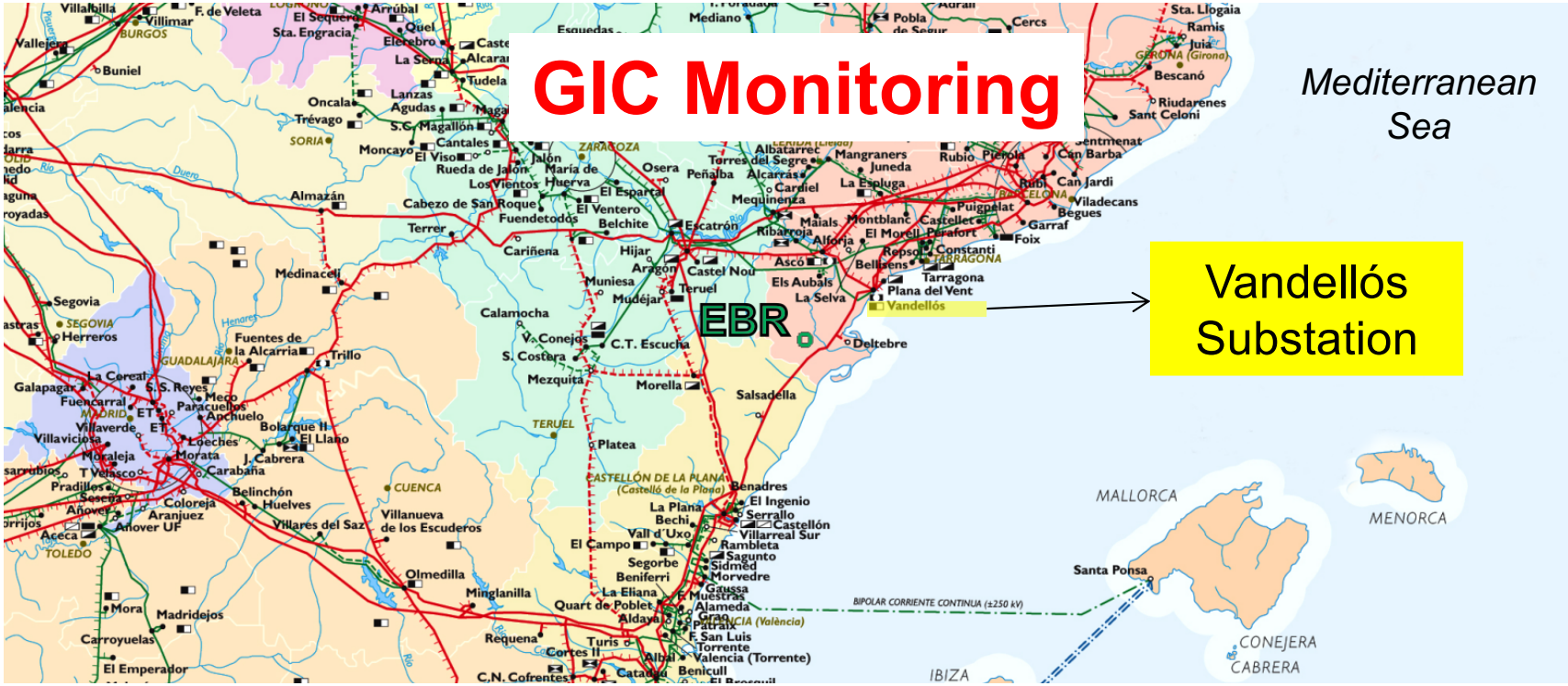

Measuring system

Neutral

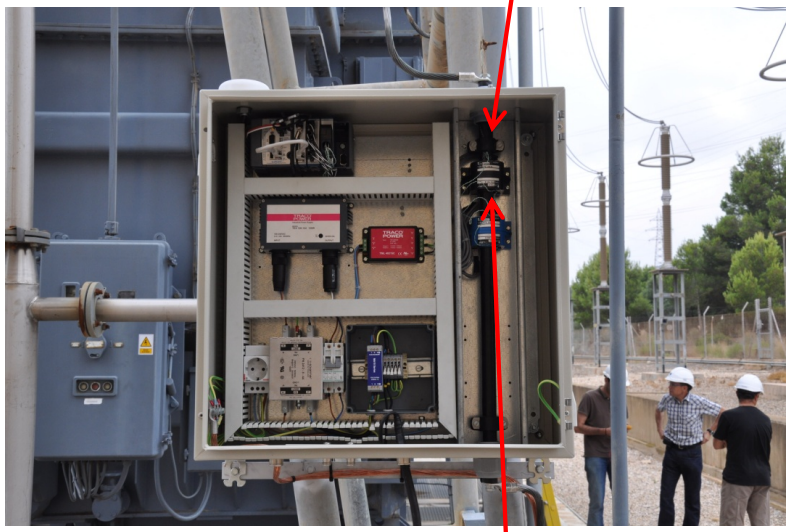

Measuring sensors

Model validation with real measurements

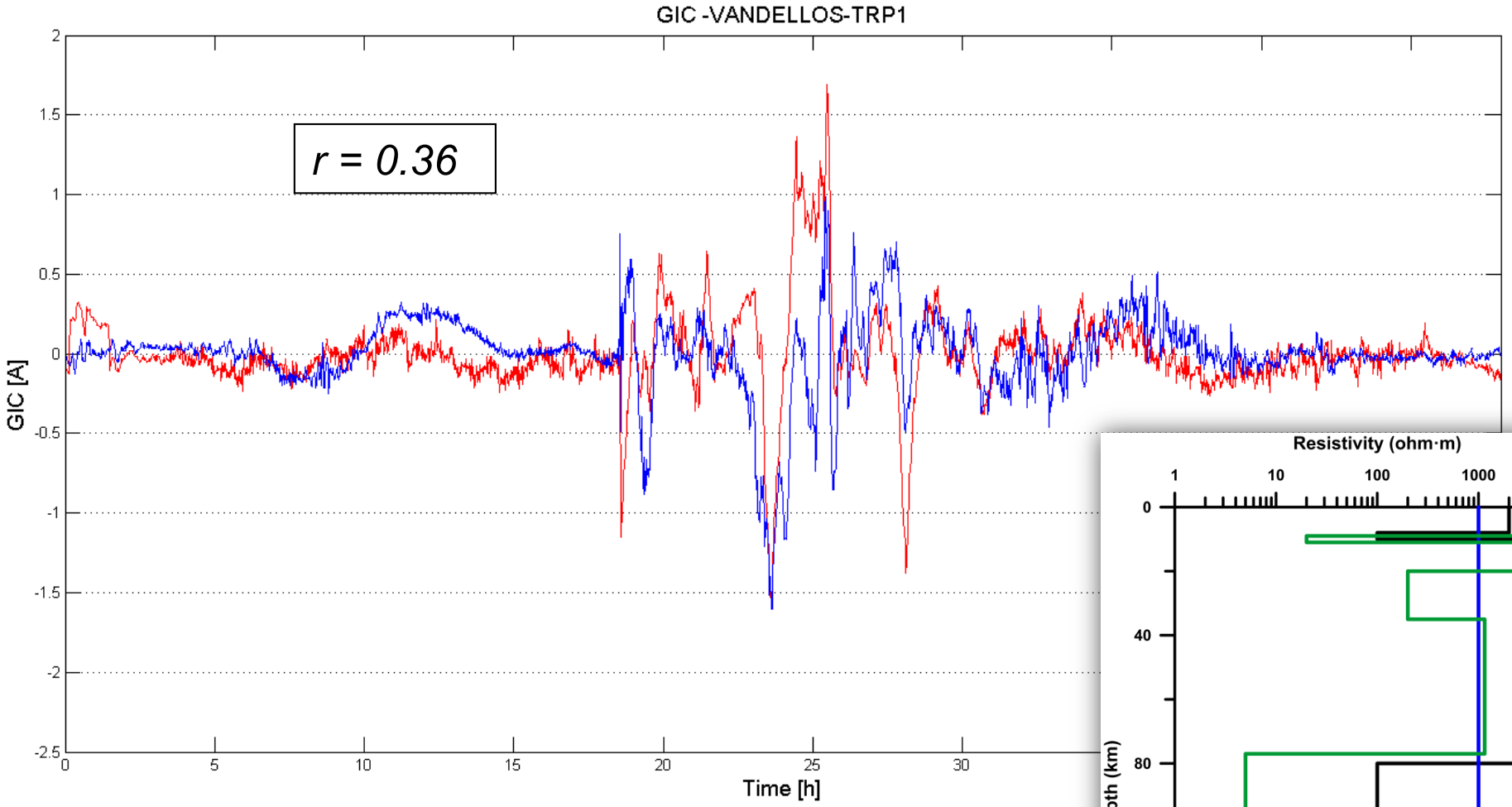

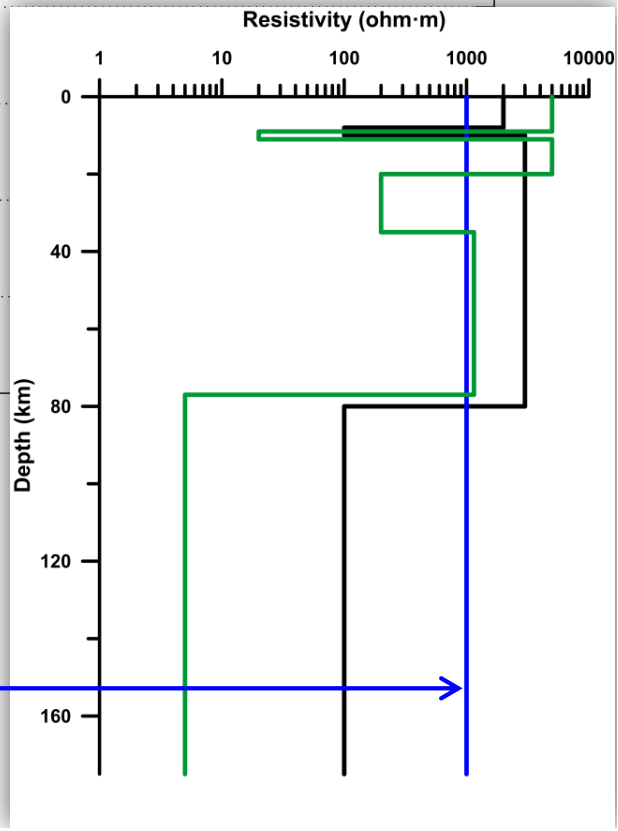

Measured (red) and calculated GIC at the TRP1 transformer of Vandellòs for 24–25 October 2011

Uniform Earth

Non uniform Earth: 1-D layered structure

$$E_{x,y}(\omega) = \pm \frac{Z(\omega) B_{y,x}(\omega)}{\mu_0}$$

$Z(\omega)$ **Surface impedance**

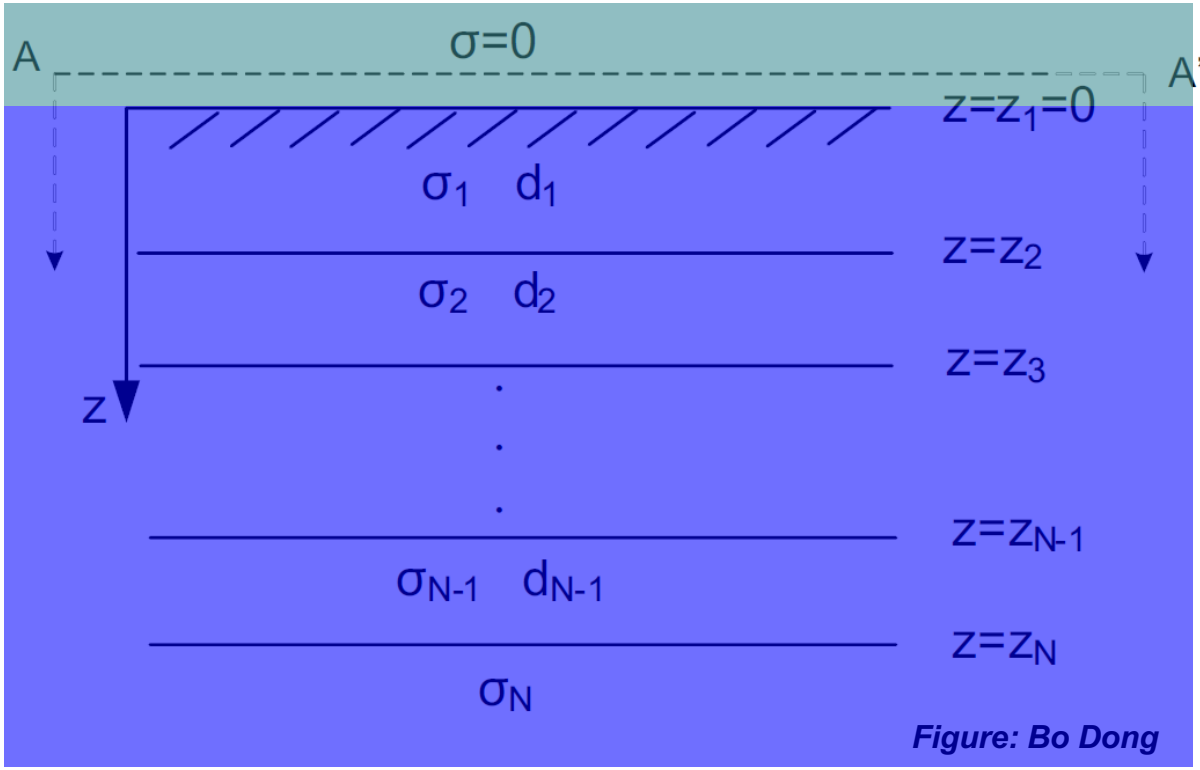

Figure: Bo Dong

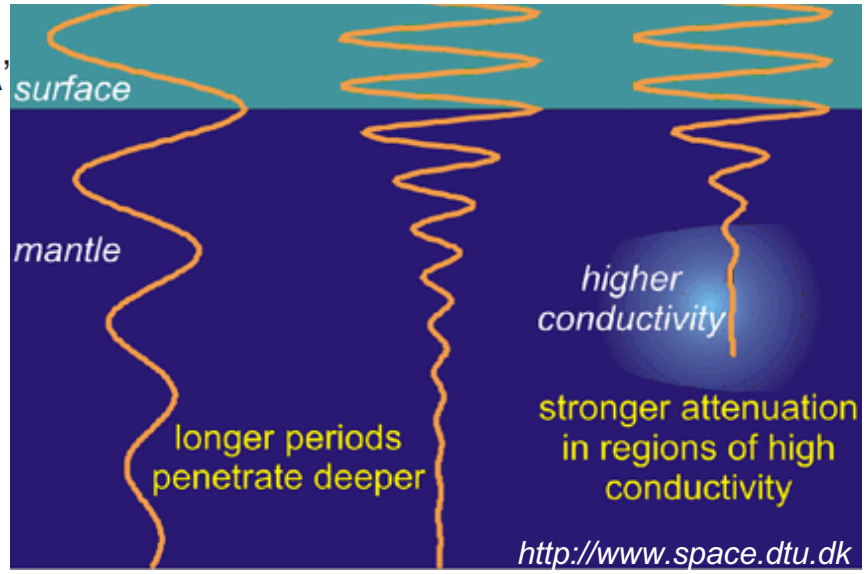

Skin depth $p(\omega) = \frac{Z(\omega)}{i\omega\mu_0}$

$$Z_N = \frac{i\omega\mu_0}{\gamma_N} \coth\left(\gamma_N d_N + \coth^{-1}\left(\frac{\gamma_N}{i\omega\mu_0} Z_{N+1}\right)\right)$$

$$\gamma_N = \sqrt{i\omega\mu_0\sigma_n}$$

Model validation with real measurements

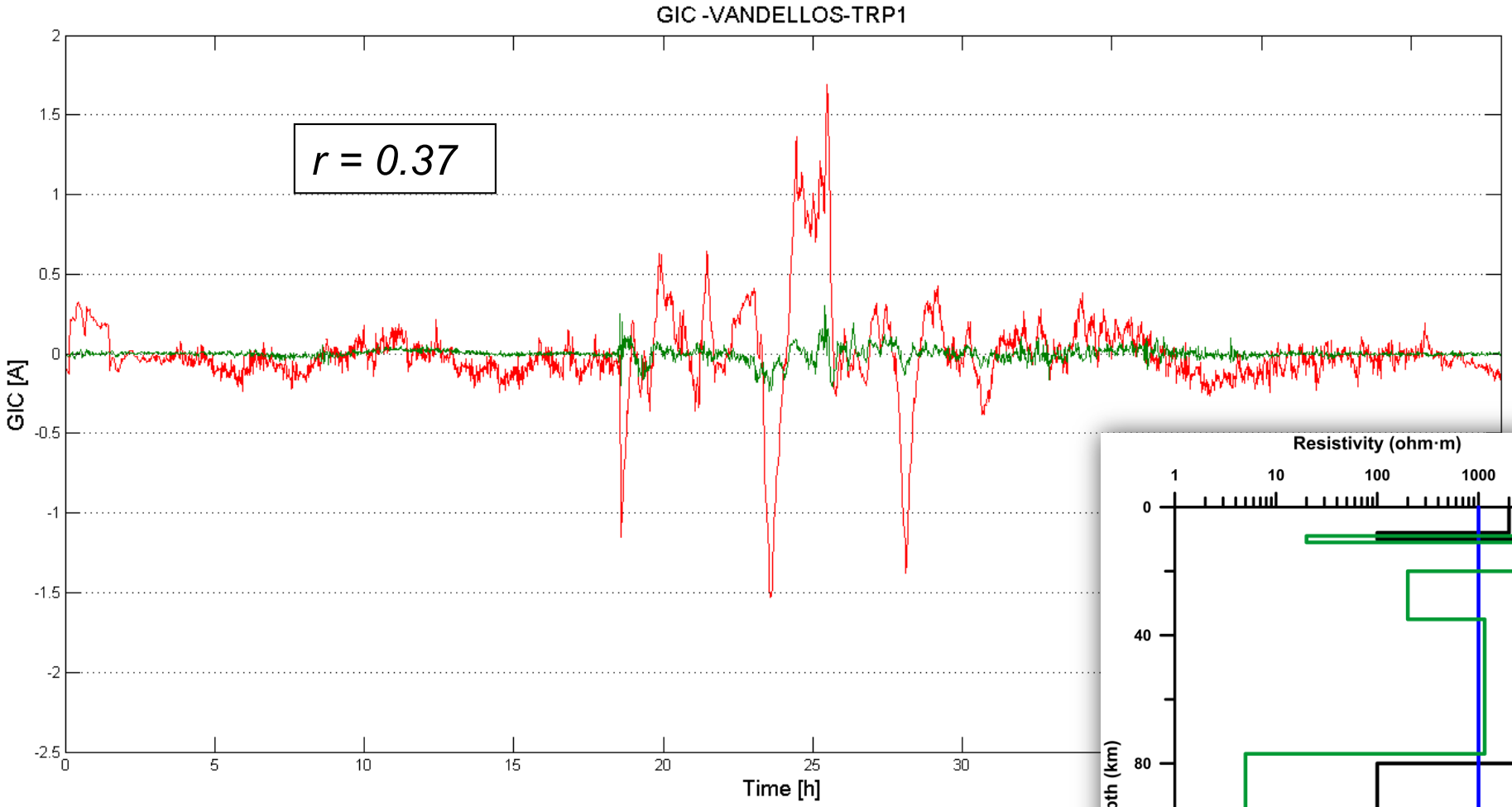

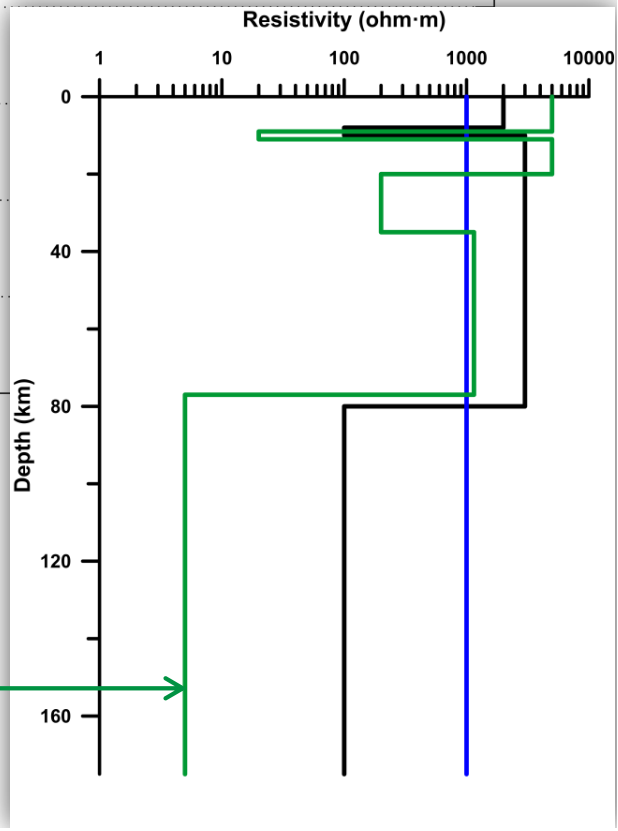

Measured (red) and calculated GIC at the TRP1 transformer of Vandellòs for 24–25 October 2011

Layered Earth

Model validation with real measurements

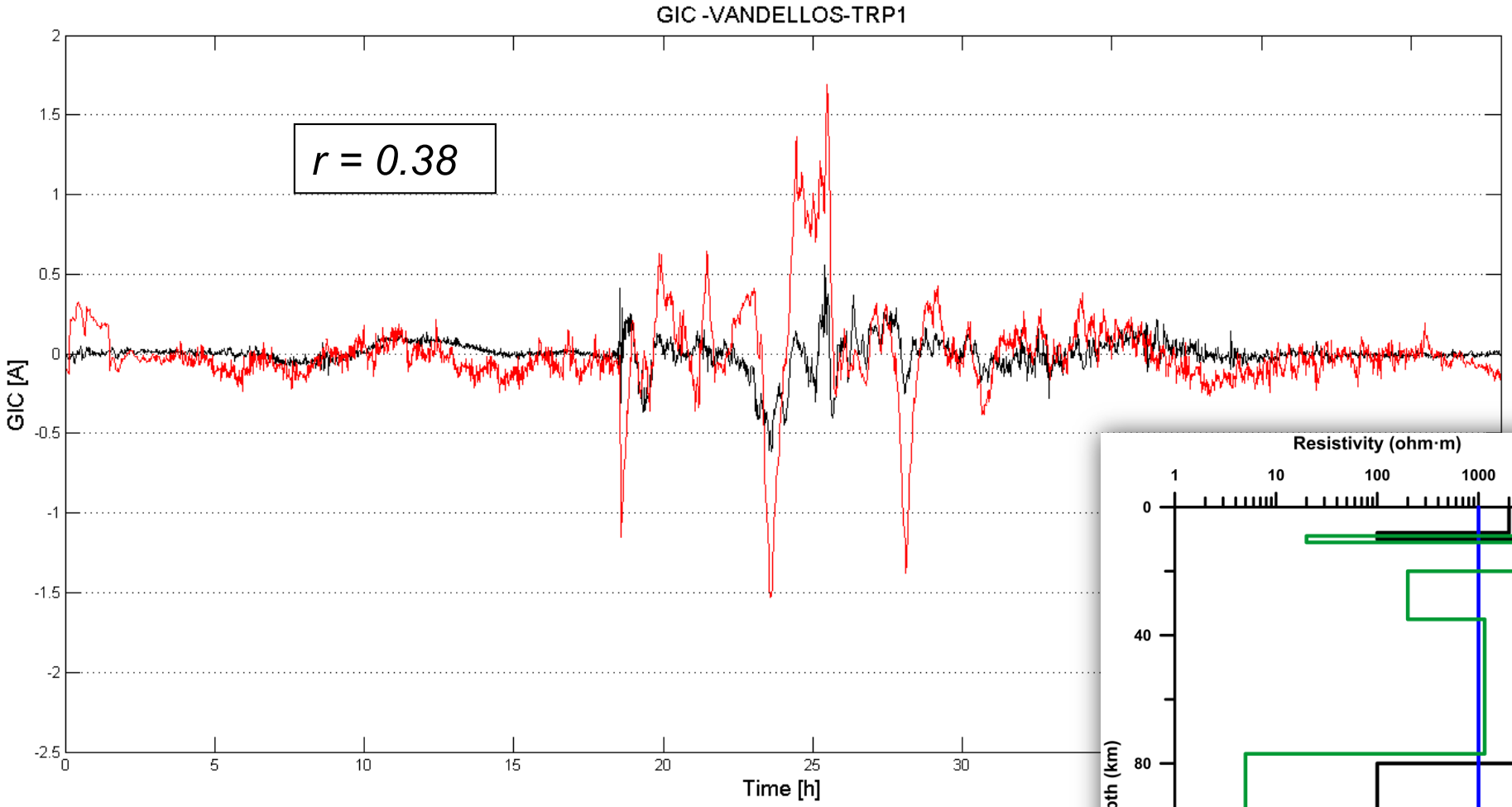

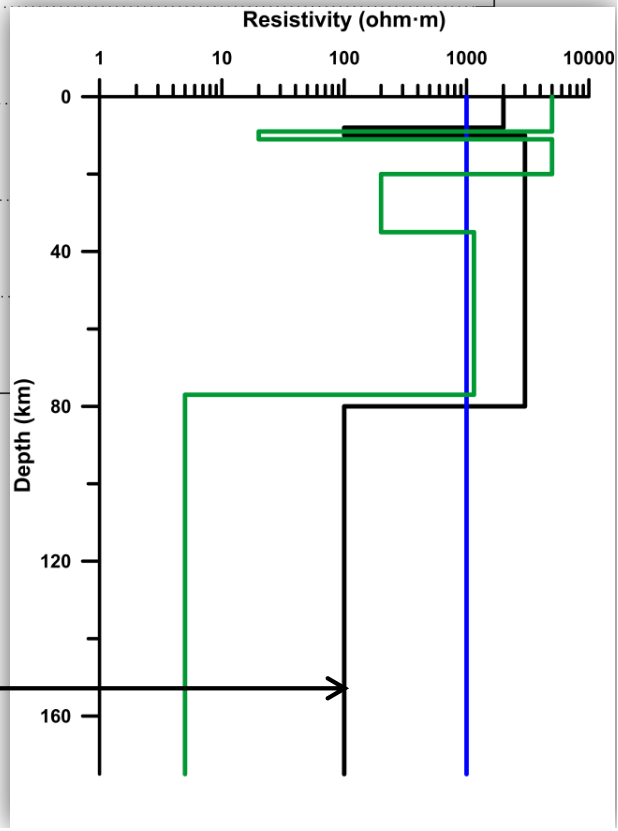

Measured (red) and calculated GIC at the TRP1 transformer of Vandellòs for 24–25 October 2011

Layered Earth

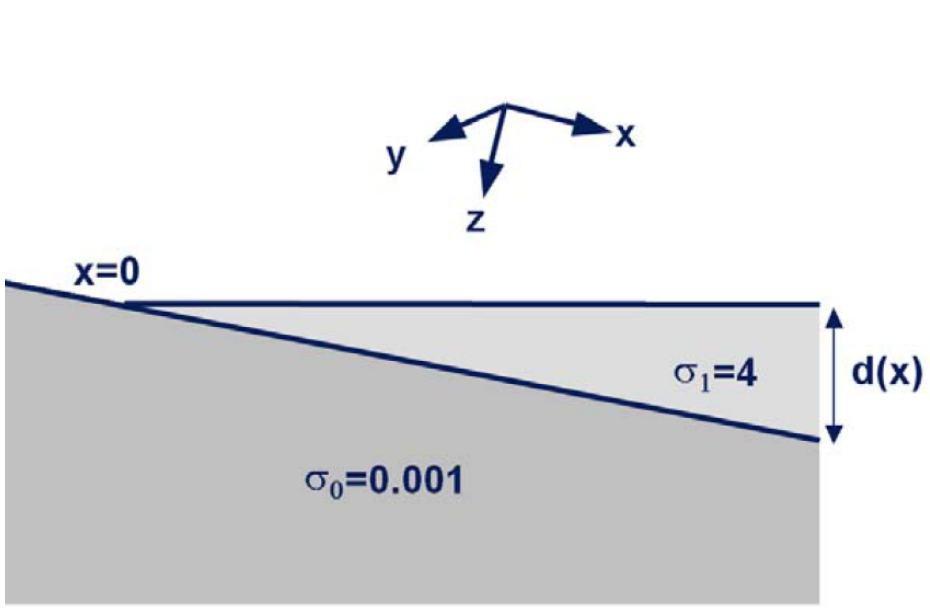

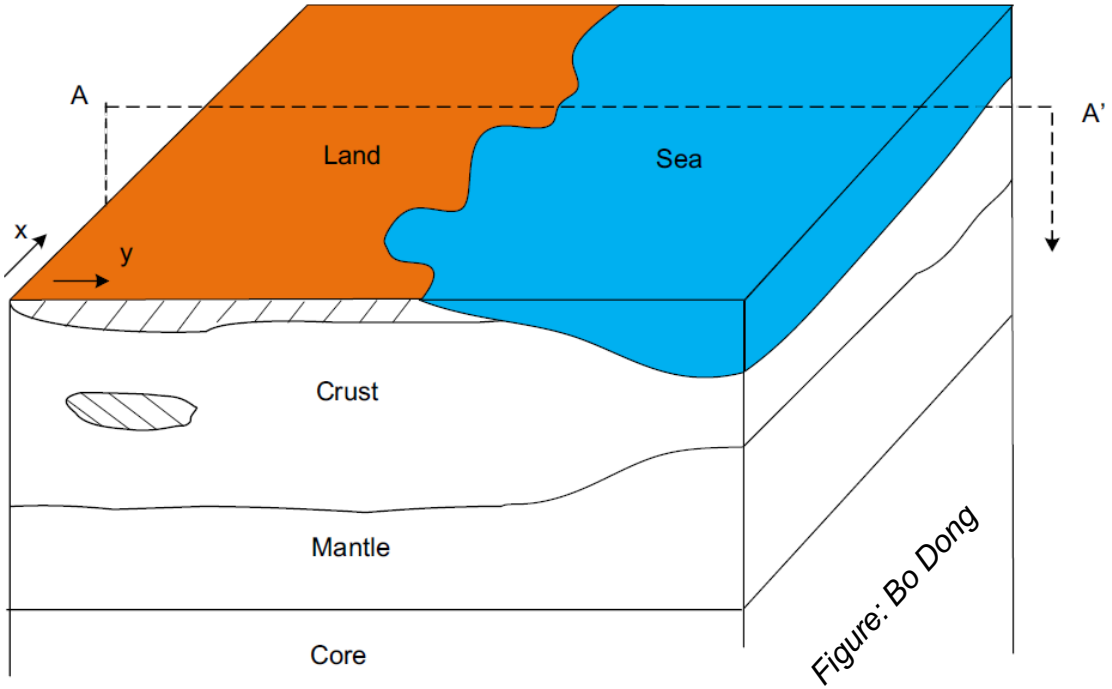

Figure: Bo Dong

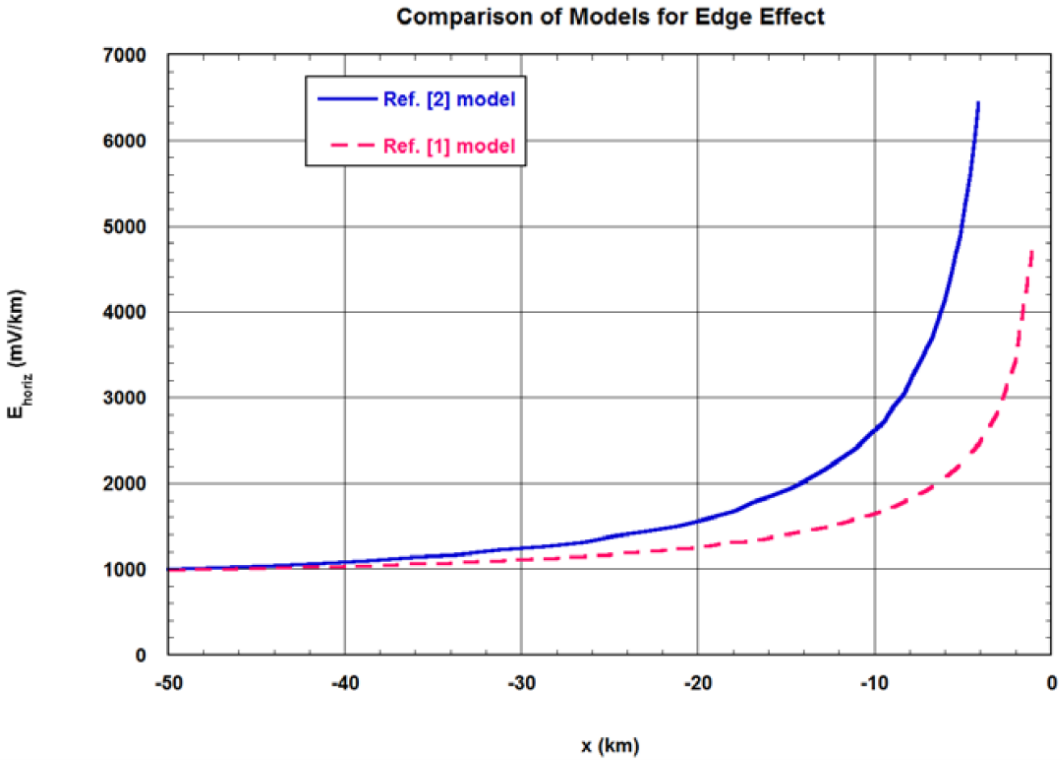

From J.L. Gilbert (2014)

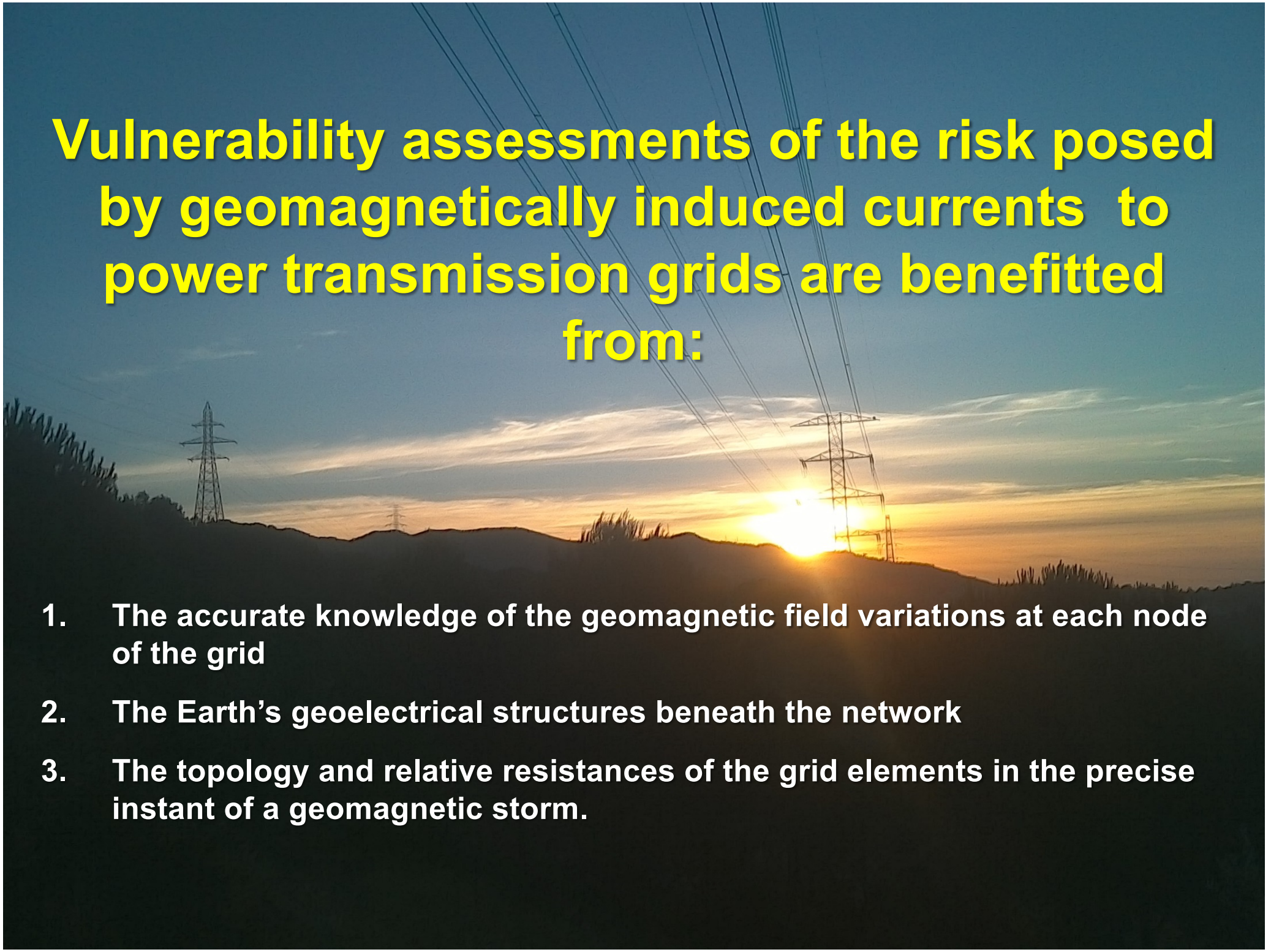

Vulnerability assessments of the risk posed by geomagnetically induced currents to power transmission grids are benefitted from:

1. The accurate knowledge of the geomagnetic field variations at each node of the grid
2. The Earth's geoelectrical structures beneath the network
3. The topology and relative resistances of the grid elements in the precise instant of a geomagnetic storm.

Geomagnetic variations interpolated from the records of several observatories with the SECS technique

- Spherical Elementary Current Systems (SECS) is an equivalent source method that models the observed ground magnetic variations in terms of their current sources, which are assumed to flow on a current sheet at the ionosphere.

-The current source is constructed from the superposition of divergence-free elementary currents flowing concentrically around the knots of a pre-defined grid.

- Amplitudes of the elementary current systems are determined by inversion of the magnetic data. The system to be solved is (**T**: transfer matrix):

$$\mathbf{B} = \mathbf{T} \cdot \mathbf{I}$$

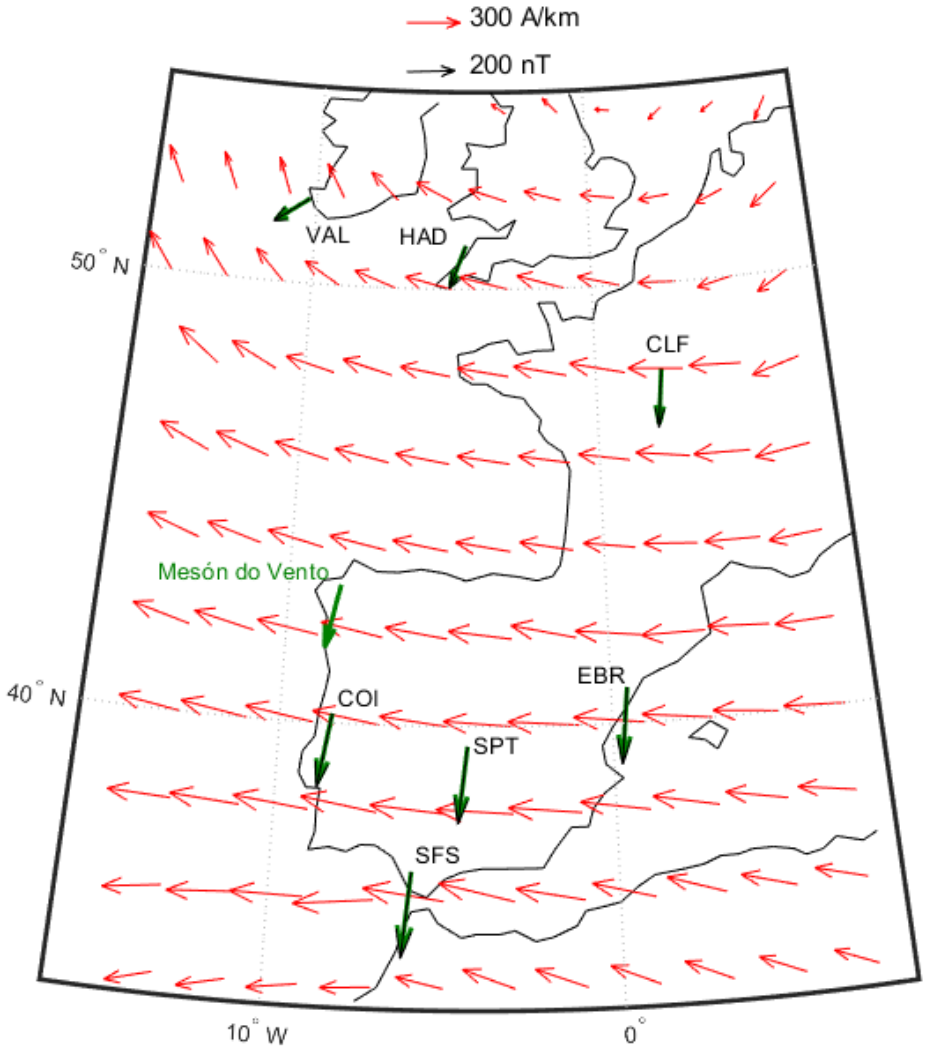

Instant of maximum disturbance during the 2015 Saint Patrick's Day storm

At mid-latitudes the source field is rather uniform and the effect of its spatial changes is not important

Any interpolation method is valid, even that of using the nearest geomagnetic observatory

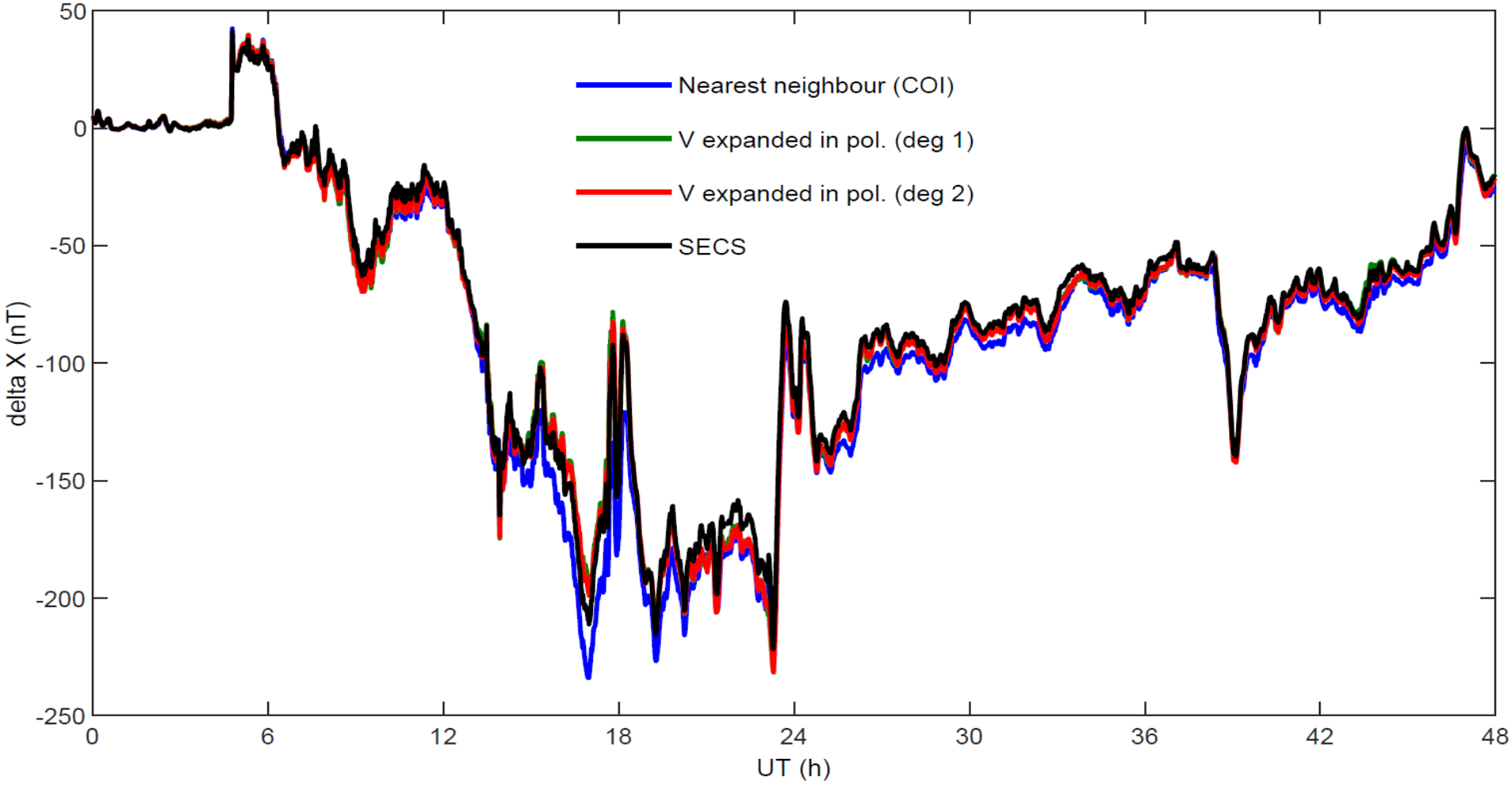

Knowledge of the geoelectrical structure → magnetotellurics

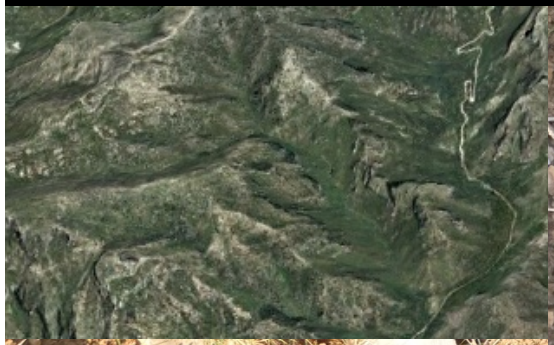

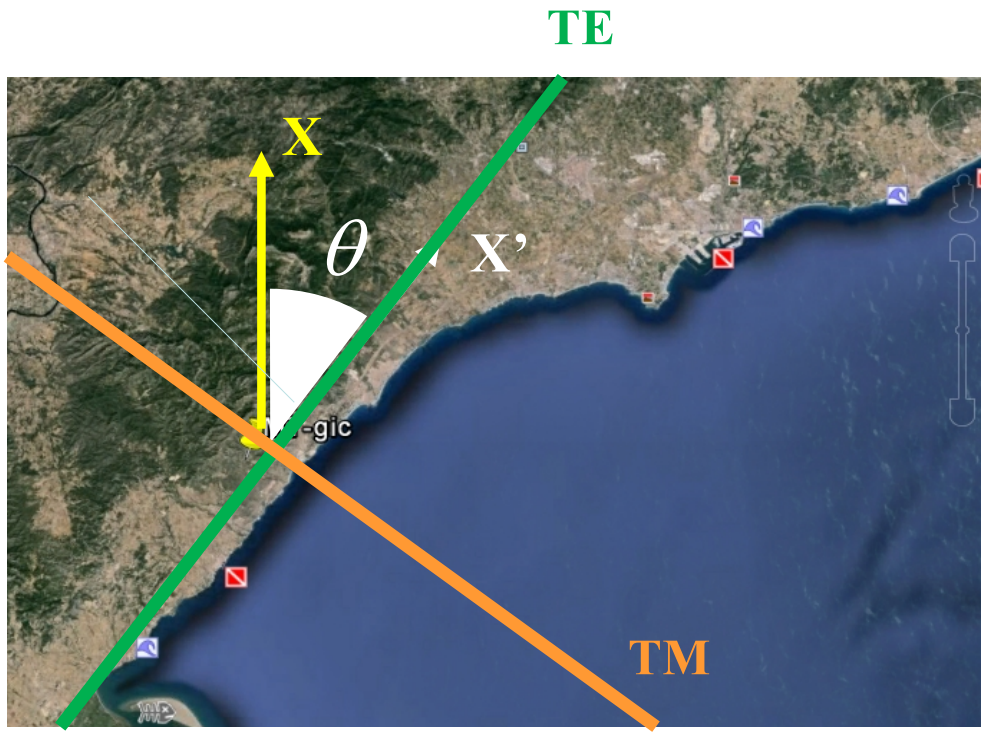
TE
X
θ
X'
TM

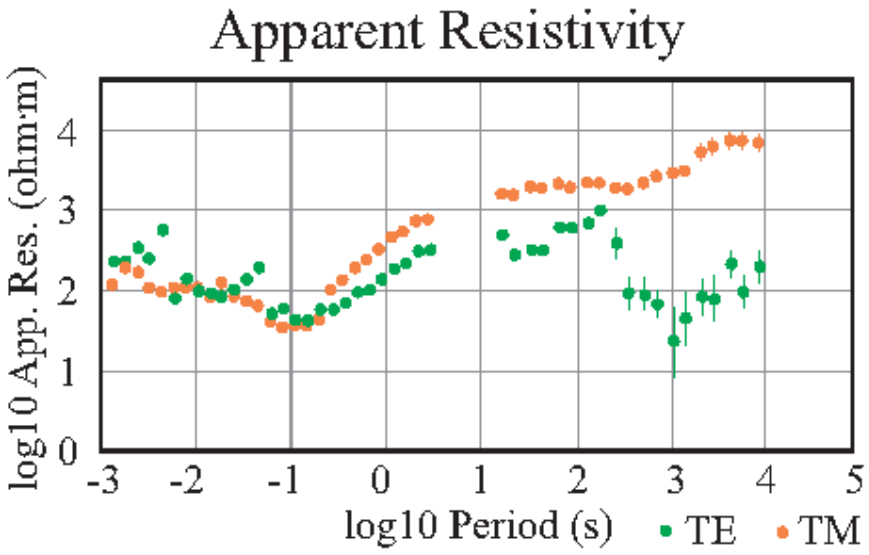
Apparent Resistivity
log10 App. Res. (ohm·m)
0
1
2
3
4
-3
-2
-1
0
1
2
3
4
5
log10 Period (s)
TE
TM

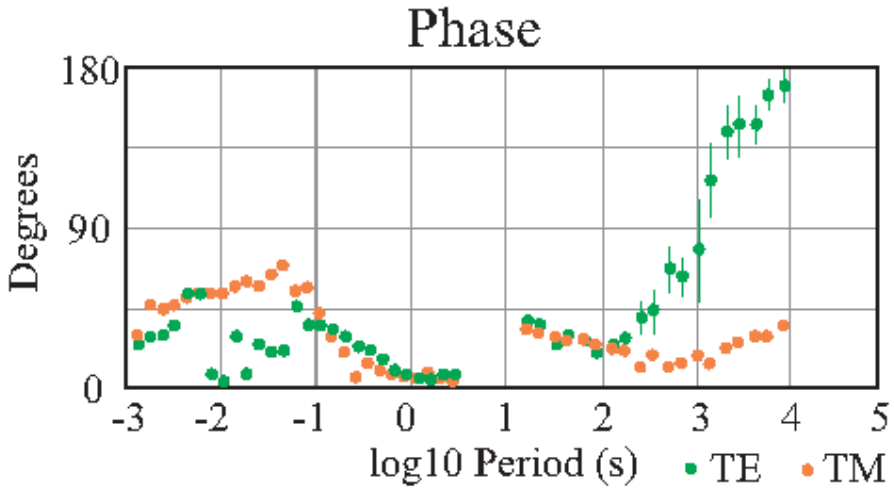
Phase
Degrees
180
90
0
-3
-2
-1
0
1
2
3
4
5
log10 Period (s)
TE
TM

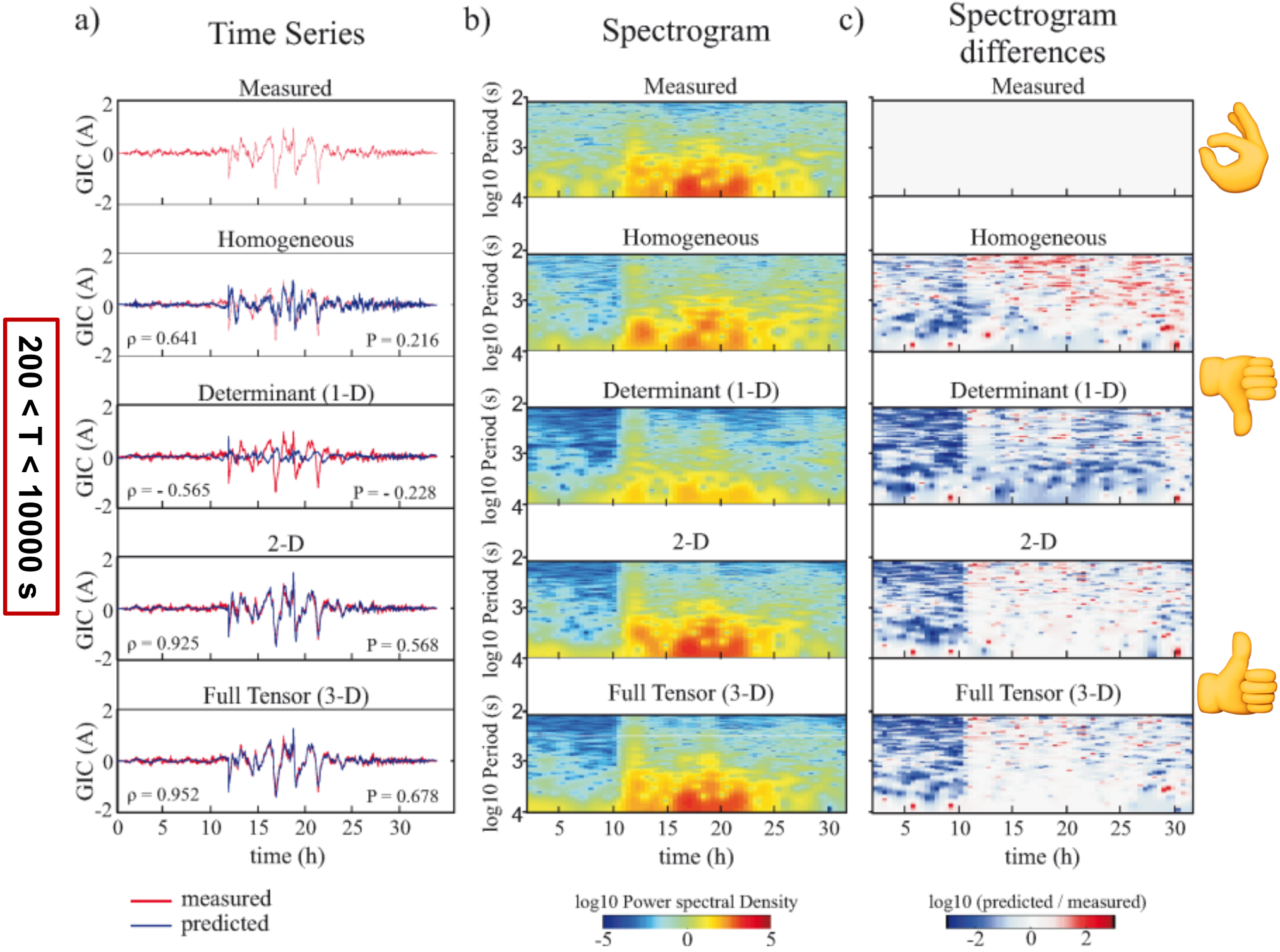
a)
Time Series
b)
Spectrogram
c)
Spectrogram differences
Measured
Homogeneous
Determinant (1-D)
2-D
Full Tensor (3-D)
GIC (A)
ρ = 0.641
P = 0.216
ρ = - 0.565
P = - 0.228
ρ = 0.925
P = 0.568
ρ = 0.952
P = 0.678
time (h)
log10 Period (s)
measured
predicted
log10 Power spectral Density
log10 (predicted / measured)
200 < T < 10000 s

Space Weather

AN AGU JOURNAL

Explore this journal >

Research Article

Improving the modeling of geomagnetically induced currents in Spain

J. M. Torta, A. Marcuello, J. Campanyà, S. Marsal, P. Queralt, J. Ledo

Accepted manuscript online: 19 April 2017 Full publication history

DOI: 10.1002/2017SW001628 View/save citation

Cited by (CrossRef): 0 articles Check for updates Citation tools

Am score

Abstract

Vulnerability assessments of the risk posed by geomagnetically induced currents (GICs) to power transmission grids benefit from accurate knowledge of the geomagnetic field variations at each node of the grid, the Earth's geoelectrical structures beneath them, and the topology and relative resistances of the grid elements in the precise instant of a storm. The results of previous analyses on the threat posed by GICs to the Spanish 400 kV grid are improved in this study by resorting to different strategies to progress in the three aspects identified above. Firstly, although at

Modelling approach:

1) Obtaining the geoelectric field by:

Surface impedance

from observatory data

$$E_{x,y}(\omega) = \pm \frac{Z(\omega) B_{y,x}(\omega)}{\mu_0}$$

2) Obtaining the induced voltages on the power grid by:

$$V_{ij} = \int_{L_{ij}} E \cdot dl$$

Length of the grid line between groundings

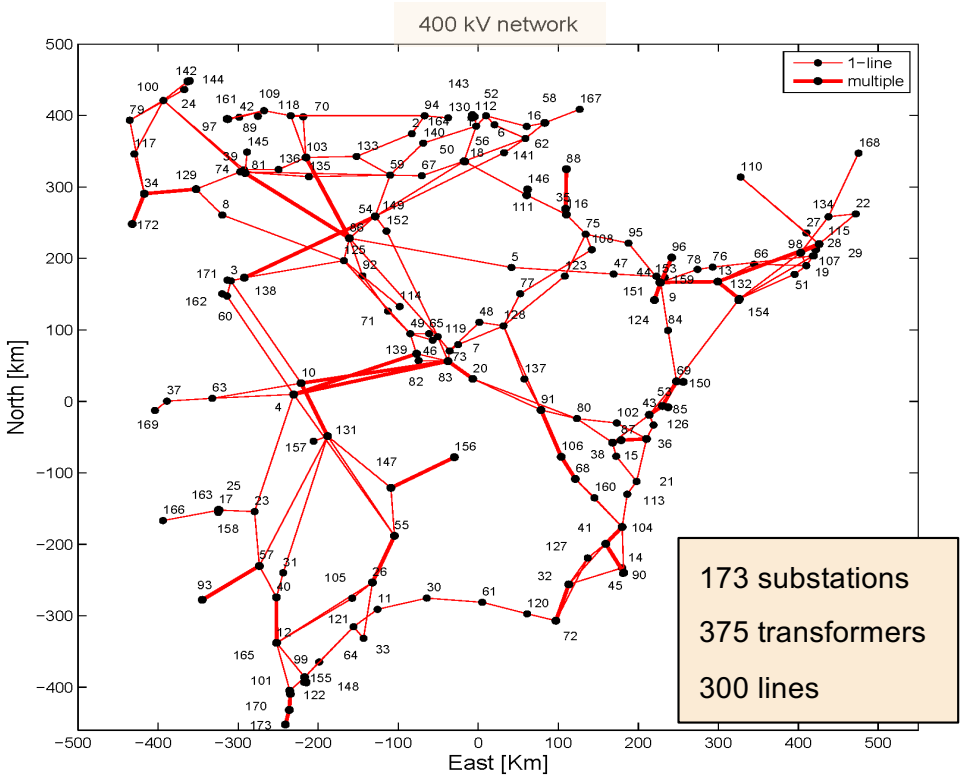

Initial Modelling:

- **Plane wave assumption** for the external source
- **Homogeneous Earth conductivity** for the induction problem
- **Lehtinen-Pirjola method** (Ohm and Kirchhoff laws in matrix form)

IBERGIC PROJECT

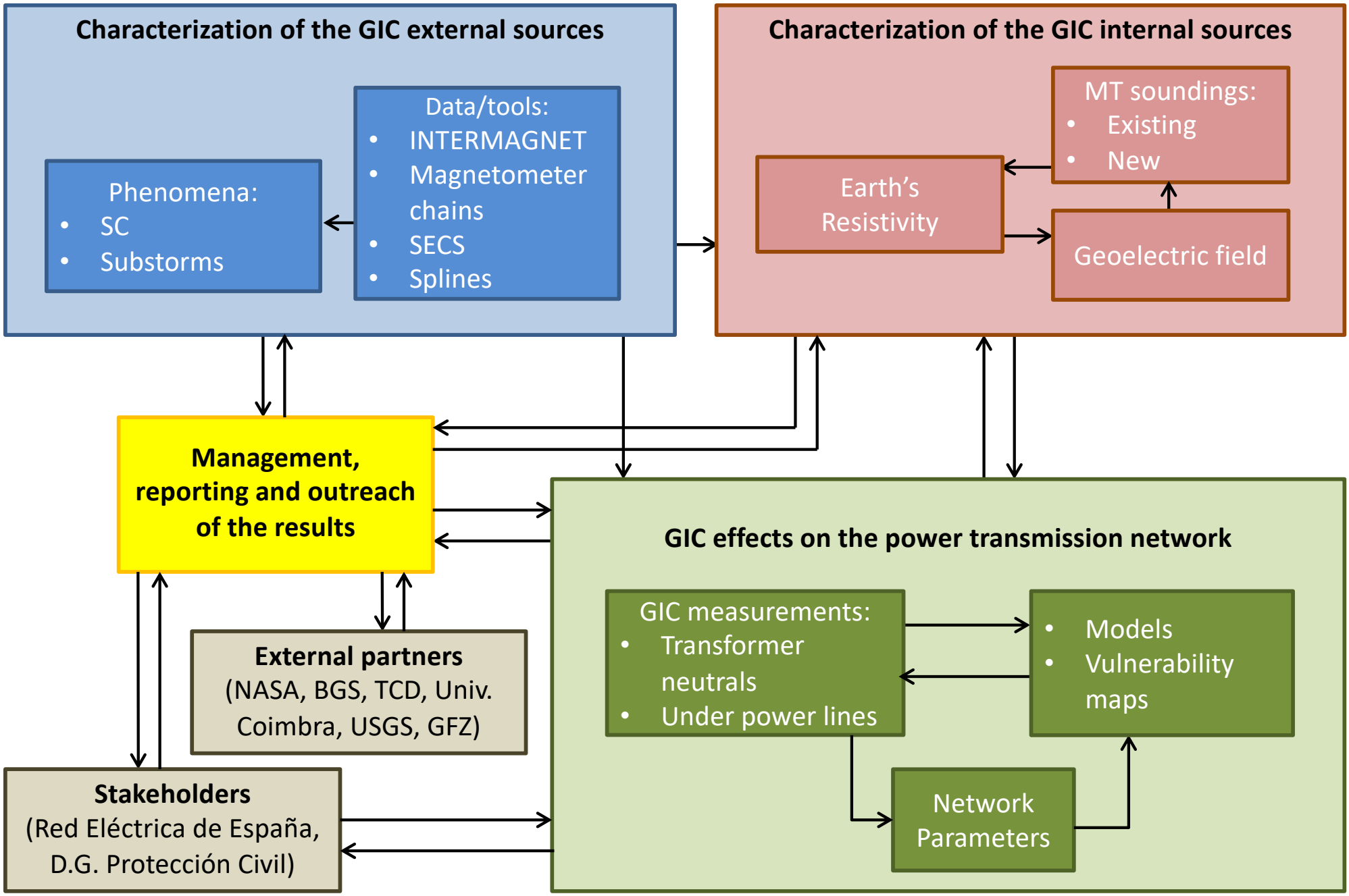

IBERGIC PROJECT

Characterization of the GIC external sources

Data/tools:
- INTERMAGNET
- Magnetometer chains
- SECS
- Splines

←

Phenomena:
- SC
- Substorms

AGU PUBLICATIONS

JGR

nal of Geophysical Research: Space Physics

RCH ARTICLE
2016JA023166

Section:
e system responses to
atrick's Day storms in
d 2015

hod proves suitable to map
DPmi current patterns

Use of spherical elementary currents to map the polar current systems associated with the geomagnetic sudden commencements on 2013 and 2015 St. Patrick's Day storms

S. Marsal[1], J. M. Torta[1], A. Segarra[1], and T. Araki[2]

[1]Observatori de l'Ebre, (OE), CSIC - Universitat Ramon Llull, Roquetes, Spain, [2]Department of Geophysics, Graduate School of Science, Kyoto University, Kyoto, Japan

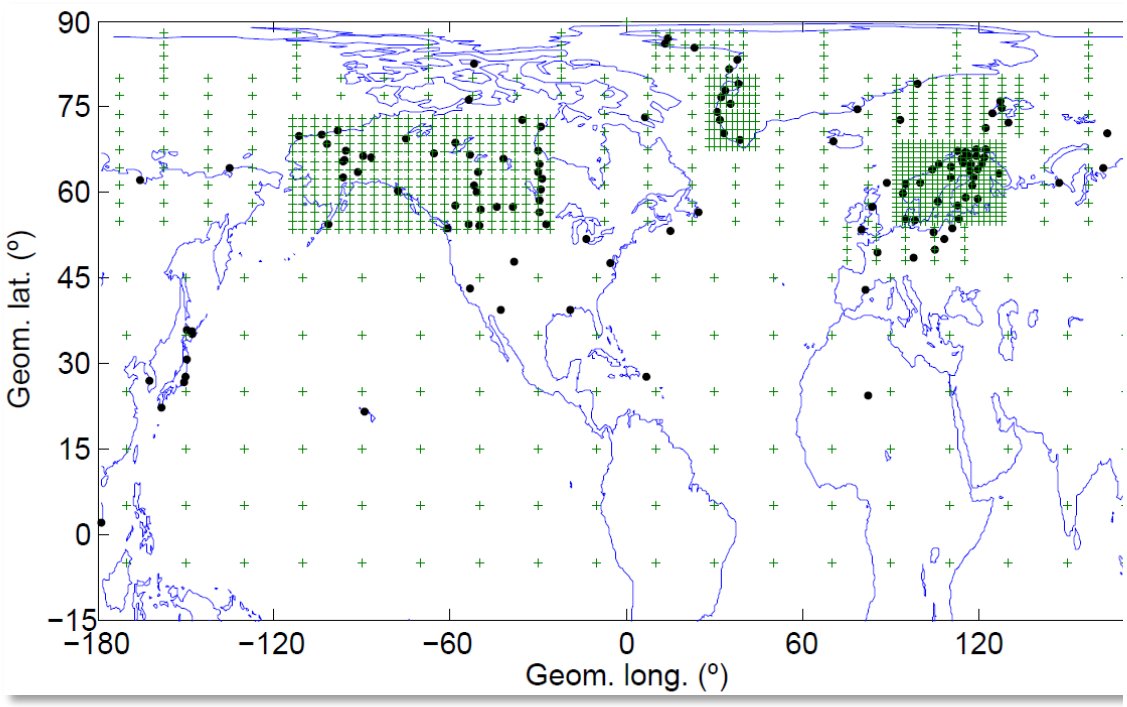

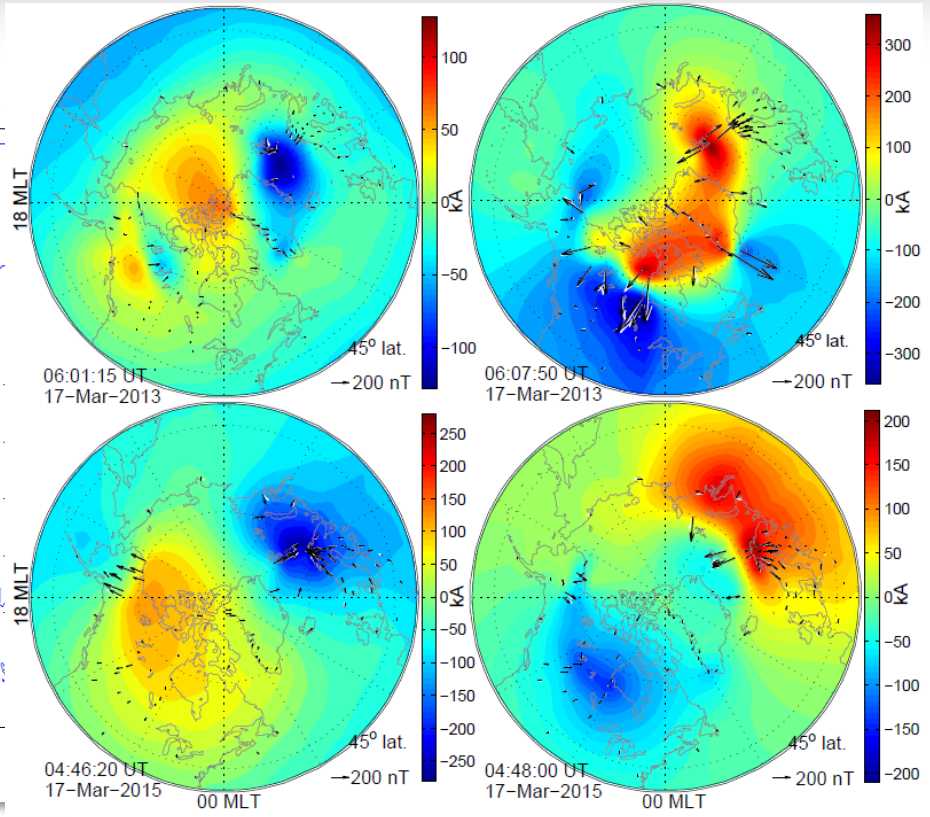

IBERGIC PROJECT

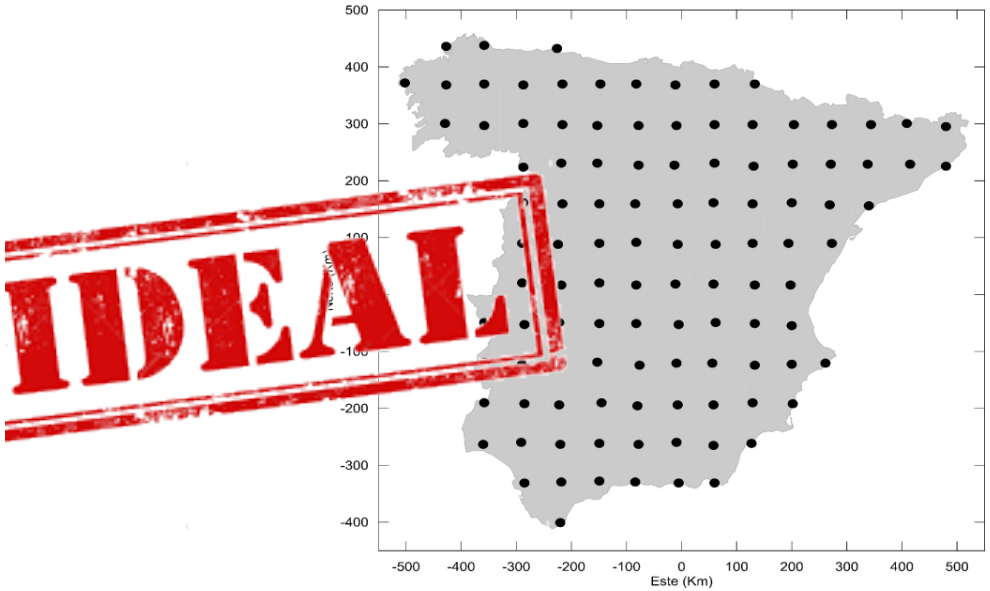

Characterization of the GIC internal sources

MT soundings:
- Existing
- New

Earth's Resistivity

Geoelectric field

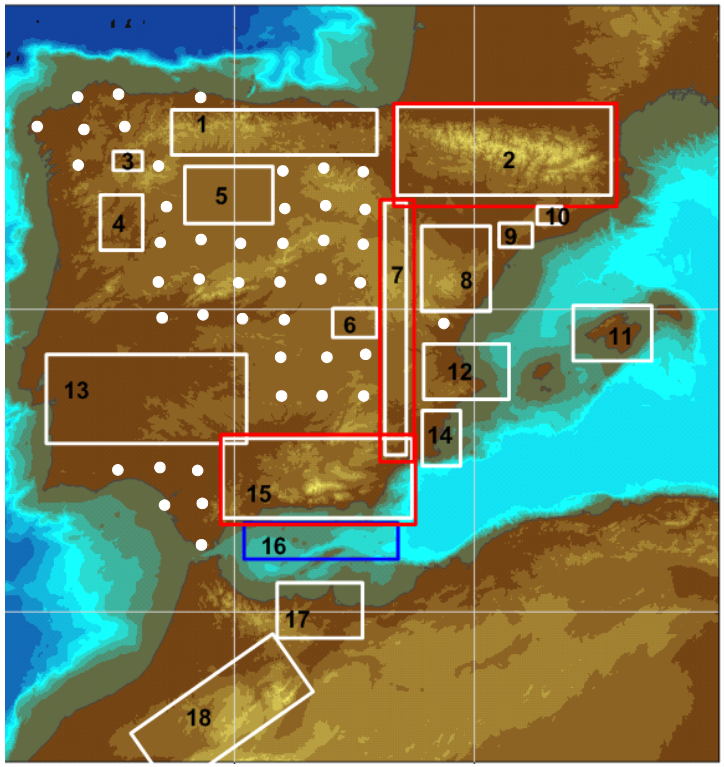

1. Cantabrian Mountains
2. Pyrenees and Ebro Basin
3. Bembibre
4. NE Portugal
5. Hontomín and Duero Basin
6. El Hito Anticline
7. Tajo Basin - Betics profile (Picasso)
8. Iberian Chain and El Maestrat
9. Montmell
10. Vallès
11. Majorca
12. Jumilla and Bicorp diapirs
13. Ossa Morena and Centro Iberia
14. Alhama de Murcia and Carboneras Fa
15. Betic Chain
16. Alboran Basin
17. Alhucemas Fault
18. Atlas Mountains

Broad Band

Long Period

Marine Survey

Knowledge of the geoelectrical structure → magnetotellurics

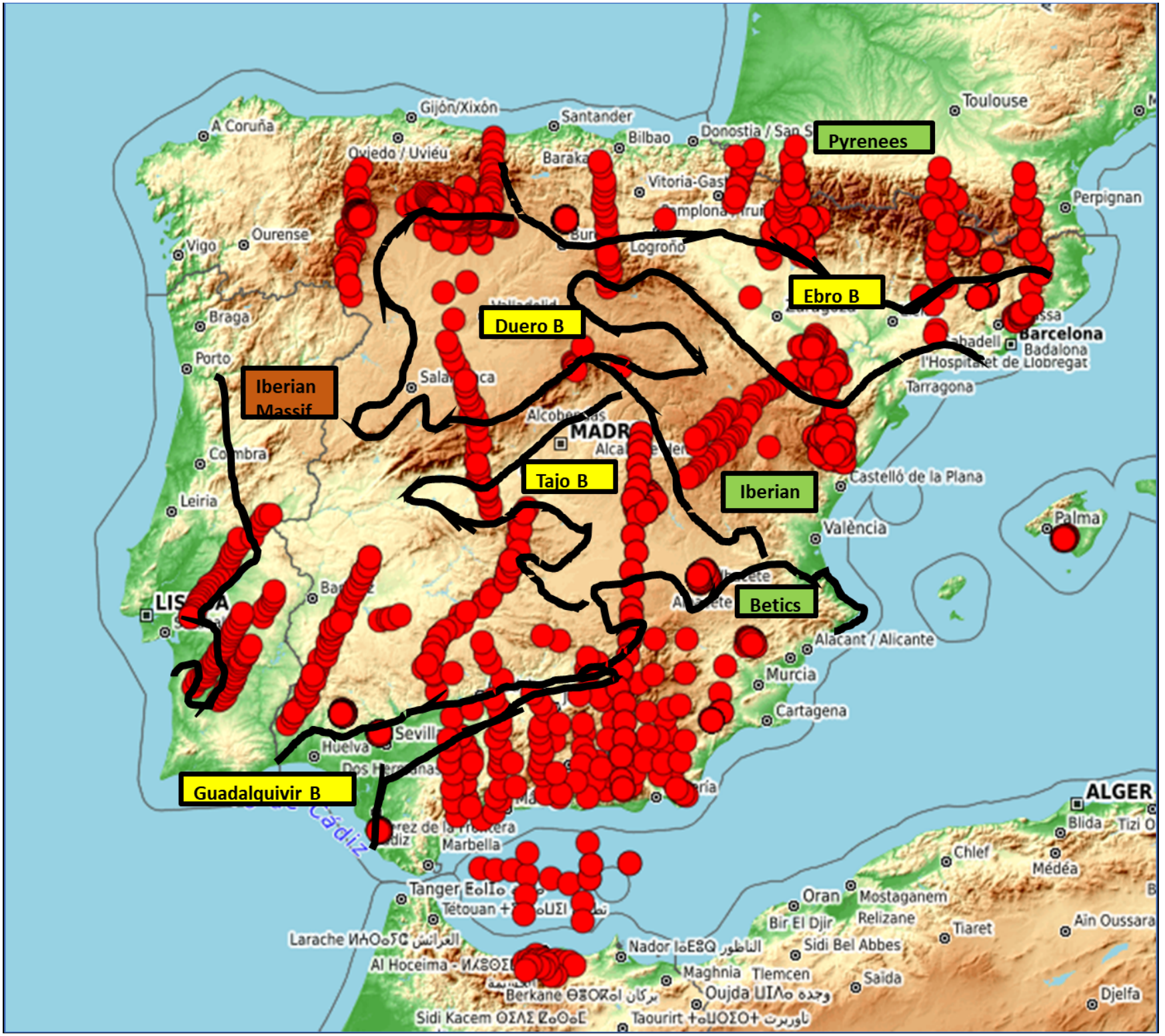
Pyrenees
Ebro B
Duero B
Iberian Massif
Tajo B
Iberian
Betics
Guadalquivir B
Gijón/Xixón
Santander
Bilbao
A Coruña
Oviedo / Uviéu
Toulouse
Perpignan
Vigo
Ourense
Braga
Porto
Barcelona
Tarragona
Coimbra
Leiria
Castelló de la Plana
Palma
València
Alacant / Alicante
Murcia
Cartagena
Sevilla
Huelva
Cádiz
Marbella
ALGER
Blida
Chlef
Médéa
Oran
Mostaganem
Relizane
Tiaret
Ain Oussara
Sidi Bel Abbes
Tlemcen
Saida
Djelfa
Maghnia
Nador
Tanger
Tétouan
Larache
Al Hoceima
Berkane
Oujda
Sidi Kacem
Taourirt

Pous et al., 2011

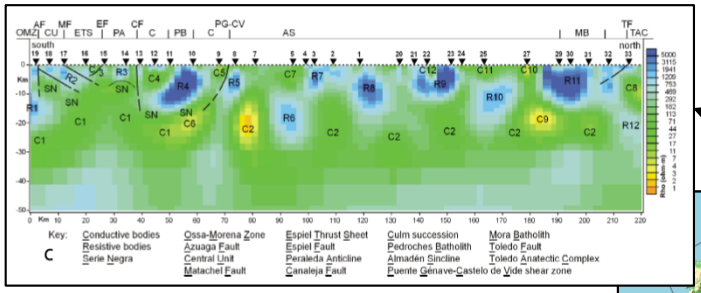

Campanyà et al., 2012

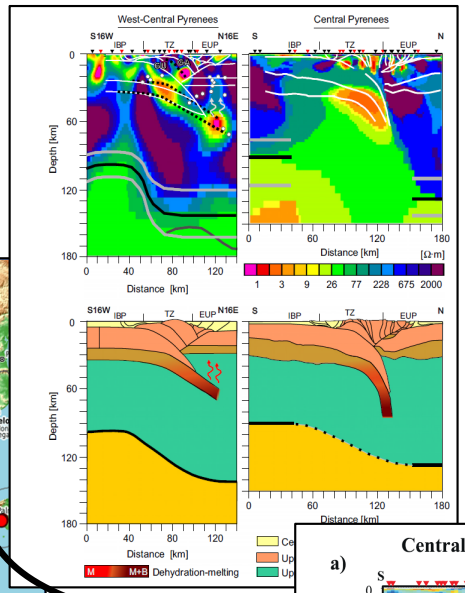

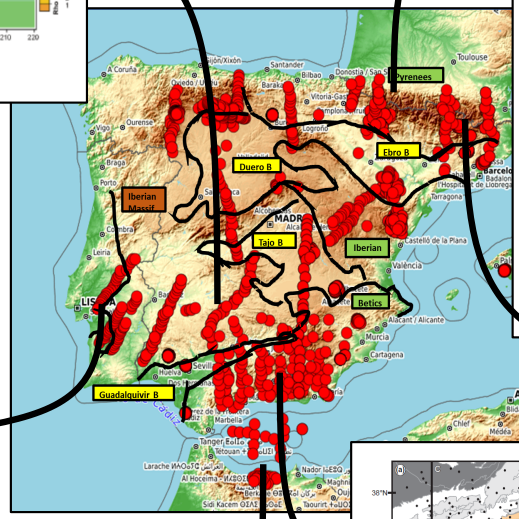

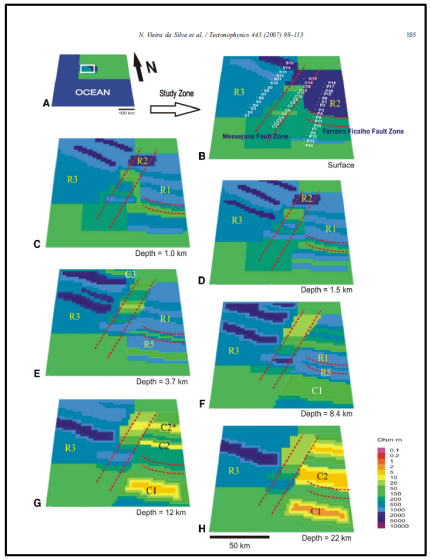

Vieira da Silva, et al. 2007

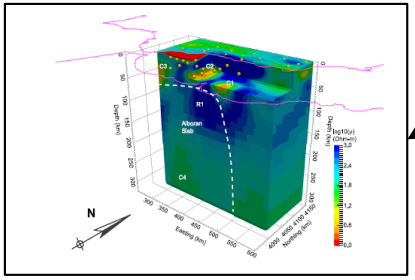

Garcia et al., 2015

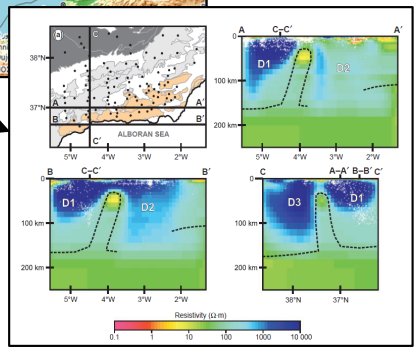

Rosell et al., 2010

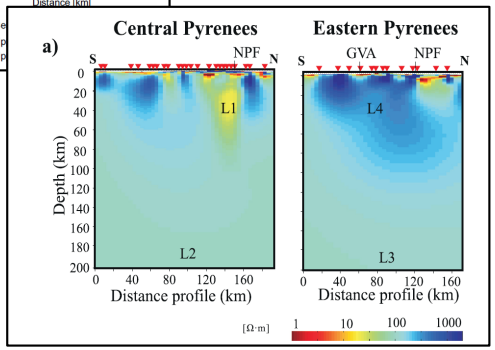

Campanyà et al., 2018

Electrical **R**esistivity **M**odel of the **I**berian **L**ithosphere

INITIAL MODEL:

ERMIL 0.0

Seismic and potential field methods

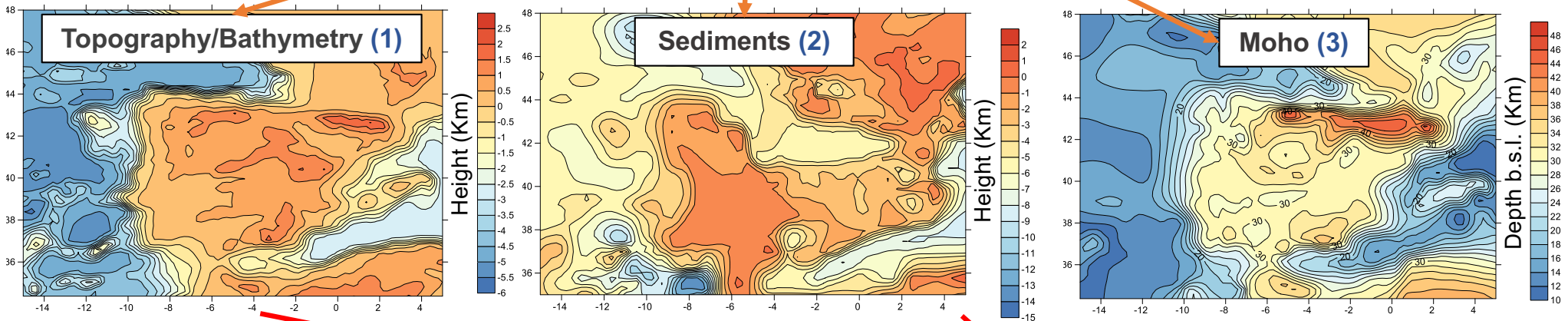

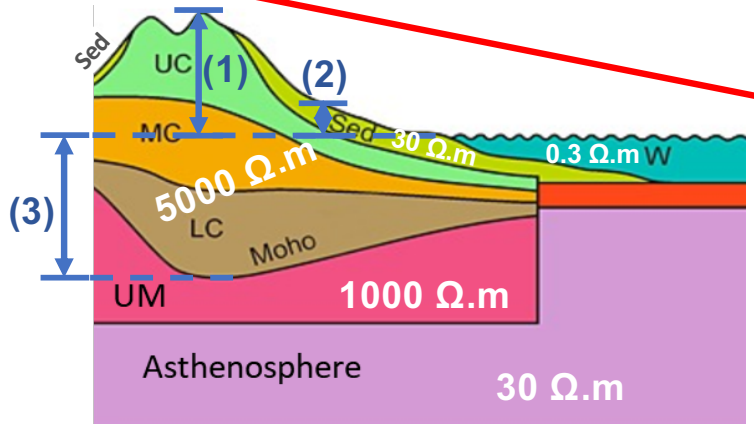

$Z(w)$

Electrical **R**esistivity **M**odel of the **I**berian **L**ithosphere

INITIAL MODEL:

ERMIL 0.0

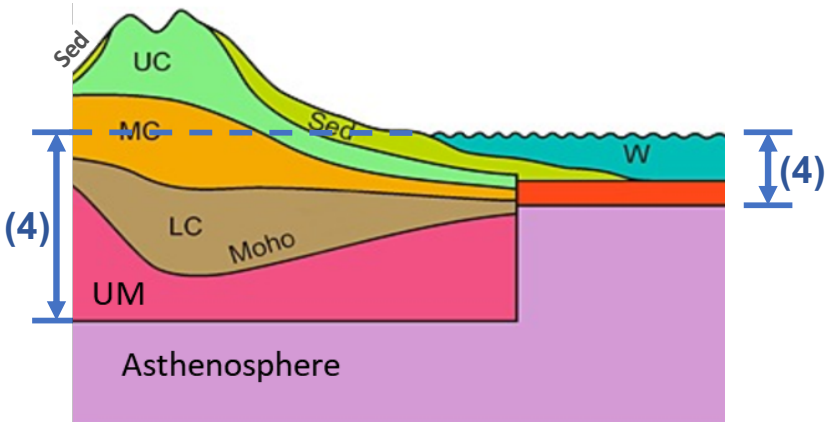

Under certain assumptions (not true in regions with a transient thermal regime or with anomalous crustal radioactivity), surface heat flow can be used as a rough proxy for the thickness of the lithosphere.

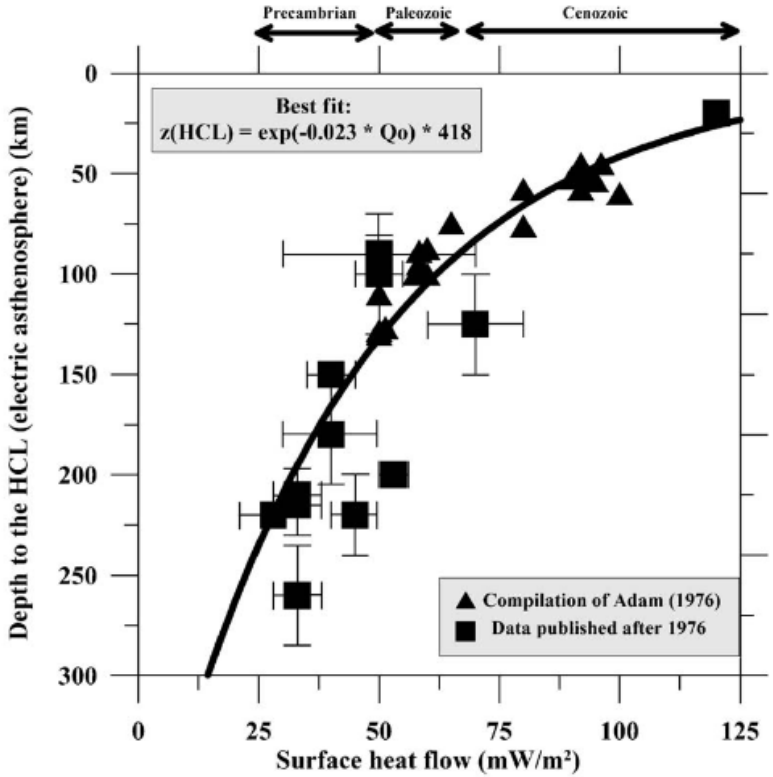

Empirical relationship between heat flow and thickness of the electrical lithosphere (Artemieva, 2006)

Electrical **R**esistivity **M**odel of the **I**berian **L**ithosphere

INITIAL MODEL:

ERMIL 0.0

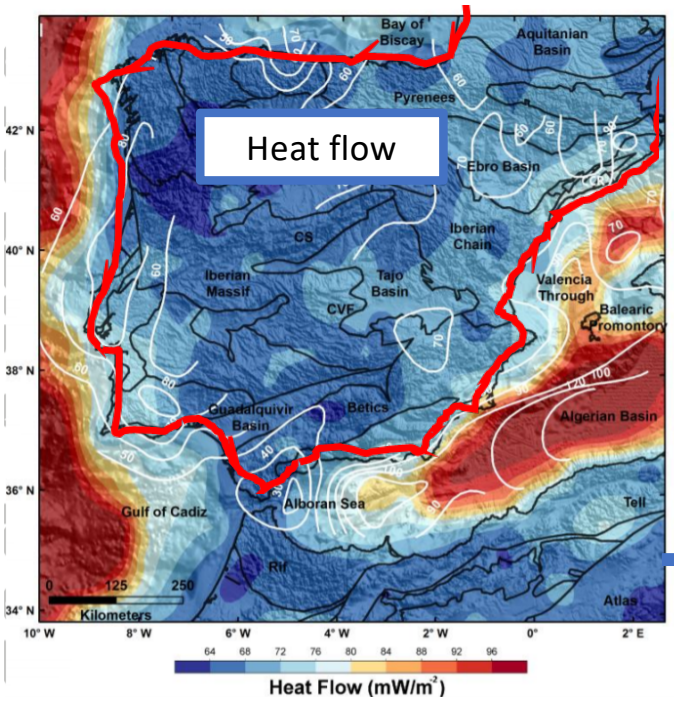

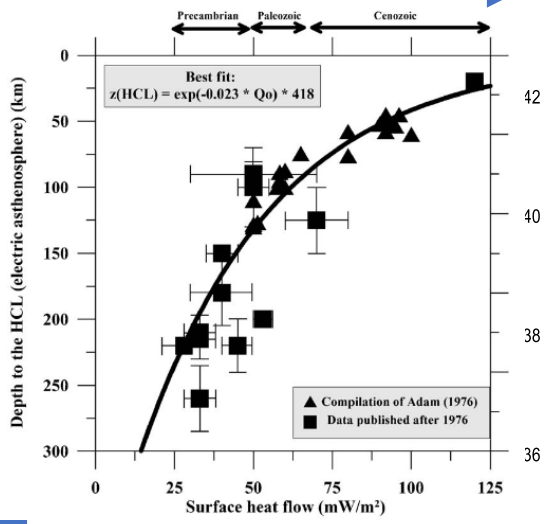

$$z_{HCL} = 418*\exp(-0.023*Q_o)$$

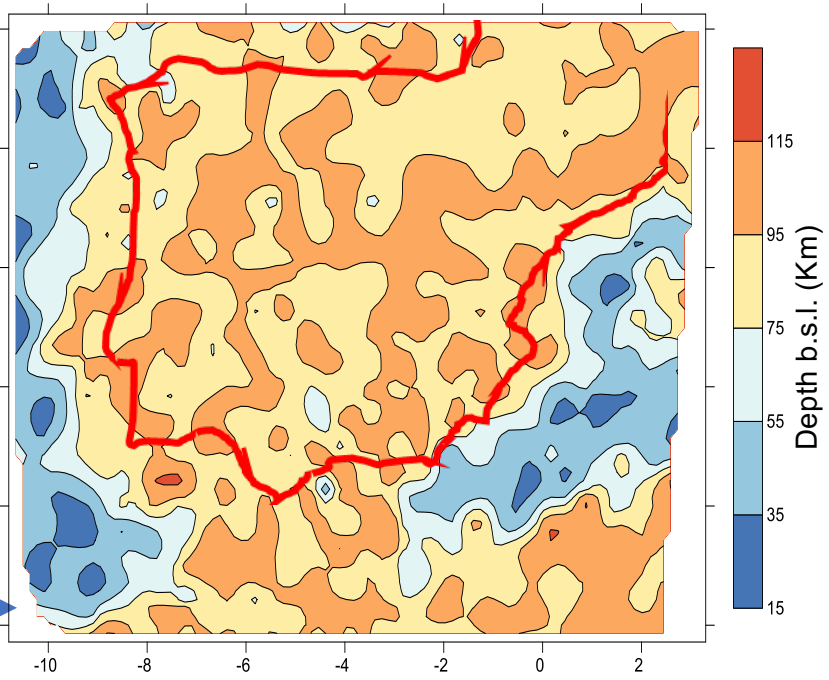

Heat flow data derived from the Curie point depth (Andrés et al., 2018).

Electrical lithosphere thickness derived from heat flow data and the equation of Artemieva (2006).

Electrical lithosphere thickness map

Electrical **R**esistivity **M**odel of the **I**berian **L**ithosphere

INITIAL MODEL:

ERMIL 0.0

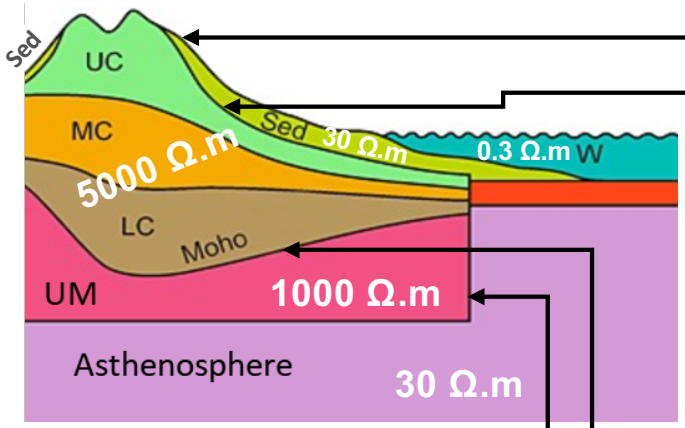

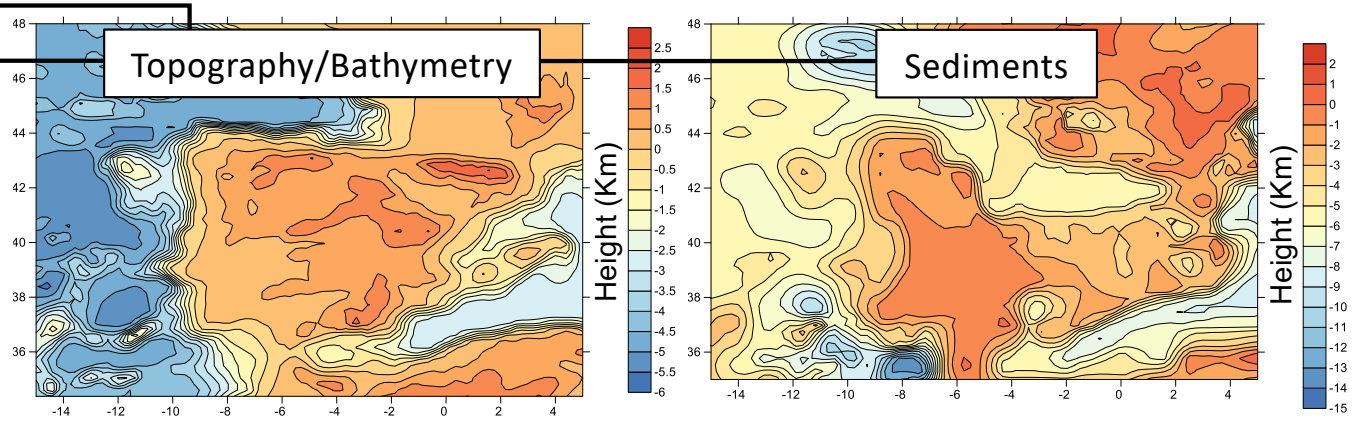

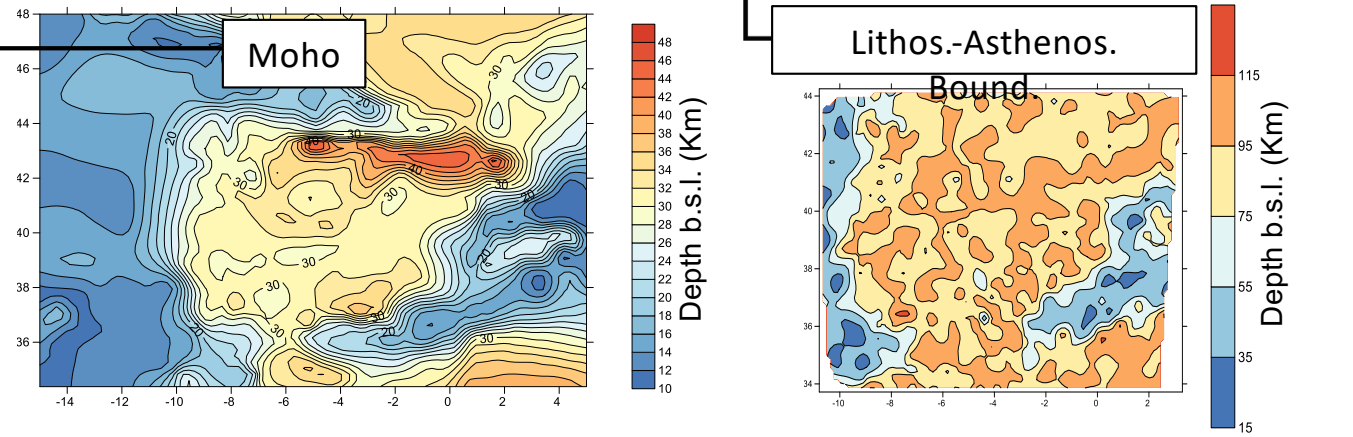

The LAB should be considered as a first order approx., given that the heat flow map is an approx. to the real values and also that the conversion formula was obtained considering tectonic scenarios that span over several tectonic periods.

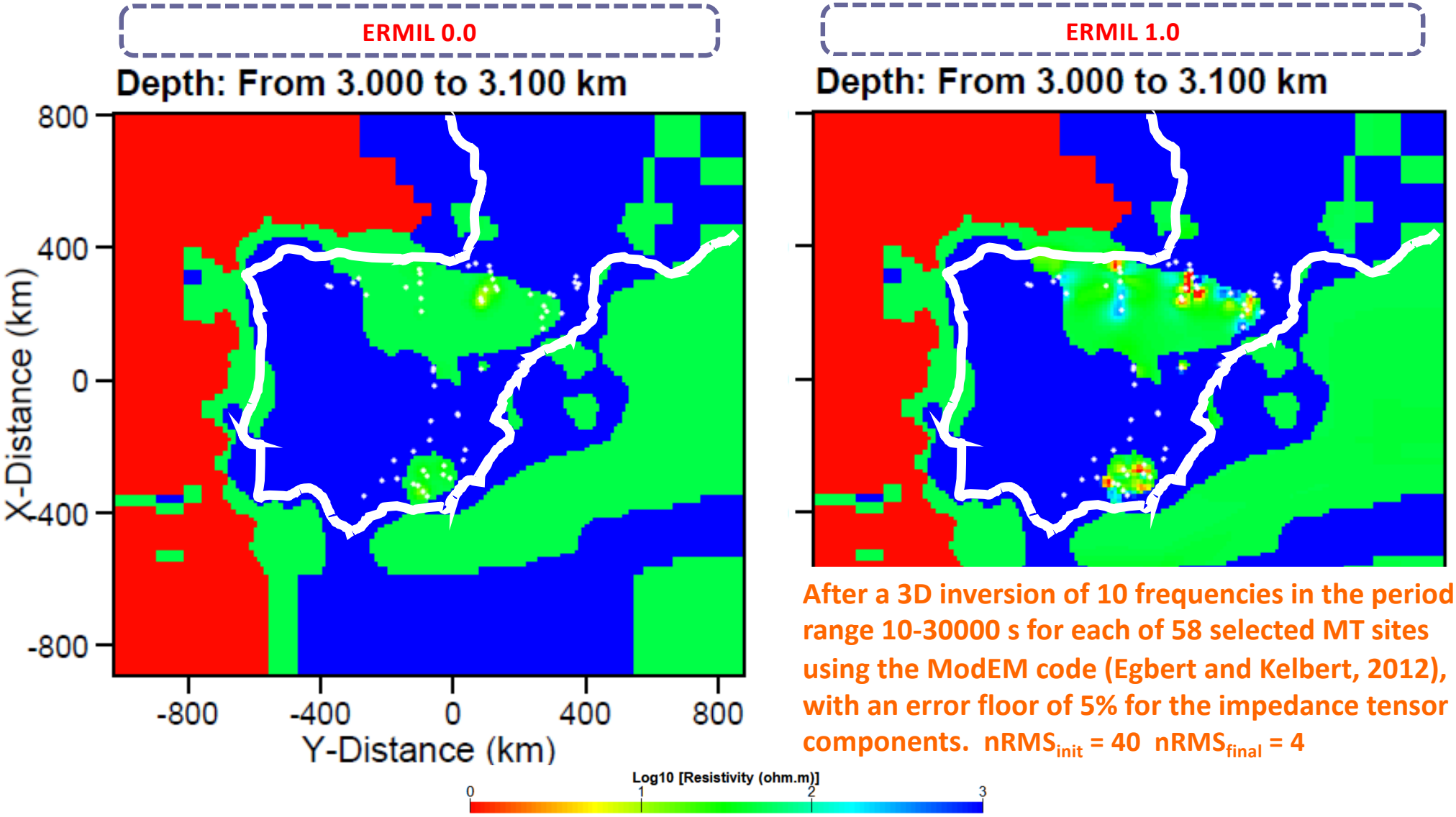

After a 3D inversion of 10 frequencies in the period range 10-30000 s for each of 58 selected MT sites using the ModEM code (Egbert and Kelbert, 2012), with an error floor of 5% for the impedance tensor components. $nRMS_{init} = 40$ $nRMS_{final} = 4$

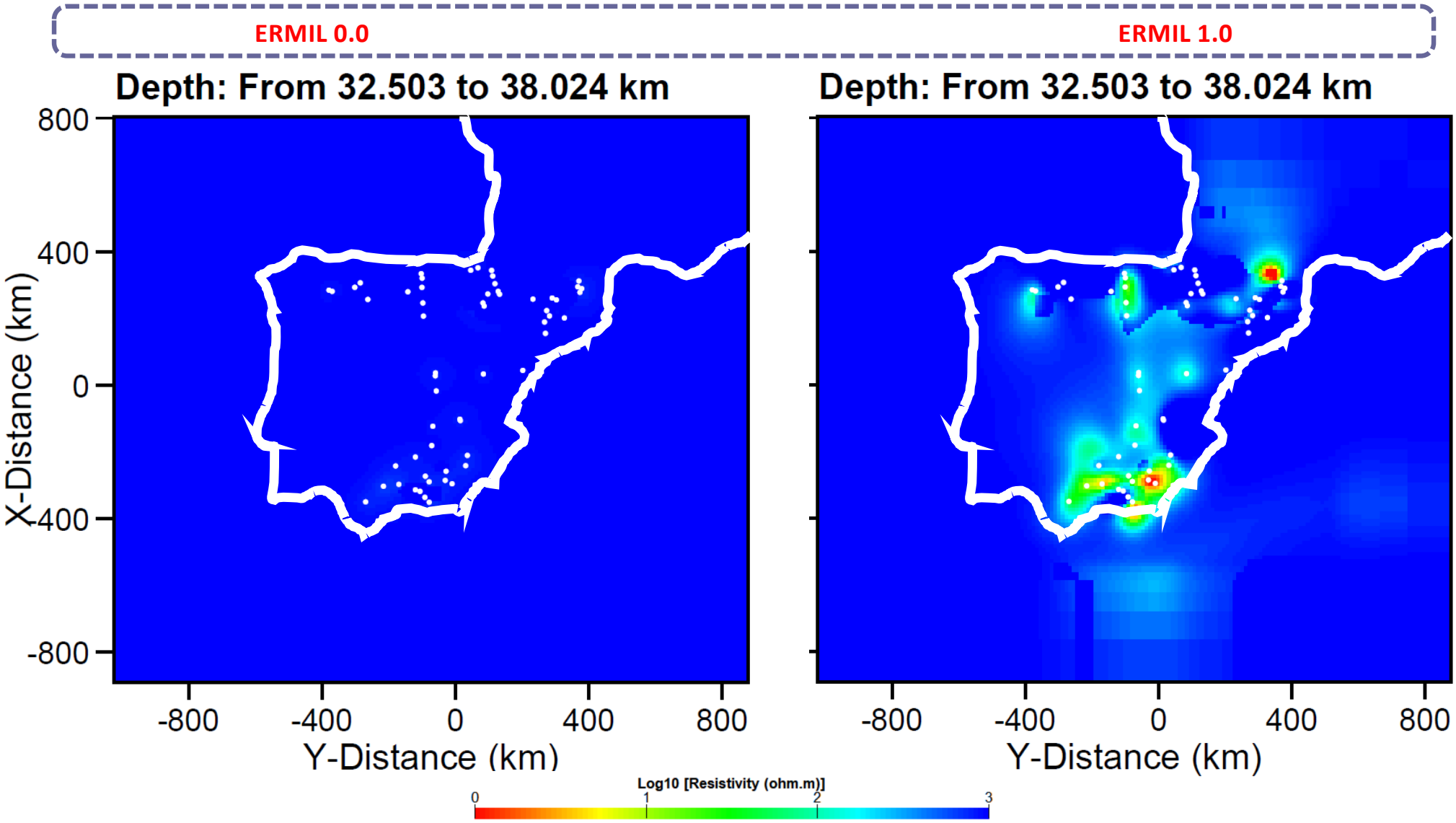
ERMIL 0.0
ERMIL 1.0
Depth: From 32.503 to 38.024 km
Depth: From 32.503 to 38.024 km
X-Distance (km)
800
400
0
-400
-800
-800
-400
0
400
800
Y-Distance (km)
Log10 [Resistivity (ohm.m)]
0
1
2
3

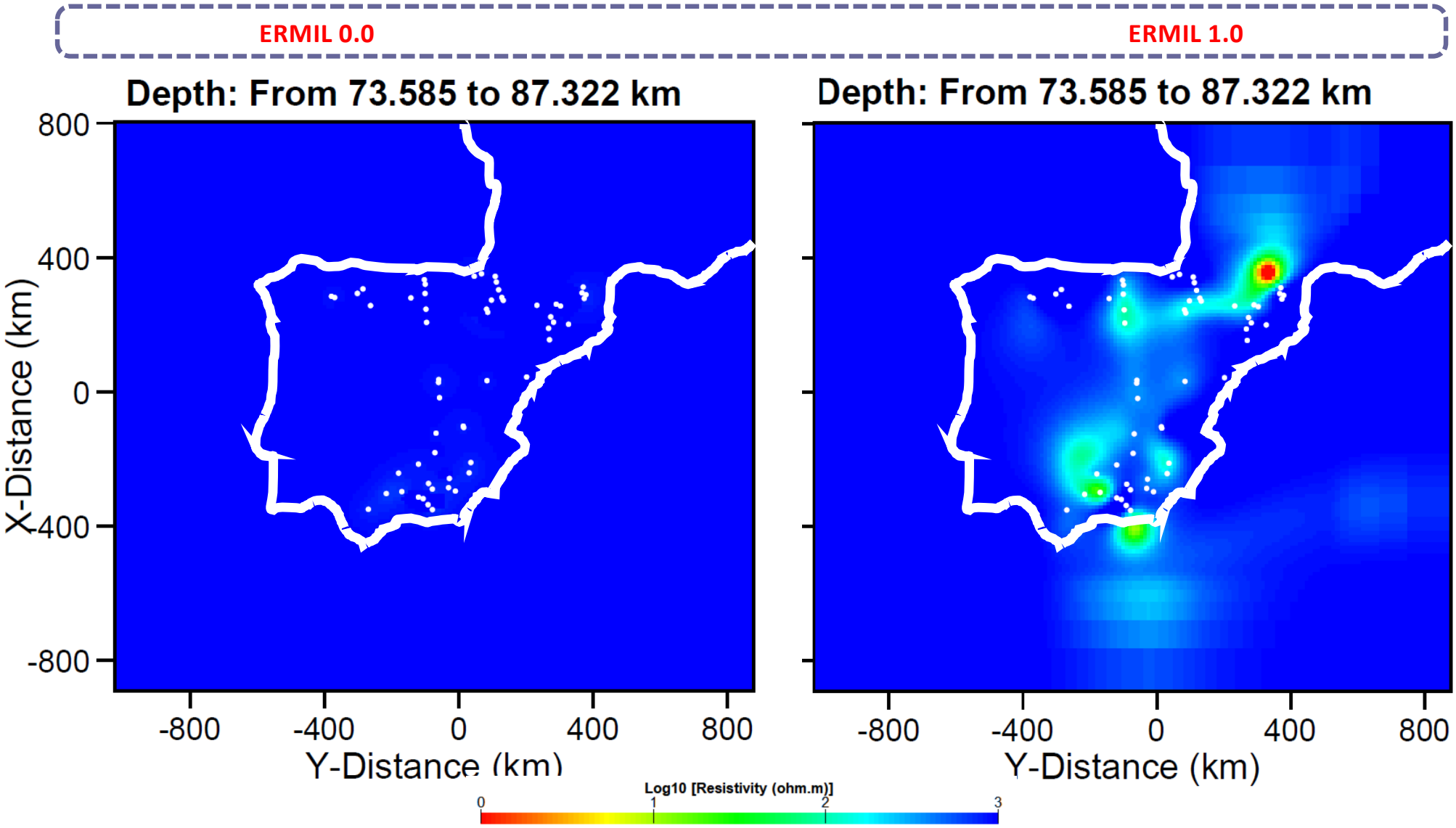
ERMIL 0.0
ERMIL 1.0
Depth: From 73.585 to 87.322 km
Depth: From 73.585 to 87.322 km
X-Distance (km)
800
400
0
-400
-800
-800
-400
0
400
800
Y-Distance (km)
Log10 [Resistivity (ohm.m)]
0
1
2
3

ERMIL 0.0

ERMIL 1.0

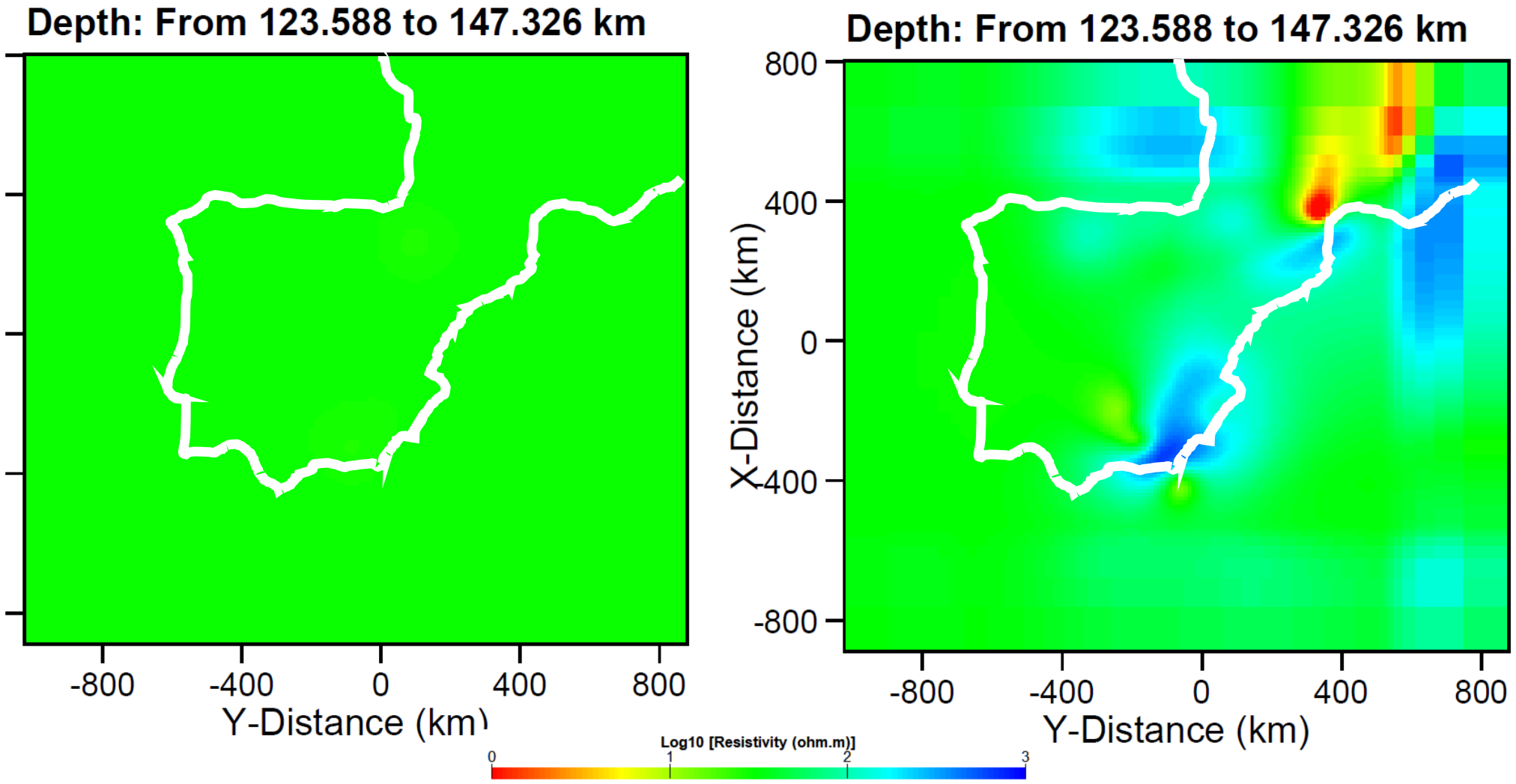

EM fields (2015-03-17, 17:20 -18:49 UT)

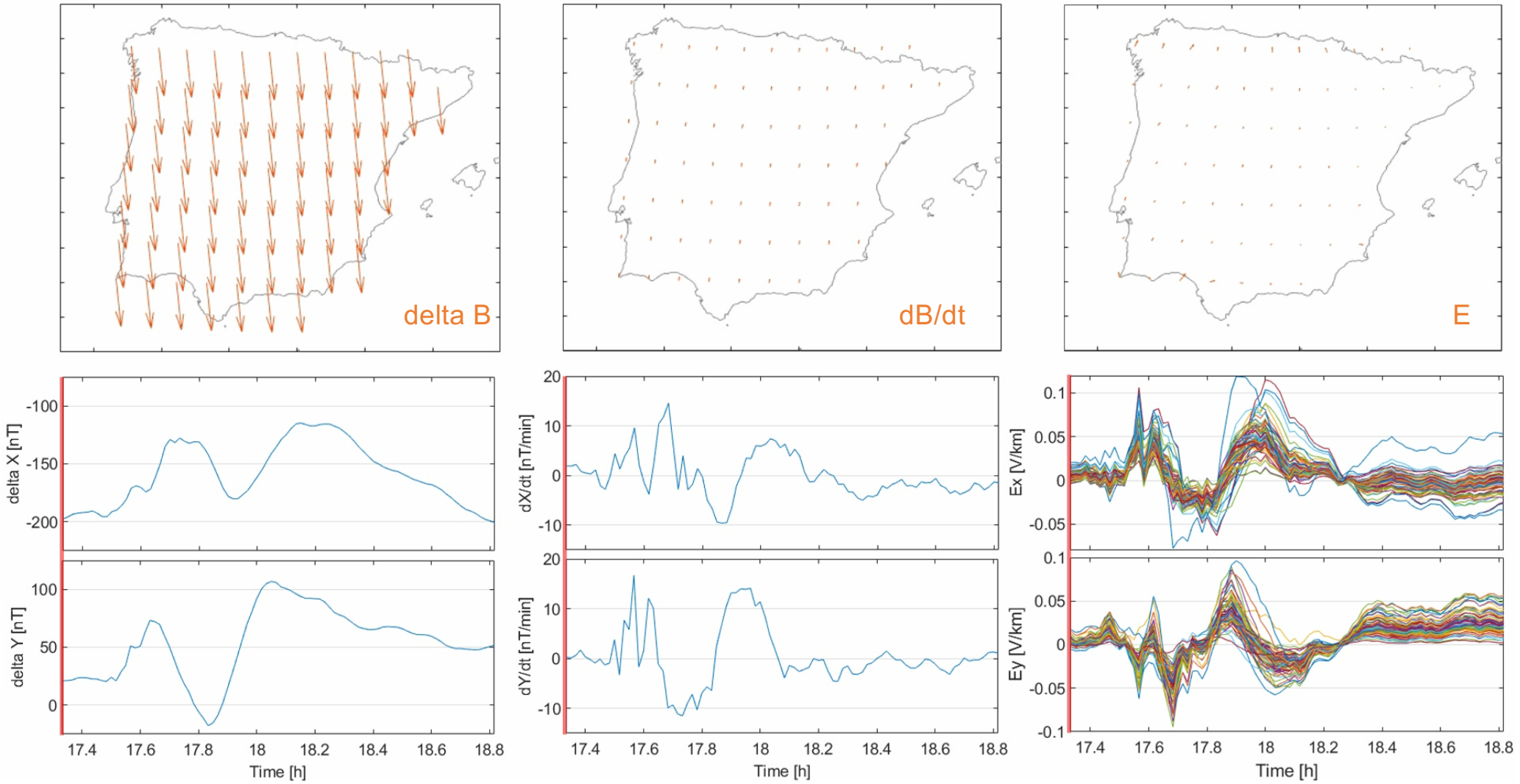

EM fields (2015-03-17, 17:53 UT)

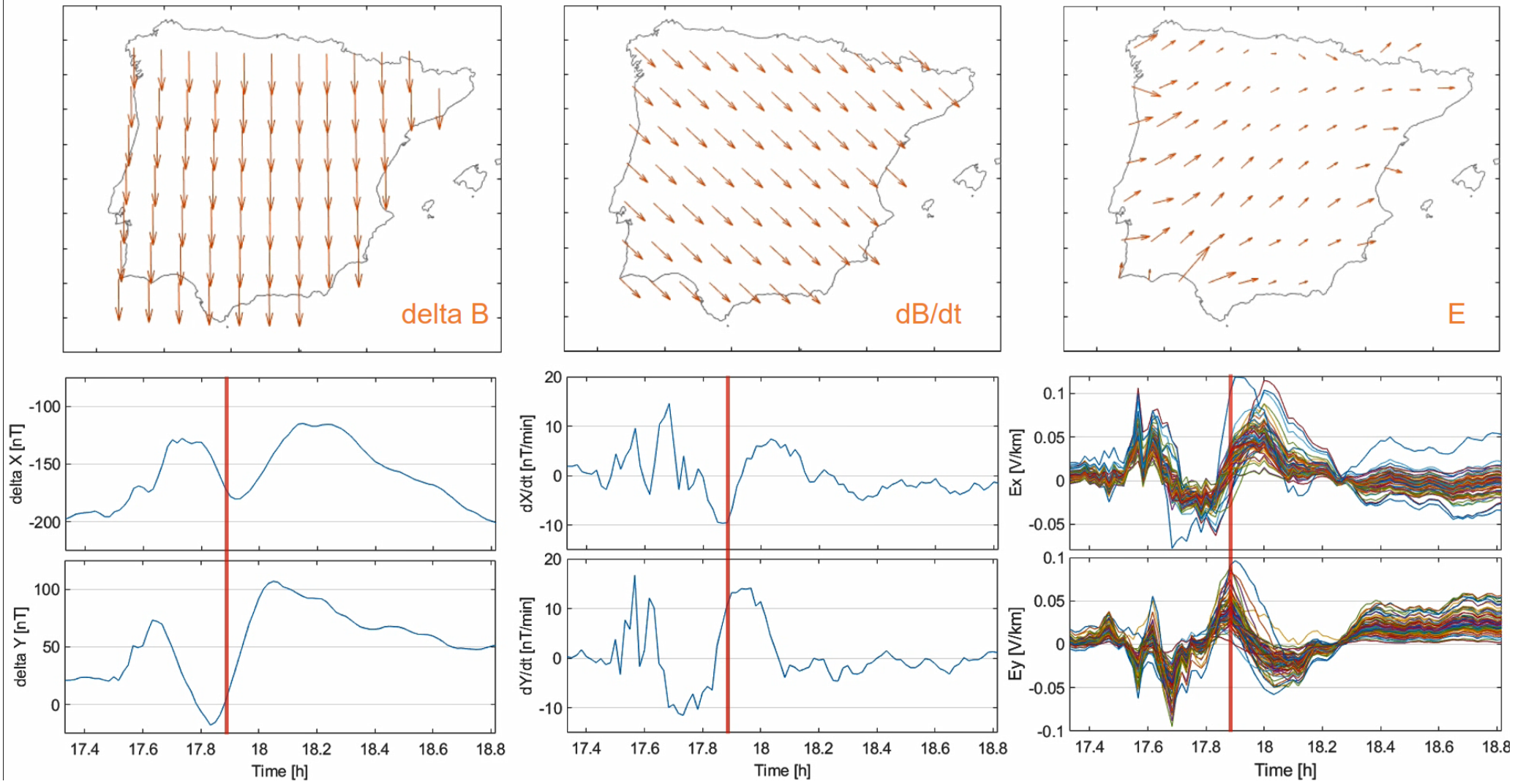

Torta et al. Earth, Planets and Space 2014, 66:87
http://www.earth-planets-space.com/content/66/1/87

Earth, Planets and Space
a SpringerOpen Journal

Vulnerability map (Torta et al., 2014)

FULL PAPER Open Access

Assessing the hazard from geomagnetically induced currents to the entire high-voltage power network in Spain

Results with homogeneous Earth's resistivity

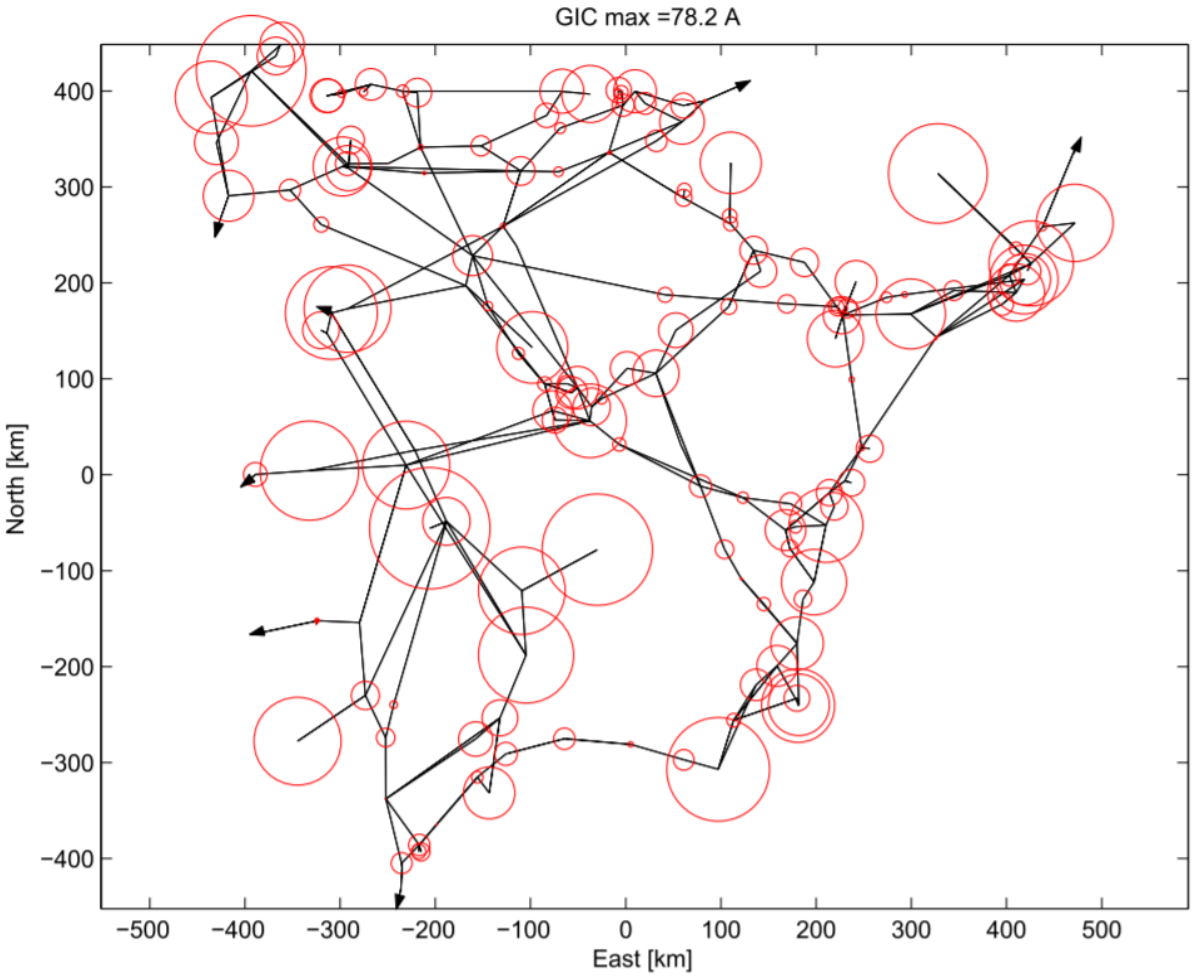

Figure 4 Maximum values of GICs under the conditions during the Halloween storm. Circles have diameters proportional to the flowing current (regardless of its sign), and a maximum of 78.2 A was observed, which was achieved at the Mesa de la Copa substation (node 157 in Figure 1). Arrowheads at the ends of some transmission lines indicate connection with foreign substations.

Vulnerability map assessment (In prep., 2019)

Results with homogeneous Earth's resistivity

Results with a 3D Earth's resistivity model

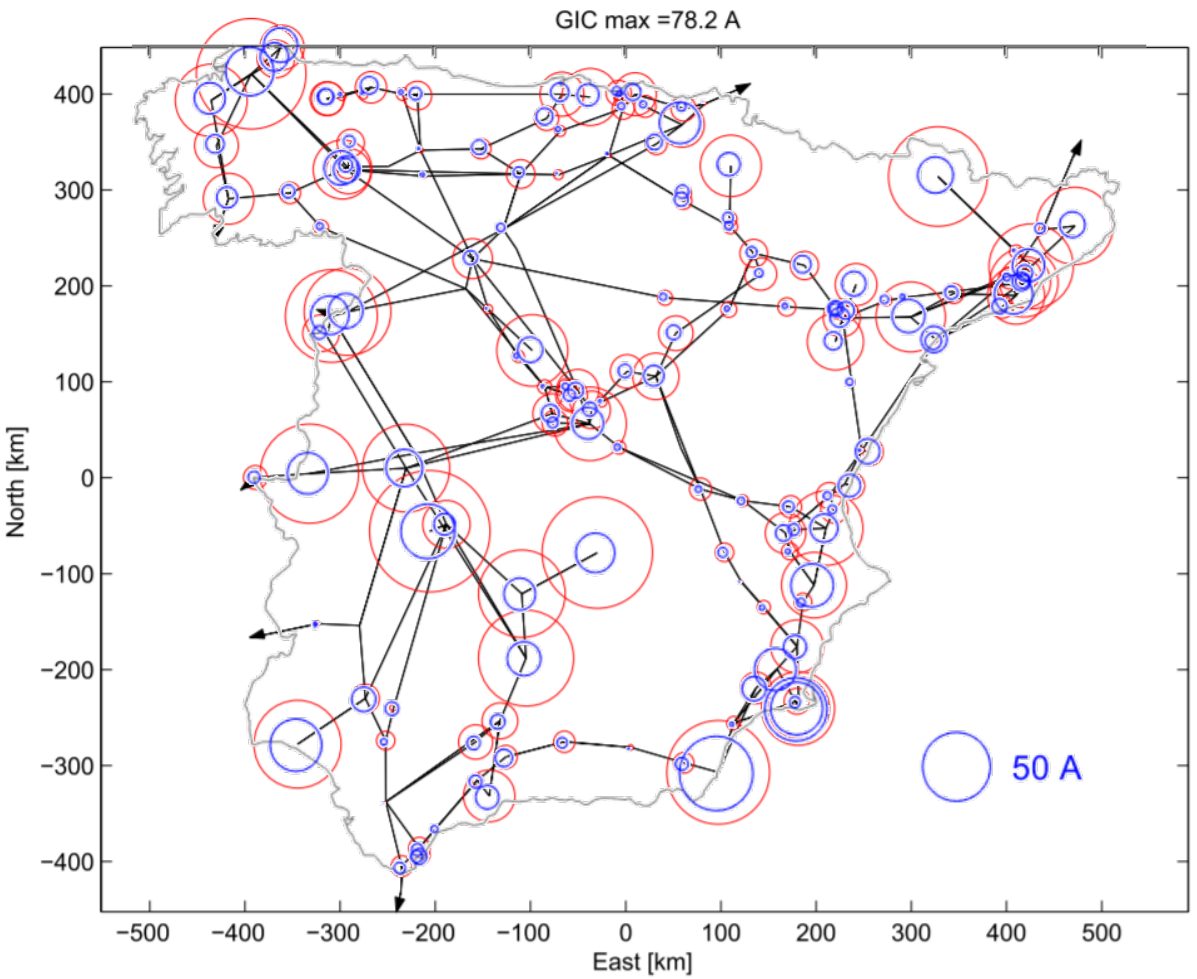

Figure 4 Maximum values of GICs under the conditions during the Halloween storm. Circles have diameters proportional to the flowing current (regardless of its sign), and a maximum of 78.2 A was observed, which was achieved at the Mesa de la Copa substation (node 157 in Figure 1). Arrowheads at the ends of some transmission lines indicate connection with foreign substations.

IBERGIC PROJECT

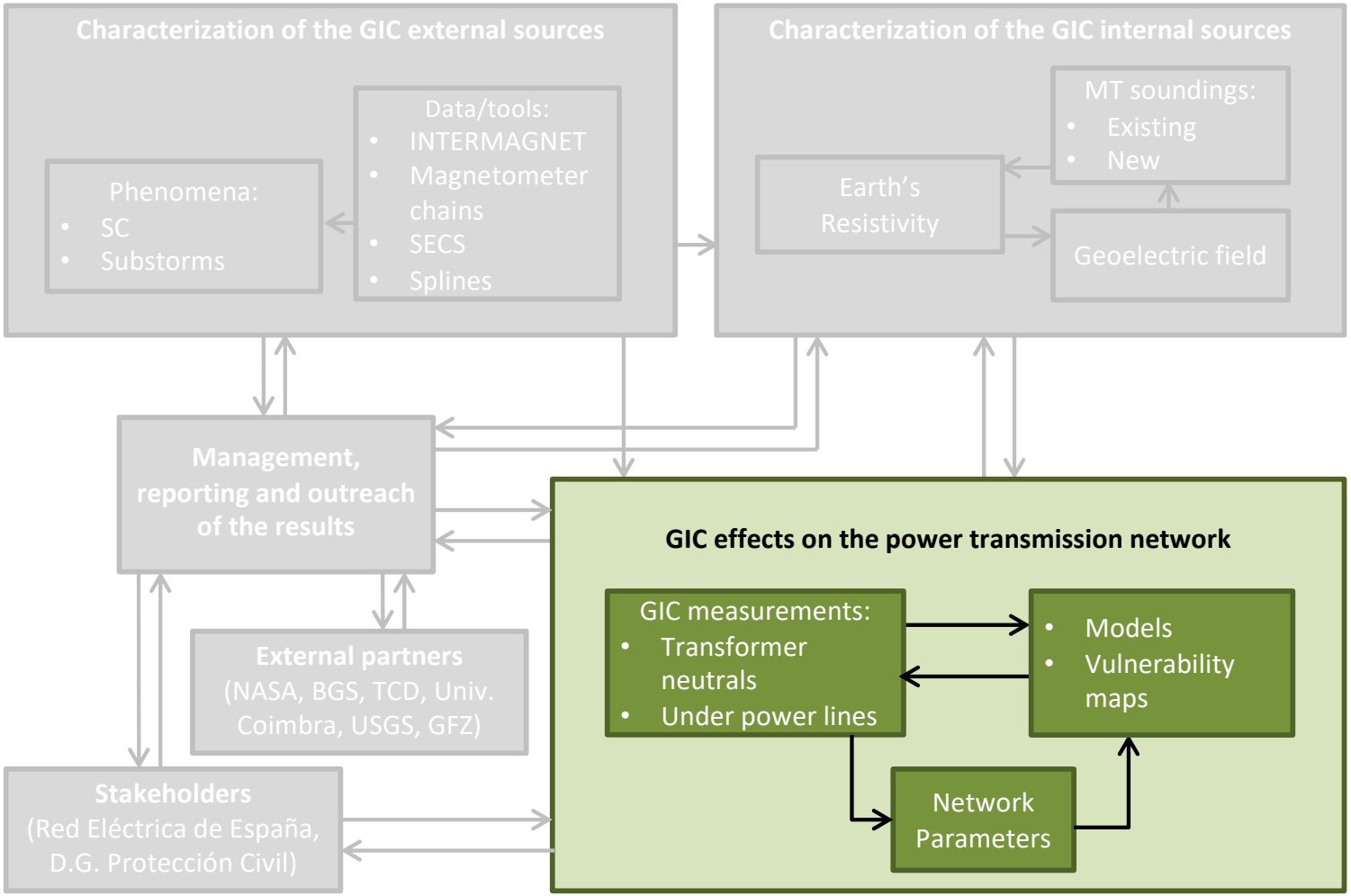

IBERGIC PROJECT

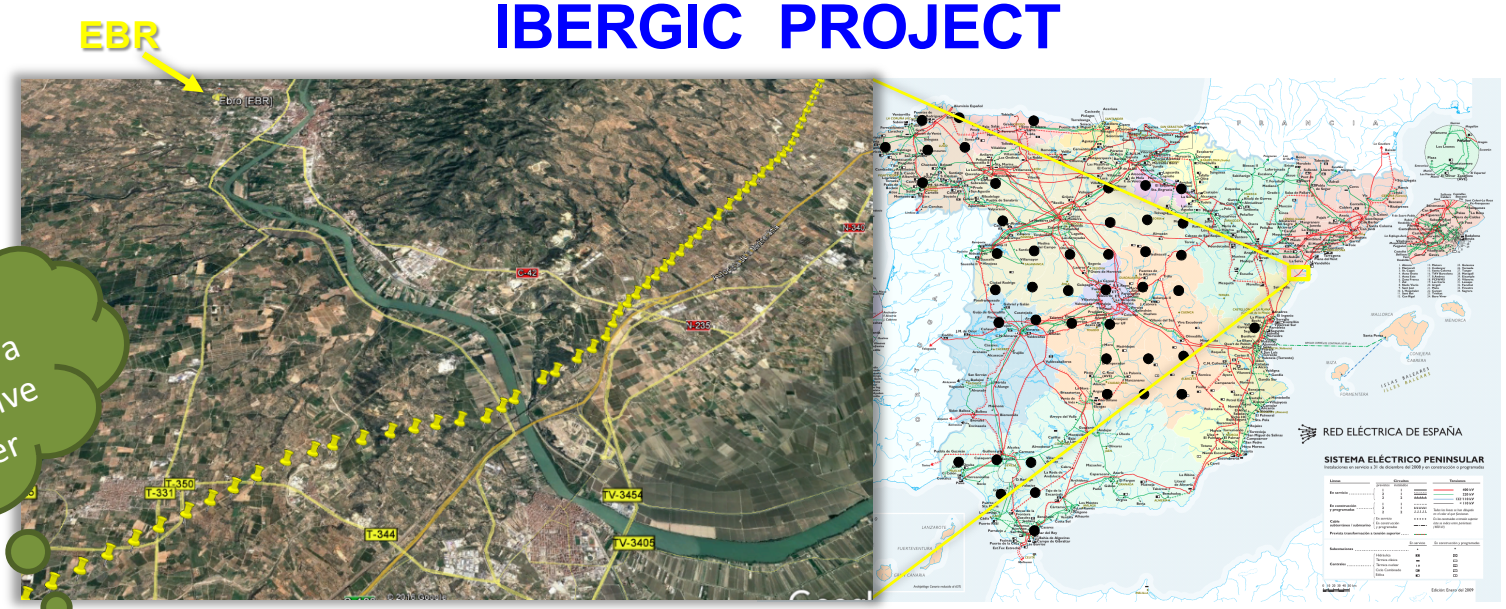

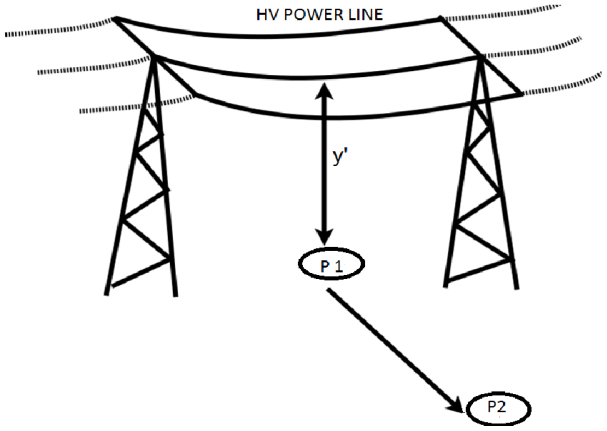

GIC effects on the power transmission network

GIC measurements:
- Transformer neutrals
- Under power lines

- Models
- Vulnerability maps

Network Parameters

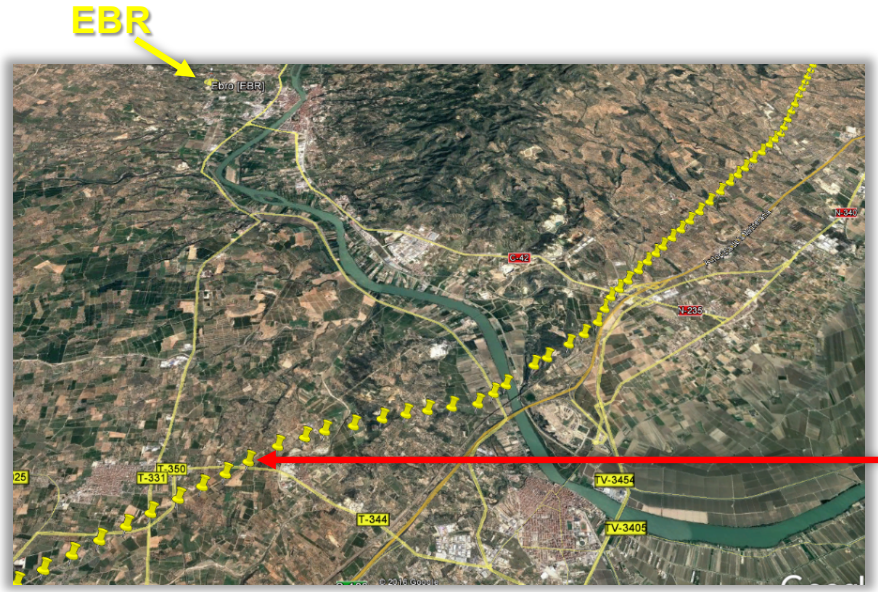
EBR
T-350
T-331
T-344
TV-3454
TV-3405

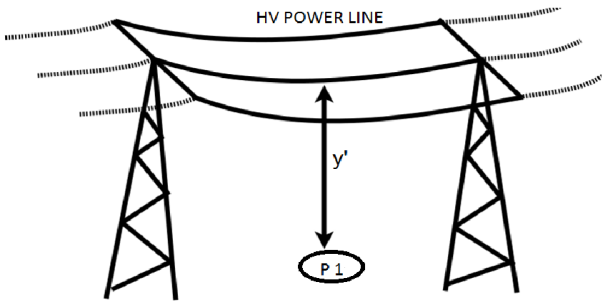
HV POWER LINE
y'
P 1

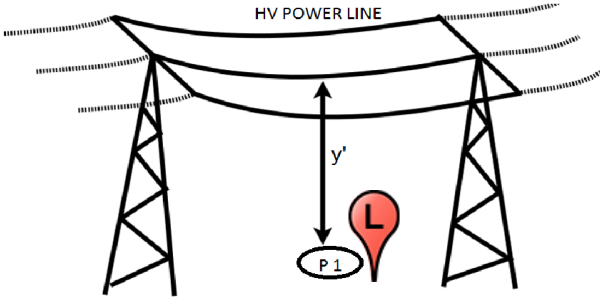

Diurnal thermal amplitude ~ 1 ºC

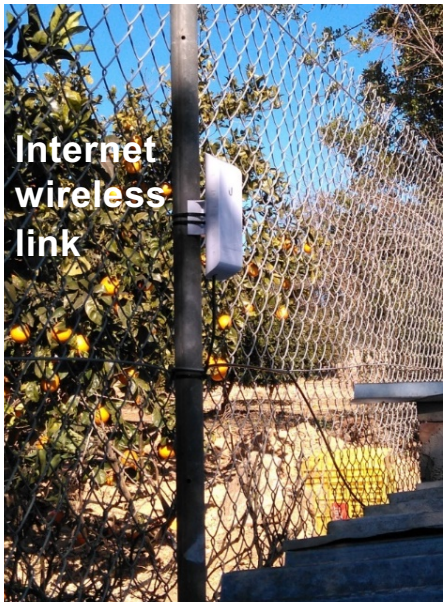

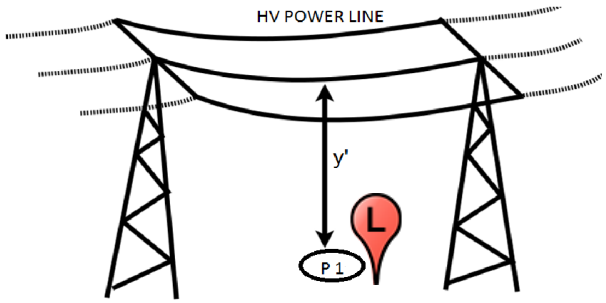

Diurnal thermal amplitude ~ 1 ºC

A second magnetometer was installed 300 m away from the power line

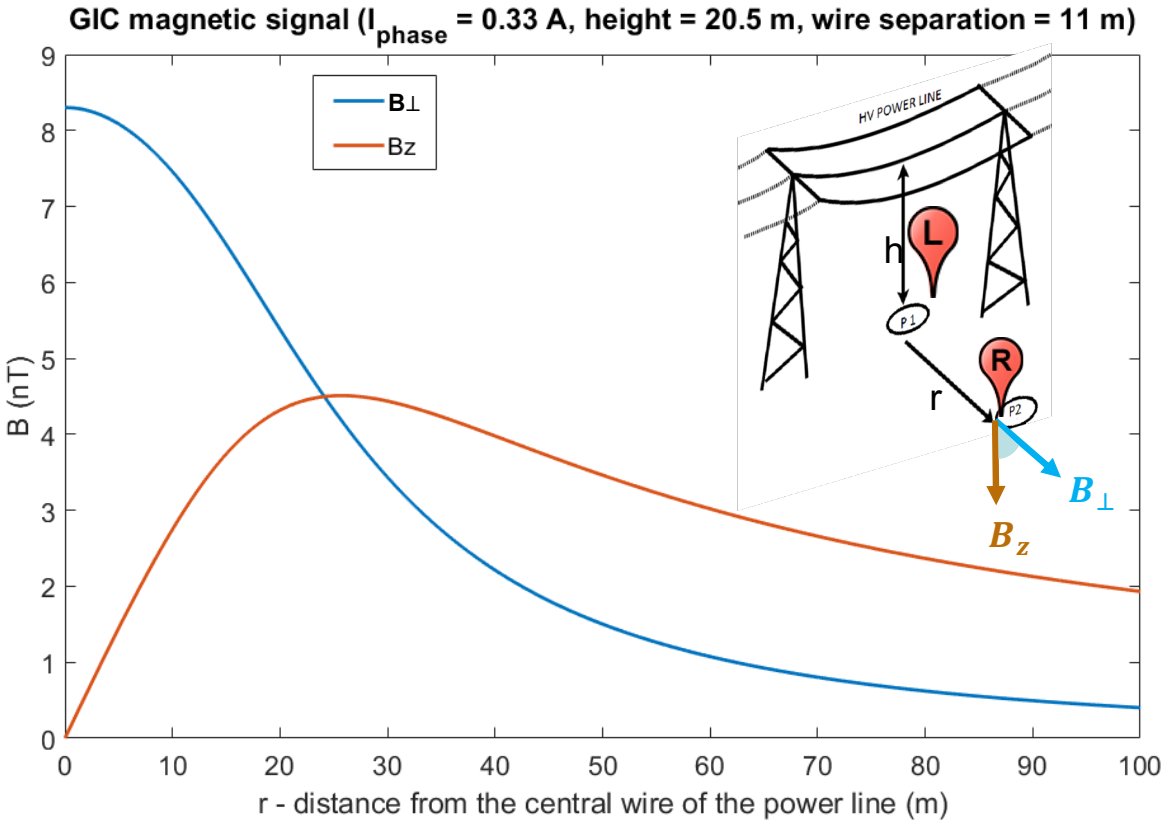

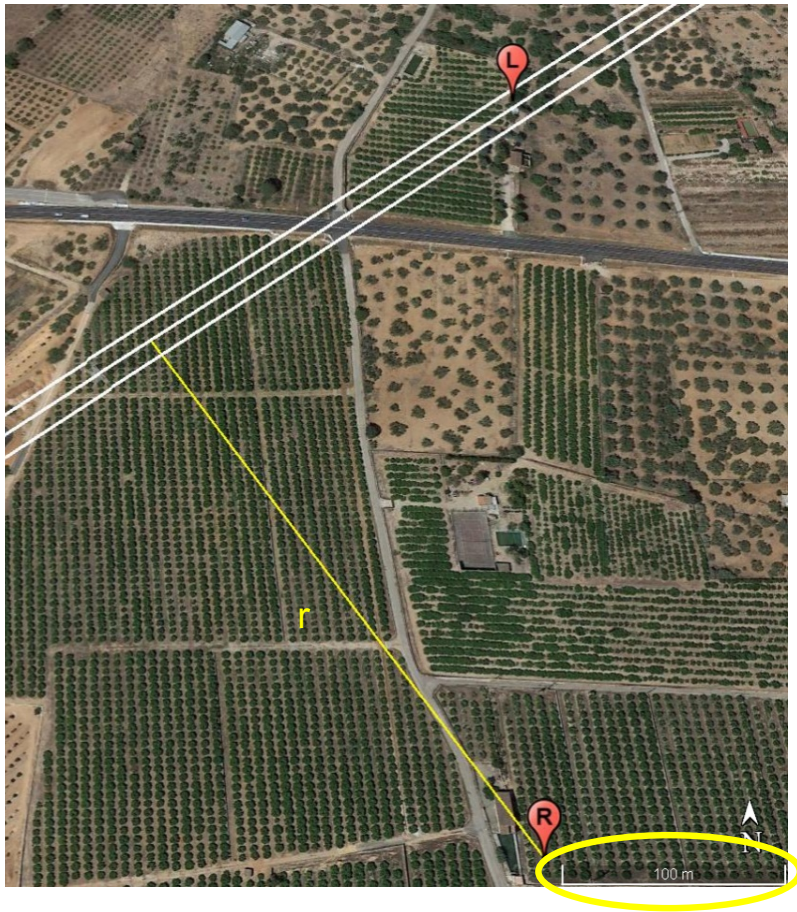

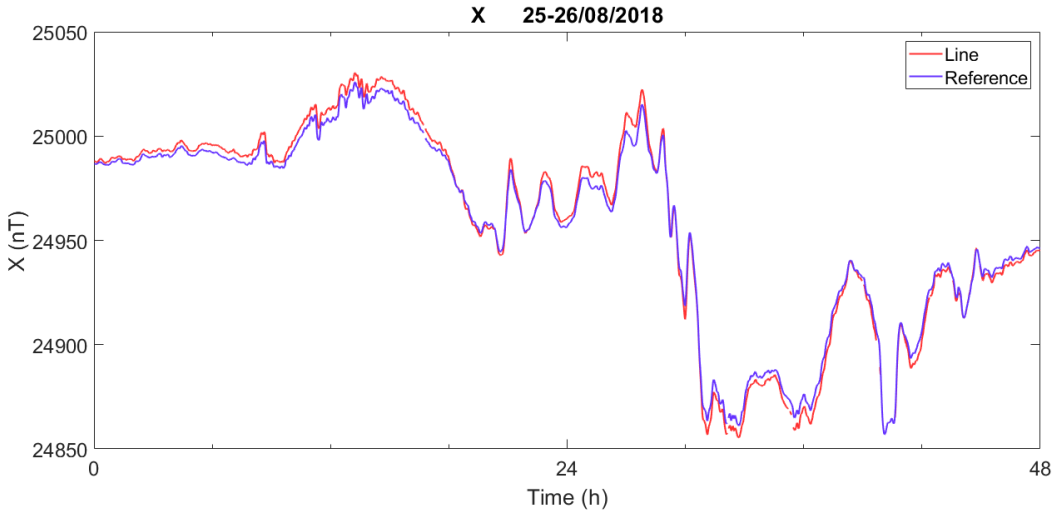
X 25-26/08/2018
25050
25000
24950
24900
24850
X (nT)
0
24
48
Time (h)
Line
Reference

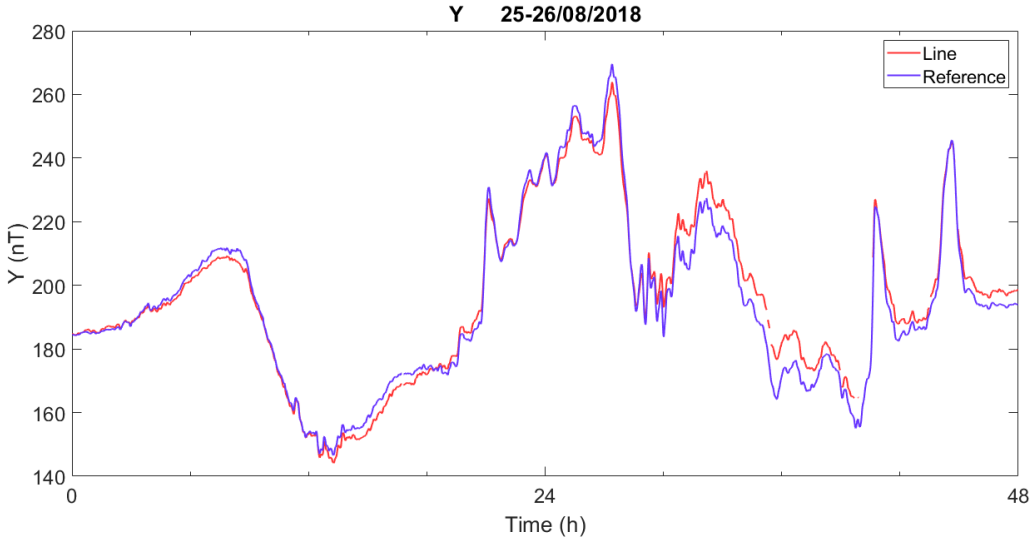
Y 25-26/08/2018
280
260
240
220
200
180
160
140
Y (nT)
0
24
48
Time (h)
Line
Reference

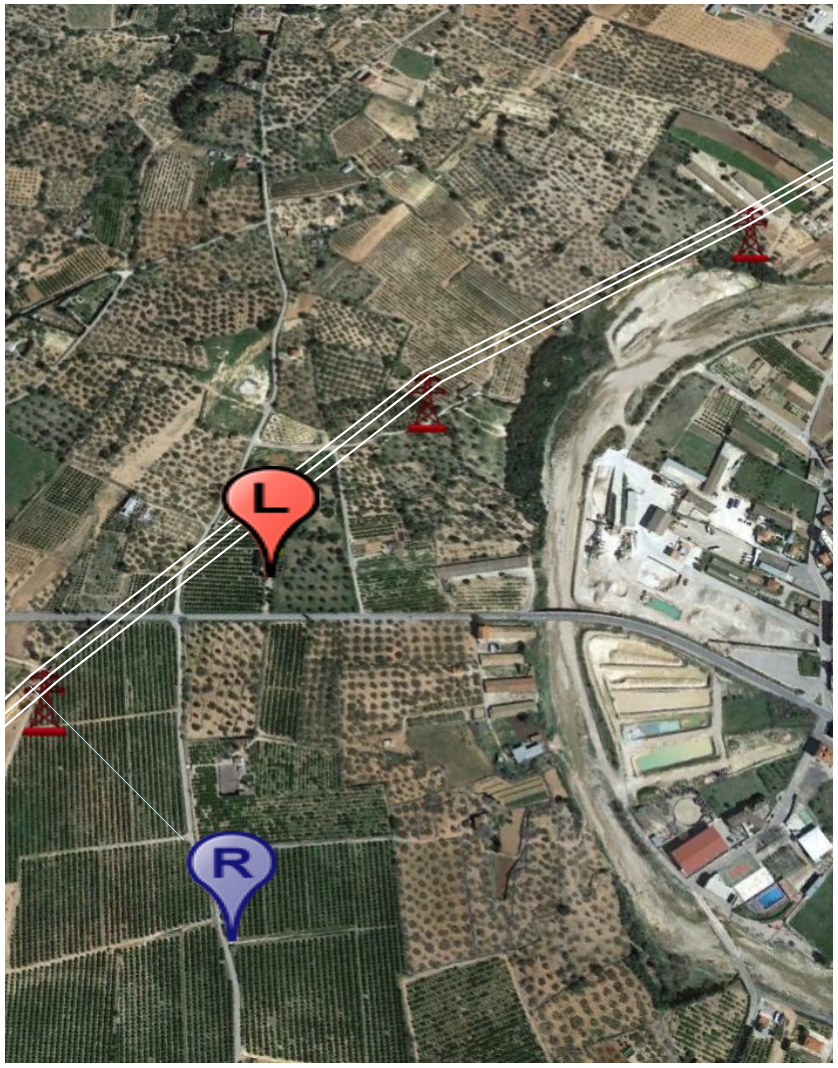
L
R

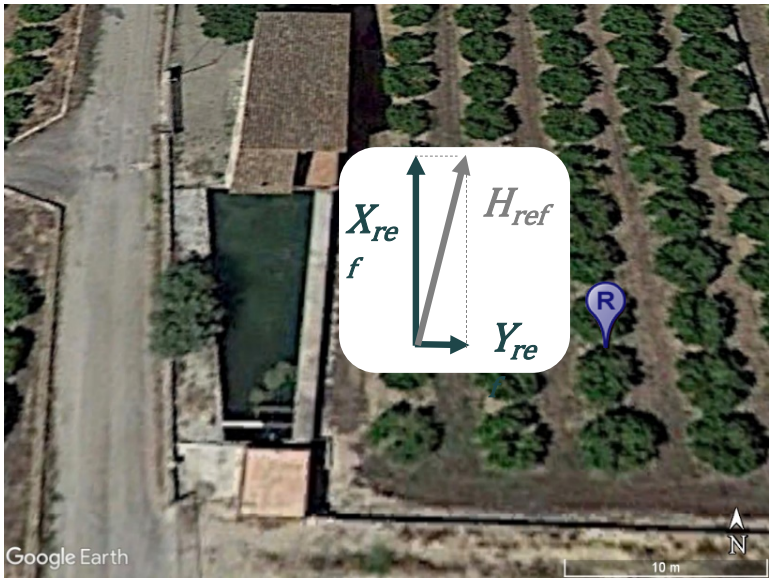

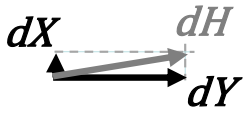

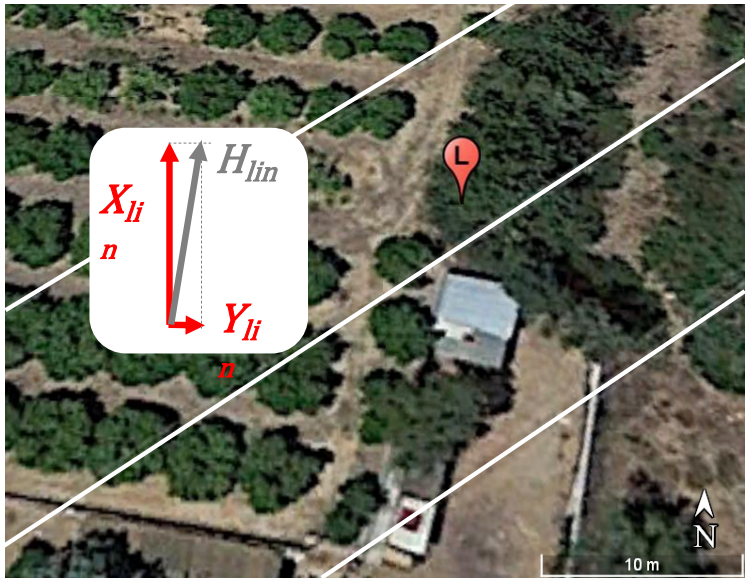

For the quietest days:

$$\begin{pmatrix} X_{ref} \\ Y_{ref} \\ Z_{ref} \end{pmatrix} - \boldsymbol{R}(\varphi,\theta,\psi)\left[\begin{pmatrix} k_X & 0 & 0 \\ 0 & k_Y & 0 \\ 0 & 0 & k_Z \end{pmatrix}\begin{pmatrix} X_{lin} \\ Y_{lin} \\ Z_{lin} \end{pmatrix} + \begin{pmatrix} b_X \\ b_Y \\ b_Z \end{pmatrix}\right] = \begin{pmatrix} \boldsymbol{dX} \\ \boldsymbol{dY} \\ \boldsymbol{dZ} \end{pmatrix}$$

vector of residuals

orientation angles

scale values

Bias fields

minimum

determined by LS

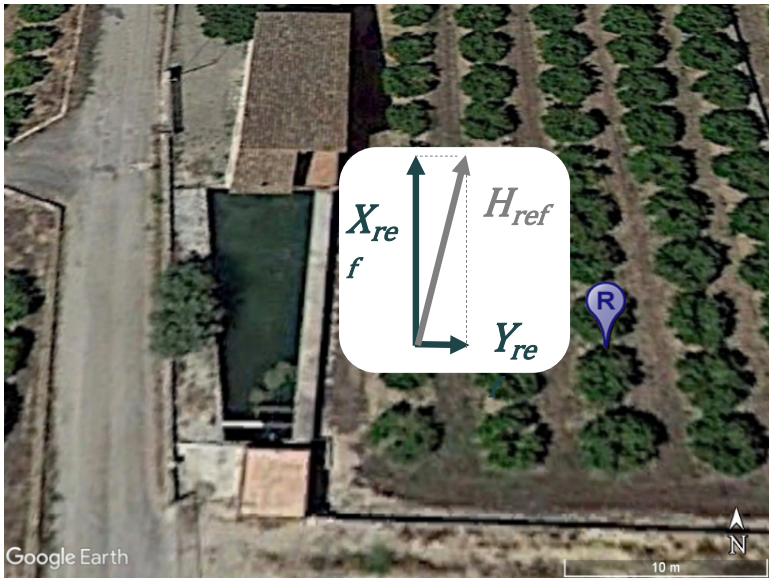

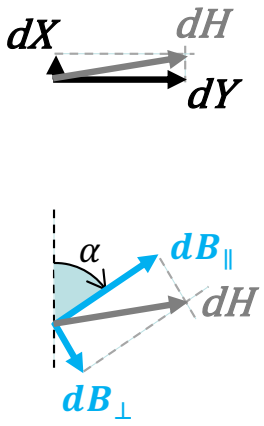

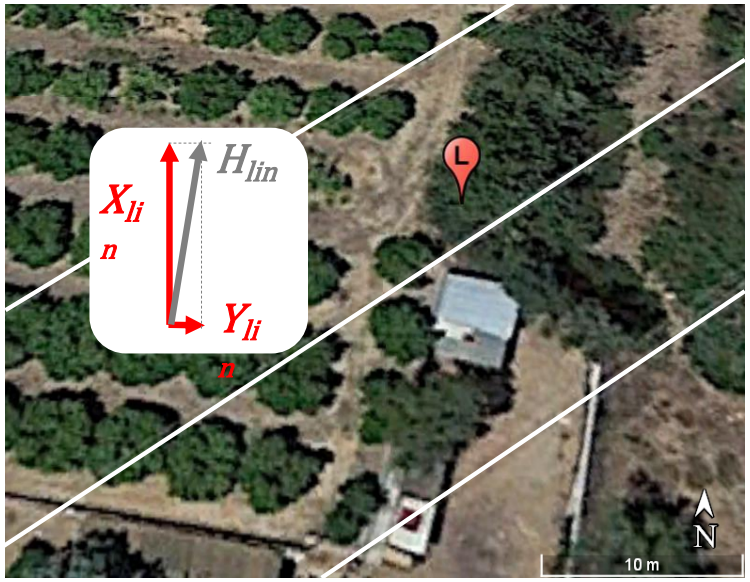

For the disturbed periods:

$$\begin{pmatrix} X_{ref} \\ Y_{ref} \\ Z_{ref} \end{pmatrix} - \boldsymbol{R}(\varphi,\theta,\psi)\left[\begin{pmatrix} k_X & 0 & 0 \\ 0 & k_Y & 0 \\ 0 & 0 & k_Z \end{pmatrix}\begin{pmatrix} X_{lin} \\ Y_{lin} \\ Z_{lin} \end{pmatrix} + \begin{pmatrix} b_X \\ b_Y \\ b_Z \end{pmatrix}\right] = \begin{pmatrix} \boldsymbol{dX} \\ \boldsymbol{dY} \\ \boldsymbol{dZ} \end{pmatrix}$$

orientation angles

scale values

Bias fields

vector of residuals

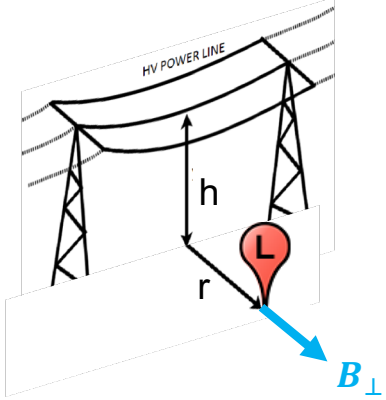

In practice $dB_{\parallel}$ should be 0

$$\begin{pmatrix} dB_{\parallel} \\ dB_{\perp} \end{pmatrix} = \begin{pmatrix} \cos\alpha & \sin\alpha \\ -\sin\alpha & \cos\alpha \end{pmatrix}\begin{pmatrix} \boldsymbol{dX} \\ \boldsymbol{dY} \end{pmatrix}$$

$$\mathbf{GIC} = \frac{dB_{\perp}}{\mathrm{GIC2B}}$$

factor dependent on the wire-wire distance, h and r, acc. Ampere's law

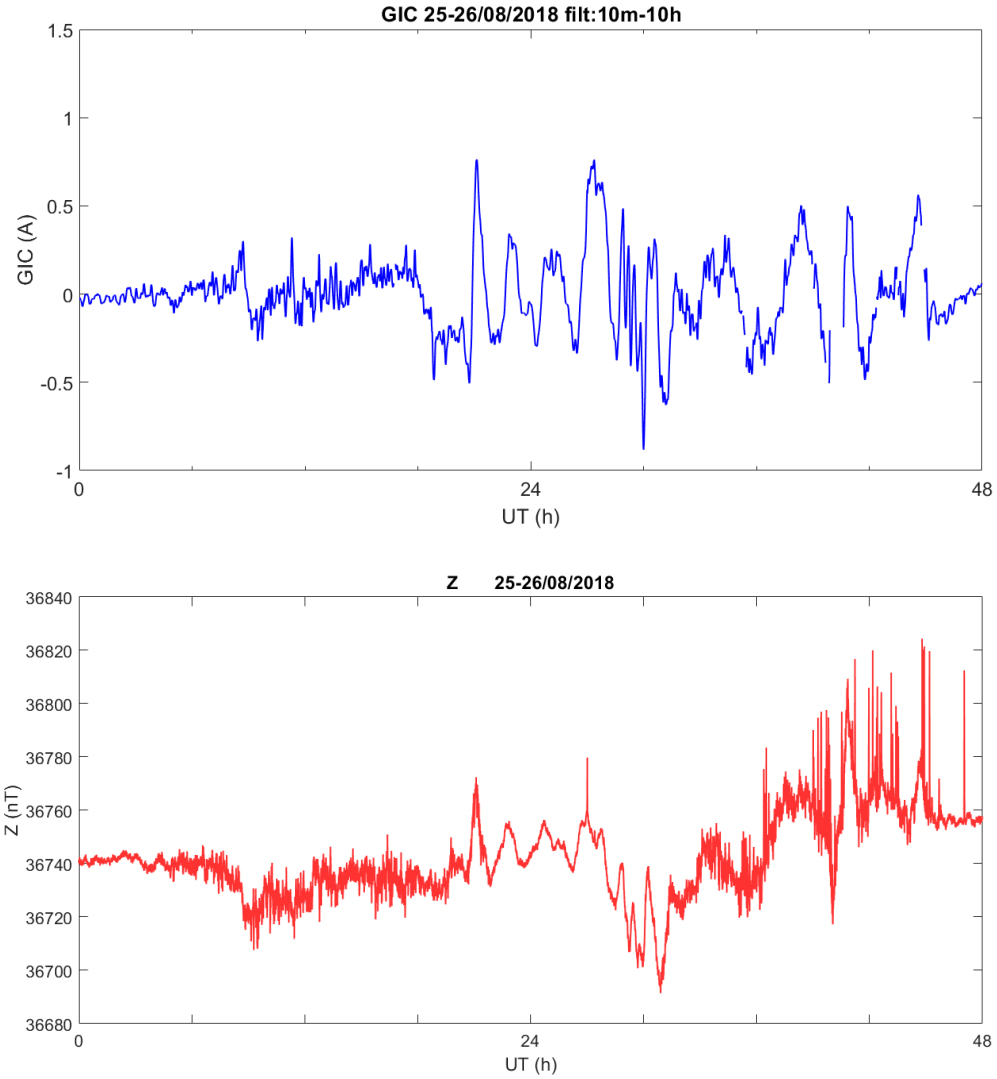
GIC 25-26/08/2018 filt:10m-10h
GIC (A)
1.5
1
0.5
0
-0.5
-1
0
24
48
UT (h)
Z 25-26/08/2018
Z (nT)
36840
36820
36800
36780
36760
36740
36720
36700
36680
0
24
48
UT (h)


L
R
2 km
Barcelona-Valencia DC powered railway
N
1 km

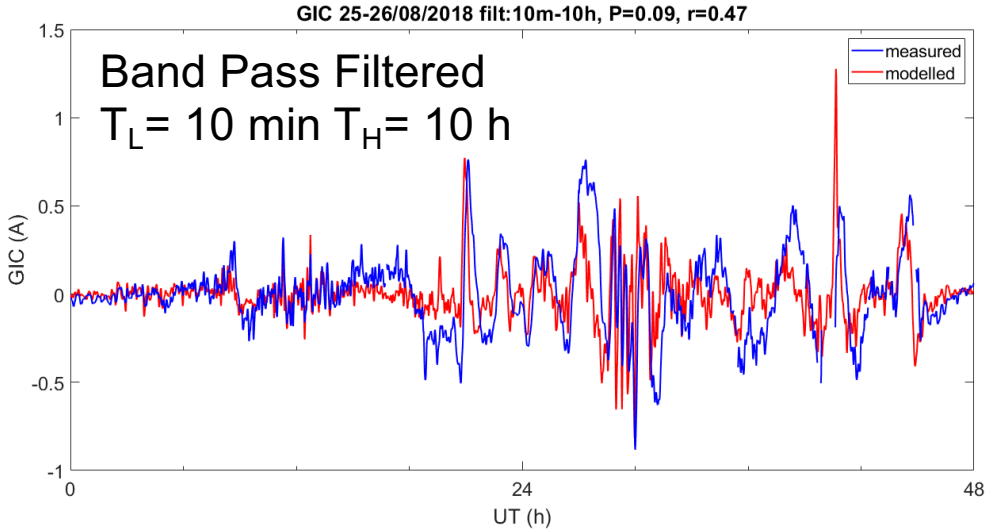

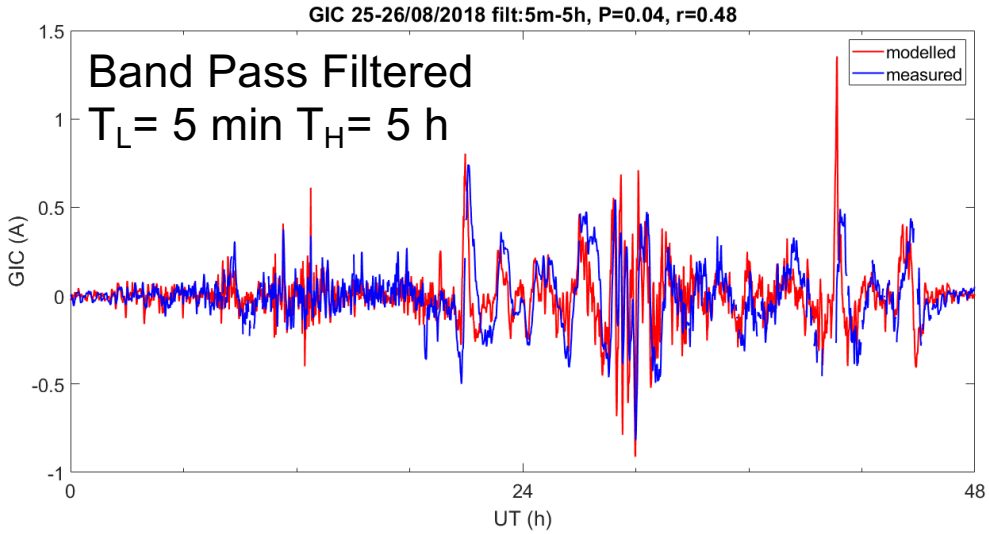

Skill scores:

P = 0.09 r = 0.47

Root mean square deviation of the residuals between our model and the observations

with:

$$P = 1 - \frac{1}{\sigma_0}\sqrt{\frac{\sum_{i=1}^{N}[(o_i - \overline{o}) - (m_i - \overline{m})]^2}{N}}$$

Standard deviation of the observations

Performance parameter (*Marsal & Torta, Space Weather, 2019*)

Observed and modelled values and their means

$$r = \frac{\overline{om} - \overline{o}\,\overline{m}}{\sqrt{(\overline{o^2} - \overline{o}^2)(\overline{m^2} - \overline{m}^2)}}$$

Correlation coefficient

P = 0.04 r = 0.48

How do we quantify the performance of our models?

Space Weather

Commentary | Free Access

Quantifying the Performance of Geomagnetically Induced Current Models

S. Marsal, J.M. Torta

First published: 02 July 2019 | https://doi.org/10.1029/2019SW002208

Abstract

We describe a metric that has been repeatedly applied to assess the performance of models aimed at predicting geomagnetically induced currents from Space Weather events. The used parameterization, based on the well-known root-mean-square error between model and observations, is simple and intuitive. Its use is exemplified, and its advantages and disadvantages are discussed, as well as its relationship with the widely extended correlation coefficient, *r*. Although the use of *r* alone is inappropriate for purposes of evaluating the agreement between model and observations, its use is recommended to complement the described performance parameter.

1 Introduction

Modeling is one of the essential activities in different branches of science and engineering with the purpose of describing either the totality or a particular aspect of an observable

P gives us an idea of the fraction of the standard deviation of the observations which can be explained by the model

Root mean square deviation of the residuals between our model and the observations

with:

$$P = 1 - \frac{1}{\sigma_0}\sqrt{\frac{\sum_{i=1}^{N}[(o_i - \overline{o}) - (m_i - \overline{m})]^2}{N}}$$

Standard deviation of the observations

Performance parameter (*Marsal & Torta, Space Weather, 2019*)

Observed and modelled values and their means

$$r = \frac{\overline{om} - \overline{o}\,\overline{m}}{\sqrt{(\overline{o^2} - \overline{o}^2)(\overline{m^2} - \overline{m}^2)}}$$

Correlation coefficient

Modeled observations with the same signal multiplied by a scale factor or shifted by a constant value will provide the same r

Inclusion of lower voltage circuits

Taking into account the 220 kV and 110 KV power systems is essential at those substations of the 400 kV grid where the systems are interconnected through autotransformers.

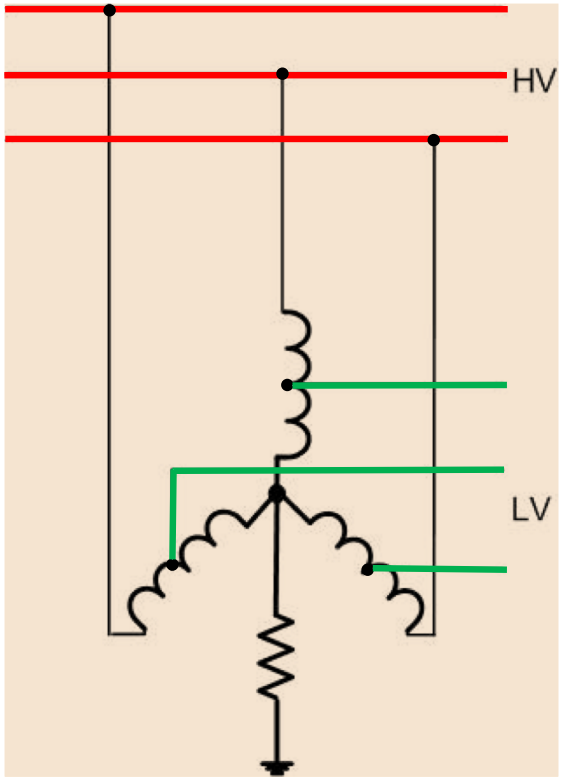

HV and LV systems are galvanically connected in autotransformers

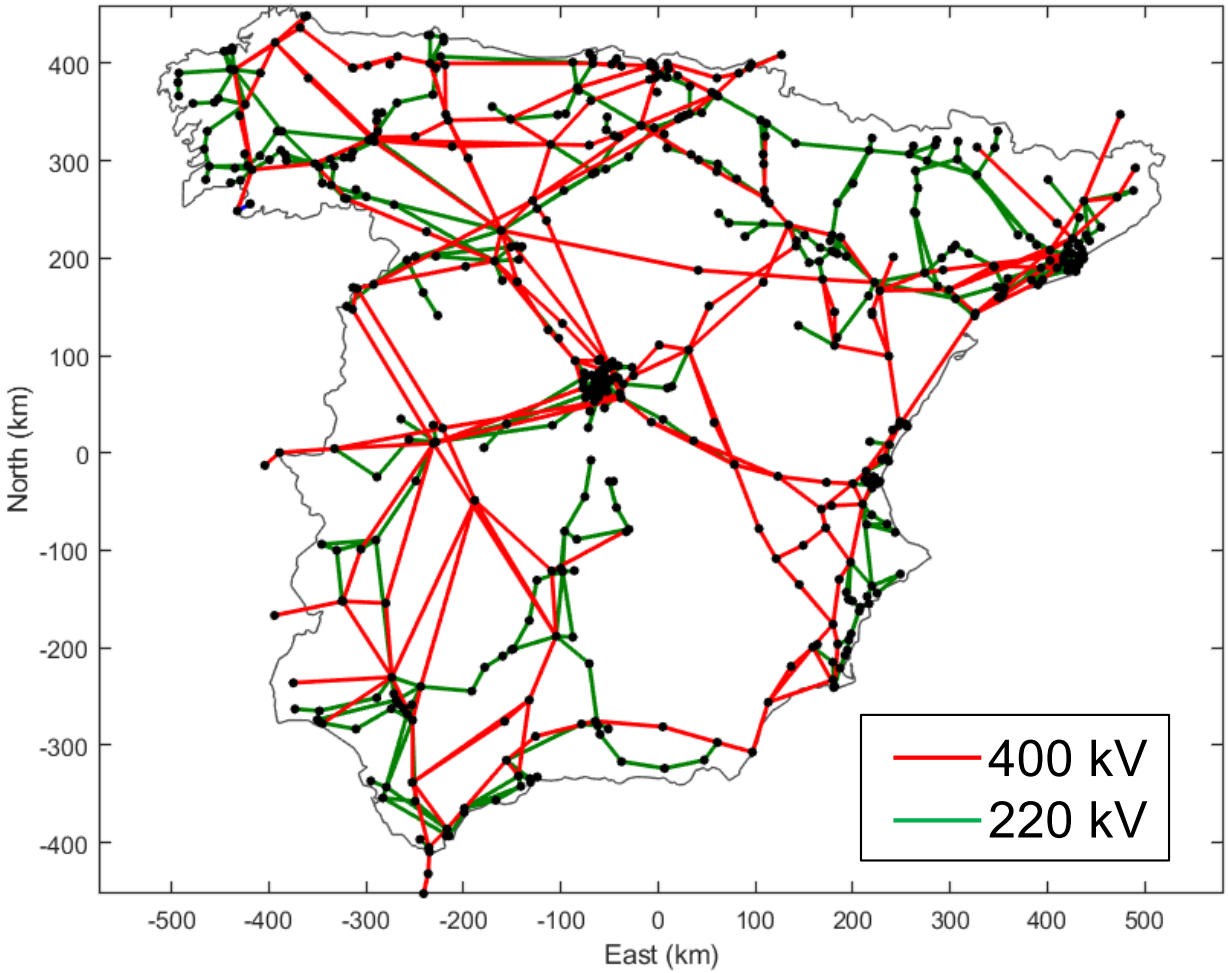

CONCLUSIONS (I)

- **Space weather is an emerging natural hazard,**
- **with incredibly important effects to our lives marked by the technological dependence (HI-LF).**
- **GIC appear in technological systems such as power transmission grids.**
- **Modelling efforts require a determination of the electric field occurring in connection with a magnetic storm at the Earth's surface,**
- **and a calculation of the resulting GIC in the conductor system after obtaining a DC model (*it is of utmost importance to know the geometrical configuration, the couplings, the connections and the resistance values*)**

CONCLUSIONS (II)

- **The forensic analysis revealed that the greatest rate of change of the geomagnetic field at Ebro Observatory reached 177 nT / min.**
- **This empirical limit is much lower than the intensities that have caused impacts on electricity networks in higher latitude regions (*"Quebec" was of 479 nT / min*), although impacts have been observed with levels < 100 nT / min.**
- **To improve the GIC modelling, MT measurements can be expressed as empirical impedance tensors.**
- **Results for both the obtaining of new models and data for their validation are still preliminary … but very promising**

Thanks for your attention!

Acknowledgements

Project *IBERGIC:* S Marsal, JJ Curto, O Cid (OE, SP); JJ Ledo, P Queralt, A Marcuello, A Martí (UB, SP); J Campanyà (DIAS, IR); L Martínez, M Quintana, J Ruperez (REE, SP)

Model validation with real measurements

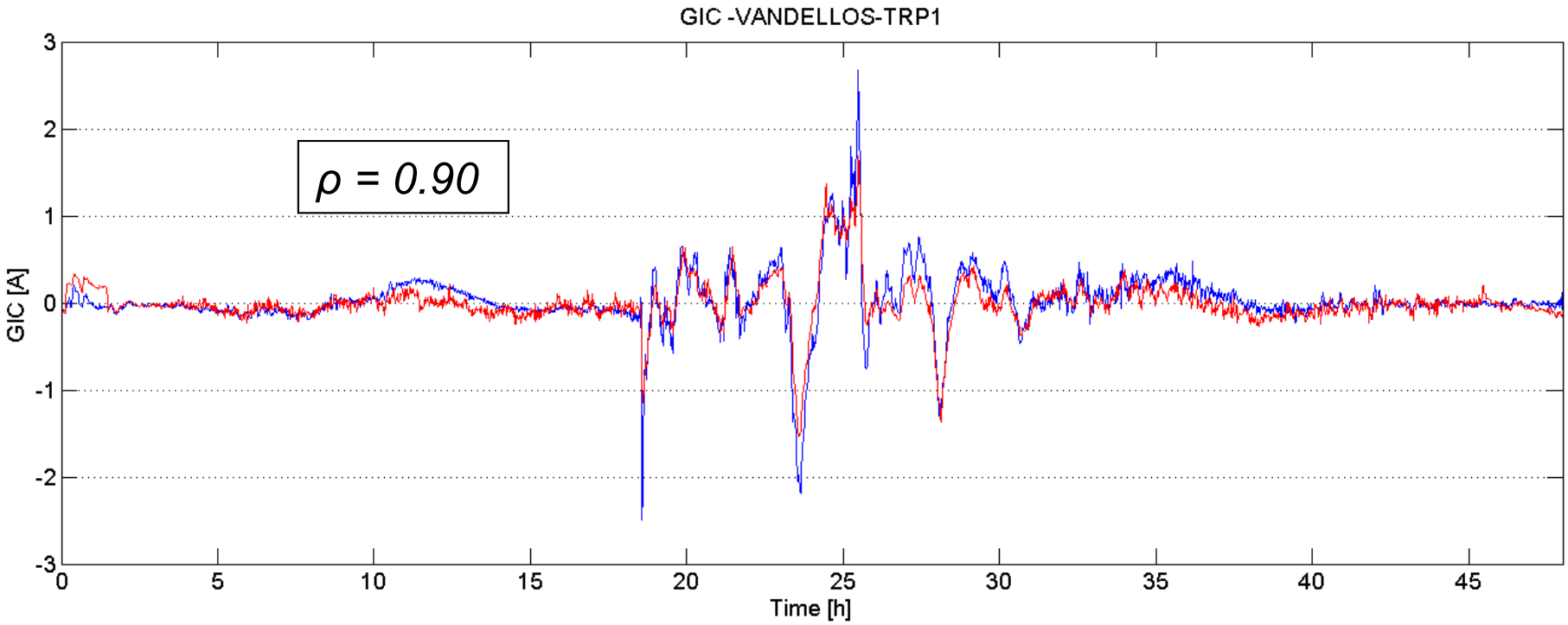

Measured (red) and calculated GIC for 24-25/10/2011

Using a 2D layered structure, with the strike direction θ assumed parallel to the coast and the Z_{TE} and Z_{TM} obtained from the MT survey:

$$GIC = \frac{1}{\mu}(a \quad b)\begin{pmatrix}\cos\theta & -\sin\theta\\ \sin\theta & \cos\theta\end{pmatrix}\begin{pmatrix}0 & Z_{TE}\\ -Z_{TM} & 0\end{pmatrix}\begin{pmatrix}\cos\theta & \sin\theta\\ -\sin\theta & \cos\theta\end{pmatrix}\begin{pmatrix}B_x\\ B_y\end{pmatrix}$$

Northward and Eastward network constants at the transformer

Saturation of Power Transformers

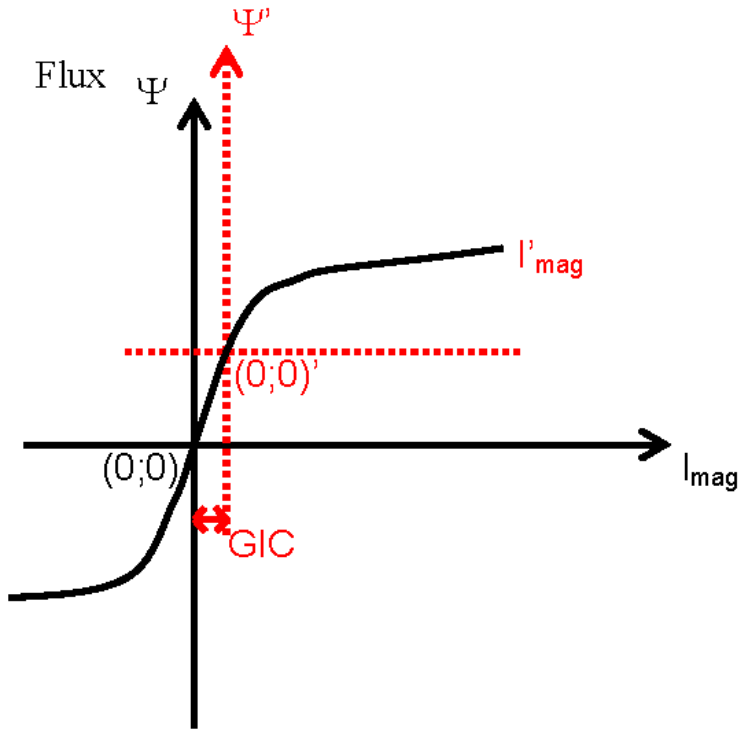

Figure 4.1 Transformer magnetisation curve in the presence of GIC [1].

A transformer core is made of high permeability ferromagnetic material such as silicon steel. Its purpose is to provide a well-defined low reluctance path for magnetic flux.The DC offset caused by the GIC causes an alignment of the core material domains in one direction and thus along the hysteresis curve causing a null point offset. To prevent transformers from becoming prohibitively expensive, their cores are designed to operate close to the saturation point of the hysteresis curve.

Saturation of Power Transformers

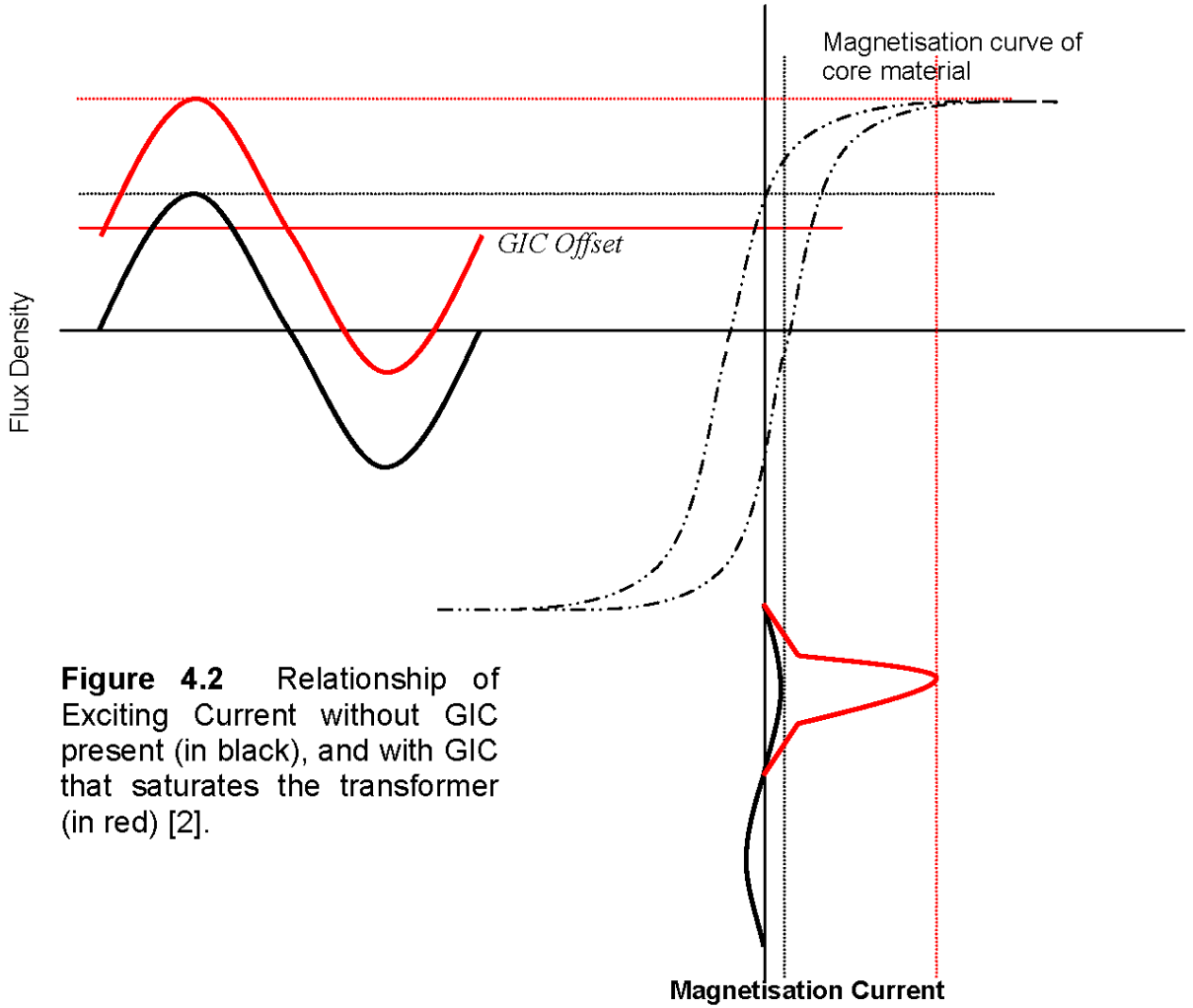

Figure 4.2 Relationship of Exciting Current without GIC present (in black), and with GIC that saturates the transformer (in red) [2].

The GIC offset can therefore cause transformers to saturate every half-cycle, hence the term half-cycle saturation, the root-cause of all power system problems that occur during geomagnetic storms. Note that magnetisation current is very small to improve transformer efficiency, therefore equally low values of GICs can cause a considerable offset.

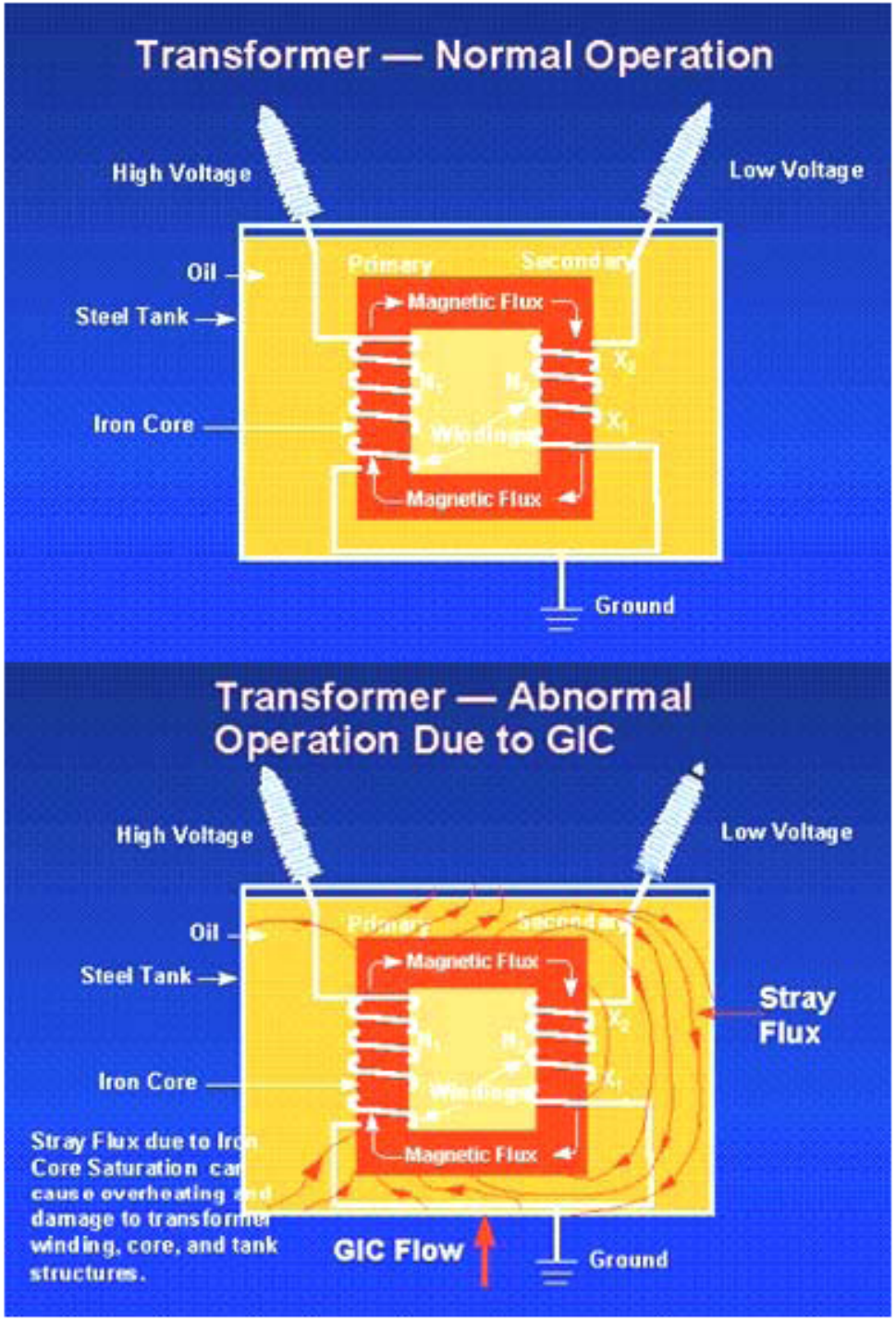

Transformer Heating

The saturation of the magnetic core will cause flux to exit the core steel for alternative paths, such as the tank wall, flux shields, clamps and other structural steel members of the transformer (see figure). The leakage flux due to core saturation initiates eddy current heating in components linked by it and creates hot spots. Hot spots can melt structural steel members and are likely to cause a cumulative damaging effect on the transformer winding insulation,leading to premature transformer failure.

SIMPLEST RAIL CIRCUIT

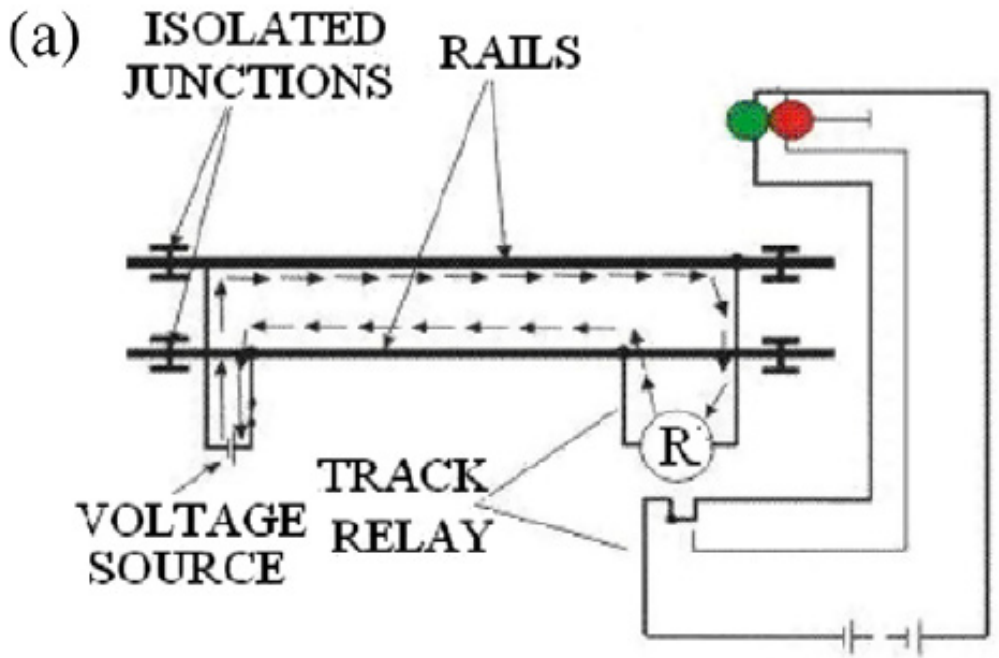

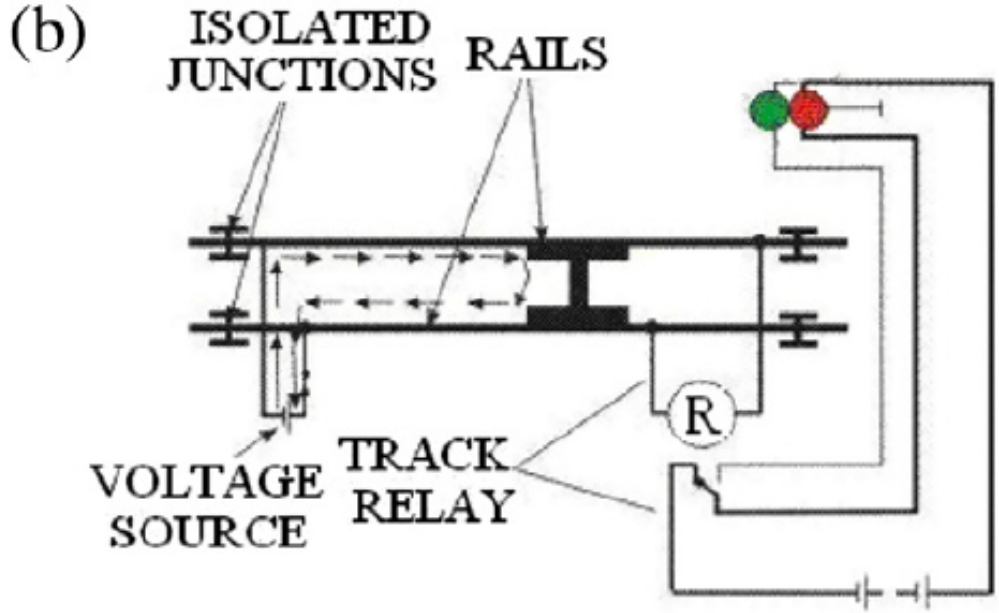

Incidents in oil and gas steel pipelines

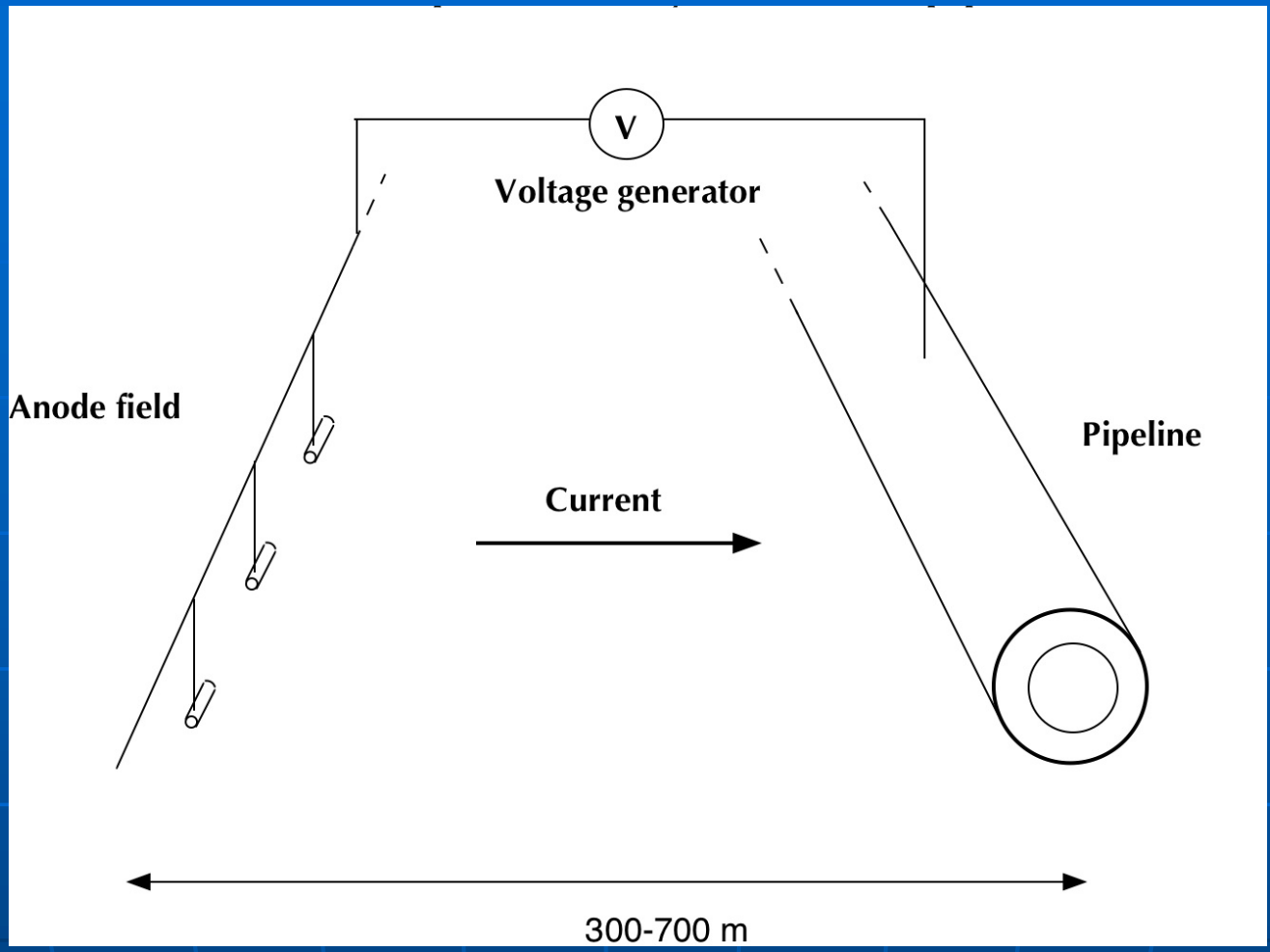

Figure: Antti Pulkkinen

- They use a cathodic protection to minimize corrosion by maintaining the steel at a negative potential with respect to ground
- GICs can cause changes in the pipeline to the ground potential, increasing the risk of corrosion in large geomagnetic storms
- They can contribute to reduce the lifetime of the pipeline